Molecular insights into pyruvate-sensing of the LytS/LytTR-type BtsS/BtsR signaling

cascade of *Escherichia coli*

Jin Qiu

München, September, 2023

Molecular insights into pyruvate-sensing of the LytS/LytTR-type BtsS/BtsR signaling

cascade of *Escherichia coli*

Jin Qiu

Dissertation zur Erlangung des Naturwissenschaftlichen Doktorgrades „Doctor rerum naturalium" (Dr.rer.nat.) an der Fakultät für Biologie der Ludwig-Maximilians-Universität München

München, September, 2023

Erstgutachter: Prof. Dr. Kirsten Jung

Zweitgutacher: Prof. Dr. Christof Osman

Tag der Abgabe: 29.09.2023

Tag der müchdlichen Prüfung: 05.12.2023

Eidesstattliche Erklärung

Hiermit erkläre ich, dass ich diese Dissertation selbstständig angefertigt und weder ganz noch teilweise einem anderen Prüfungsausschuss vorgelegt habe. Ich habe nicht versucht, die Dissertation einzureichen oder die Promotionsprüfung auf andere Weise abzulegen.

München, den September. 2023

Jin Qiu

Statutory declaration and statement

I hereby declare that I completed this thesis independently and that it has not been submitted to another examination board in whole or in part. I have not attempted to submit the thesis or take the Ph.D. exam in any other way.

München, den. September.2023

Jin Qiu

Contributions to Publications presented in this Thesis

Citations in Chapter:

1.3.6, 1.3.7, 2.2.2, 2.2.3, 2.2.6-9, 3.1, 3.2.1, 3.3, part of 4.4 with marks in front of paragraph

Jin Qiu, Ana Gasperotti, Nathalie Sisattana, Martin Zacharias, and Kirsten Jung. The LytS-type histidine kinase BtsS is a 7-transmembrane receptor that binds pyruvate. mBio. doi: 10.1128/mbio.01089-23. Online ahead of print.

Author contributions

Jin Qiu, Data curation, Investigation, Methodology, Writing the original draft, review and editing. Ana Gasperotti, Investigation, Supervision, Writing the review and editing. Nathalie Sisattana, Data curation, Methodology, Supervision, Writing the review and editing. Martin Zacharias, Conceptualization, Investigation, Writing the review and editing, Software, Visualization. Kirsten Jung, Conceptualization, Formal analysis, Funding acquisition, Project administration, Supervision, Writing the original draft, review and editing

We hereby confirm the above statements:

Jin Qiu   Prof. Dr. Kirsten Jung

我走了很远的路，换这一次红袍加身

Contents

10

Abbreviations

aa	amino acid
ABC	ATP-binding cassette
APS	ammonium persulfate
ATP	adenosine- 5'-triphosphate
Ala or A	alanine
Arg or R	arginine
Asn or N	asparagine
Asp or D	aspartic acid
BACTH	bacterial adenylate cyclase two-hybrid assay
BCIP	5-bromo-4-chloro-3-indolyl phosphate
BSA	bovine serum albumin
bp	base pair
CA	catalytic and ATP-binding
CM	cytoplasmic membrane
CP	cytoplasm
Cya	adenylate cyclase
cAMP	cyclic adenosine-5'-monophosphate
Cys or C	cysteine
DRaCALA	differential radial capillary action of ligand assay
DDM	dodecyl-beta-D-maltosid
DTT	dithiothreitol

DHp   dimerization and histidine-phosphorl transfer

dNTPs   deoxynucleotide triphosphates

epPCR   error-prone PCR

E. coli   *Escherichia coli*

EV   empty vector

ECF   extra-cytoplasmic function

F   phenylalanine

F_B fraction of ligand bound to protein

GAF   cGMP-specific phosphor-diesterases, adenylyl cyclases, and *E. coli* FhlA

Gln or Q   glutamine

Glu or E   glutamate

HK   histidine kinase

HAMP   histidine kinase, adenylyl cyclase, methyl-accepting chemotaxis protein, and

                   phosphatase

His or H   histidine

IPTG   isopropyl-β-D-thiogalactopyranoside

K_d dissociation constant

KML   modified LB medium in which NaCl is substituted for with KCl

Lac   lactate

LB   lysogeny broth

Lys or K   lysine

PCR   polymerase chain reaction

PP   periplasm

PAS   Per-Arnt-Sim proteins

Pyr   pyruvate

PTS   phosphotransferase system

POE-PCR   prolonged overlap extension PCR

PAGE   polyacrylamide gel electrophoresis

REC   receiver domain

RLU   relative light units

RM   random mutagenesis

RMSD   root-mean-square deviation

RR   response regulator

SDS   sodium dodecyl sulphate

Suc   succinate

Ser or S   serine

T_m melting temperature

Thr or T   threonine

Trp or W   tryptophan

Tyr or Y   tyrosine

TCEP   tris (2-carboxyethyl) phosphine

TCS   two-component system

TM   transmembrane

TMR-LYT   transmembrane receptors of the LytS-YhcK type

MD   molecular dynamics

nanoDSF   nano differential scanning fluorimetry

NBT   nitro blue tetrazolium

NC   negative control

Met or M   methionine

Val or V   valine

WT   wild type

w/v, v/v   weight per volume, volume per volume

List of figures and tables

Figures

Tables

Summary

LytS/LytTR-type histidine kinase/response regulator systems regulate pathogen-specific mechanisms during infection of human or plant hosts. *Escherichia coli* has two LytS/LytTR systems, BtsS/BtsR and YpdA/YpdB. The histidine kinase BtsS is a high-affinity sensor for extracellular pyruvate and interacts with response regulator BtsR to activate the expression of *btsT,* which encodes a symporter for pyruvate and H^+. This thesis describes new insights into the molecular mechanism of how pyruvate binding triggers the signal transduction process.

It was experimentally shown that BtsS is a seven-helix receptor, with its N-terminus located in the periplasm. Using a screening assay based on site-directed mutagenesis, the pyruvate-binding site was identified within the membrane-spanning domains of BtsS. It is a small cavity, and pyruvate forms interactions with the side chains of arginine 72, arginine 99, cysteine 110, and serine 113, located in the transmembrane helices III, IV and V, respectively. The interactions between pyruvate and these four amino acids were further confirmed by molecular dynamics simulation studies.

In addition, three other amino acids in BtsS were found to be important for structure and signal transduction. Arginine 192 (helix VII) plays a role in the interaction with BtsR. Serine 25 (helix I) is important for conformational dynamics, as BtsS variants in which Serine 25 has been replaced by alanine or valine maintain the signal transduction system in an ON state. Cysteine 15 is likely involved in the formation of a disulfide bridge, but this is not essential for signal transduction *in vivo* under the conditions tested.

In previous studies, the autophosphorylation activity of BtsS was not detectable. Here, for the first time, BtsS was shown to have very low autophosphorylation activity in the presence of Mg^{2+}-ATP, which was approximately 10-fold higher when Mn^{2+}-ATP was used. The predicted

phosphorylation site at histidine 382 was confirmed. Moreover, the autokinase activity of BtsS could be stimulated in the presence of pyruvate. Measurements of *in vitro* autophosphorylation activity were used as a parameter to determine the molecular effects of individual amino acid replacements in BtsS, and the effects resulted not only in massive changes in activity levels but also in pyruvate-independent activity for many variants.

The elucidation of the pyruvate-binding site of BtsS opened the possibility of redesigning BtsS into a sensor of pyruvate-like ligands such as lactate, which can be used as a biosensor in medicine. The required workflow and a high-throughput screening system were established.

1 Introduction

All the organisms are exposed to fluctuating environments. They have to evolve some strategies to live in these changing environments. As for bacteria, signaling transduction systems play a very important role in these processes for cell-cell communication or cell-environment communication (1). Thereby, bacteria can detect the extracellular conditions and cell status and deal with these changes. In general, bacterial signal transduction can be divided into three stages (2) (FIG 1.1). (i) Reception, a ligand binds to the receptor protein inserted in the membrane or located inside of the cell. (ii) Transduction, a process of activating a series of proteins embedded on the membrane or inside the cell by adding or transferring the phosphate group. (iii) Response, the change that occurs in the cell by creating some signal outputs, e.g., regulation of certain genes expression, protein activation and so on (3).
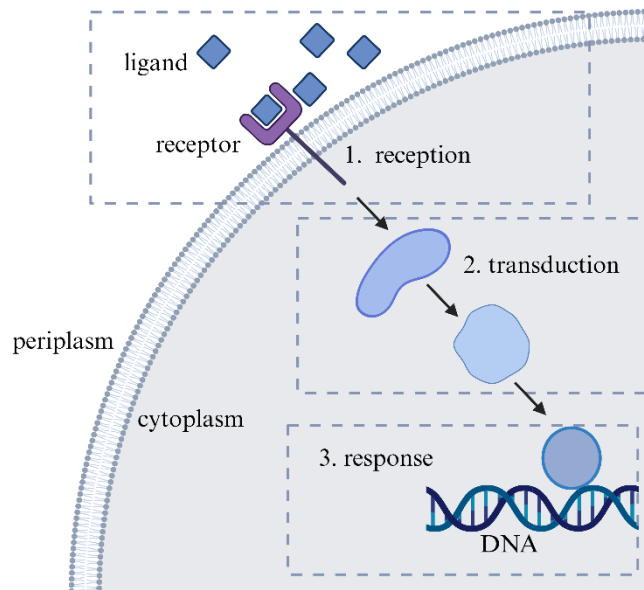
FIG 1.1 Schematic overview of three stages of signal transduction. (i) Reception, a ligand binds to the receptor protein inserted in the membrane or located inside of the cell. (ii) Transduction, the process of activating a series of

proteins embedded in the membrane or inside the cell by adding or transferring the phosphate group. (iii) Response, the change that occurs in the cell by creating the signal output. The figure was created with BioRender.com.

1.1 Signaling transduction in bacteria

Bacteria are equipped with three major classes of transmembrane signaling systems (FIG 1.2). One is the membrane-integrated one-component system (often belongs to the ToxR-like receptors family), containing a periplasmic sensor domain and a cytoplasmic DNA binding domain (4). Another class is two-component systems (TCSs), composed of a membrane-integrated sensor histidine kinase (HK) and a cognate soluble response regulator (RR). It is the major system for bacteria to sense environmental stimuli (5). The third class is the extra-cytoplasmic function (ECF) sigma factors, which are small regulators binding to the RNA polymerase to trigger gene transcription. Many bacteria have several ECF sigma factors and the corresponding regulators are outnumbering amount of sigma factors (6).
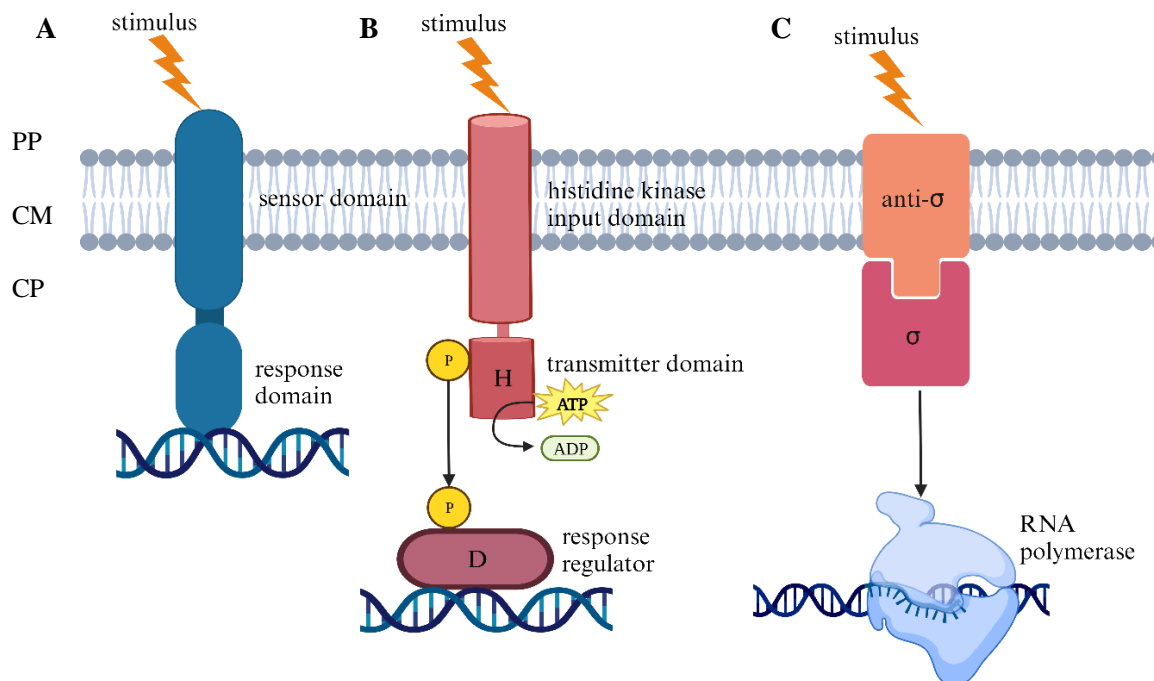
FIG 1.2 Three major classes of signaling transduction process in bacteria. (A) One-component system, consisting of sensor and DNA-binding domain, (B) two-component systems with a membrane-anchored histidine kinase (HK) and a cytoplasmic response regulator (RR), and (C) extra cytoplasmic function (ECF) sigma factors (σ) and the anti-sigma factor (anti-σ) for stimulus perception. PP - periplasm, CM - cytoplasmic membrane, CP - cytoplasm. The figure was created with BioRender.com.

1.2 Two component systems (TCSs)

TCSs are the most widely occurring signal transduction systems in bacteria and also exist in some fungi and plants. Upon stimulus perception from the environment, HKs will auto-phosphorylate in a conserved histidine residue, where the high energy γ-phosphor group provided by ATP is received. This process requires dimerization of HKs (7). Then, the phosphoryl group will be transferred to a conserved aspartate in the receiver domain of the RR, which can cause the conformational changes of the regulator, resulting in altered gene expression or protein activation. Most HKs are bifunctional, as these are displaying also a phosphatase activity to dephosphorylate the RR to stop the signaling transduction process (8-12).

The number of TCSs differs from species to species, depending on the natural host. Most species contain more than one TCS that regulate a wide variety of behaviors, for example metabolism and motility, virulence and development. There is no TCS in *Mycoplasma genitalium* (13), while 30 HKs and 32 RRs are annotated in *Escherichia coli* (14) and 132 HKs and 119 RRs in *Myxococcus xanthus* (15). Some TCSs have been extensively studied and their phenotypes and functions were elucidated. For example, AgrC/AgrA from *Staphylococcus aureus* is related to pathogenesis (16); ApsS/ApsR from *Staphylococcus epidemidis* is involved in antimicrobial peptide resistance (17); BvgA/BvgS in *Bordetella pertussis* is physiologically link to toxin and adhesin expression and biofilm formation (18); CheA/CheB/CheY in *E. coli* is related to

chemotaxis (19); CitA/CitB in *E. coli* uptakes citrate (20); Evgs/EvgA in *E. coli* is physiologically involved in multiple drug resistance (21); KdpD/KdpE in *E. coli* is a high-affinity K^+ transport system (22); PhoP/PhoQ in *E. coli* and *Staphylococcus enterica* is responsible for bacterial virulence (23); BtsS/BtsR in *E. coli* is for pyruvate response (24).

1.2.1 Histidine kinase (HK)

HK consists of an N-terminal input domain and a C-terminal transmitter domain. The input domains are variable in sequence and architecture, evolved to sense many different environmental signals and containing e.g., GAF domains (c<u>G</u>MP-specific phosphor-diesterases, <u>a</u>denylyl cyclases, and *E. coli* <u>F</u>hlA), PAS domains (contained in <u>Per-Arnt-S</u>im proteins) and HAMP domains (<u>h</u>istidine kinase, <u>a</u>denylyl cyclase, <u>m</u>ethyl-accepting chemotaxis protein, and <u>p</u>hosphatase). GAF domain comprises a five or six anti-parallel β-sheet to bind a variety of small ligands, including cGMP, cAMP, heme and it exists in around 9% of all HKs (25). HAMP domain, present in around 31% of HKs (26), converts signal-triggered transmembrane motions into receptor outputs (27). It is still not clear whether it is a unique property for all proteins to have HAMP domains and how the transmembrane signaling transmits. Around 33% of HKs contain one or more PAS domain. Studies found some ligand-binding pockets in PAS domain allow kinase to accommodate different small molecules with different binding patterns to sense variable environmental changes (28).

The transmitter domain is more conserved harboring a signal transmission domain. It is composed of a <u>d</u>imerization and <u>h</u>istidine-phosphoryl transfer domain (DHp), designated as H-box with conserved histidine residue, and <u>c</u>atalytic and <u>A</u>TP-binding (CA) domain, designated as N, G1, F, and G2 boxes since the conserved residues in these boxes are involved in ATP binding. DHp domain is known as the His kinase A domain in Pfam and CA domain is known as HATPase_c (29). CA domain binds ATP and transfers phosphoryl group to the DHp domain. A loop including

the F-box acts as an ATP cover (ATP-lid), which lengths are different in different families and it can interact with RR for signal transduction. Besides, DHp domain forms a coiled-coil structure by DHp four-helix bundle after dimerization (30). The coiled-coil structure consists of α helices within seven residues in every two turns. Normally the first and forth amino acids are hydrophobic, which are on the same side of a helix and interact with the corresponding amino acids on the other monomer helix (31). Movement at this coiled coil structure will cause the change of position or distance of amino acids, which is an important way to transmit the signal (32).

1.2.2 Response regulator (RR)

The RR is an essential cytoplasmic protein executing the cellular outputs in response to the stimulus received by the HK. Most of the RRs comprise two domains, a conserved N-terminal receiver domain (REC) and a C-terminal effector domain (33). They are connected with each other by a linker. The effector domains are very diverse according to different outputs (34). In addition, the linkers connecting these two domains are also variable in sequence and length, ranging from 40 to more than 180 amino acids (35). The phosphoryl group in REC domain will be transferred to a conserved aspartate residue, which will cause the conformational changes (36). The activated RR will then trigger DNA-binding (37-40), RNA-binding (41, 42), enzymatically active (43-45) and protein-binding (46, 47).

The architecture of REC domains of RR is similar, which have a five-stranded β-sheet with two α-helices on one side and three α-helices on the other side. While the sequences of this domain are quite diverse (26). One aspartic acid residue is conversed at the end of the third β-strand which receives the phosphoryl group from HK (26)(48). Another two conserved ones are aspartate and glutamate, within a loop involved in Mg^{2+}or Mn^{2+}-ion binding, which participates the phosphorl-transfer step. Other conversed residues are threonine or serine (Thr or Ser) located at the end of the

β4 chain and phenylalanine or tyrosine (Phe or Tyr) in the middle of the β5 chain, which are named as switch residues (49, 50). RRs phosphorylation and conformational changes are similar, but the degree of structural change differs. Phosphorylation of conserved aspartic acid residues causes rearrangement of switch residues and conformational change of the REC domain (49, 50). Their side chains keep away from or towards phosphorylation center to pose the active and inactive conformations, respectively (51, 52).

1.3 Signaling transduction mechanism

1.3.1 Stimulus perception

There are three different mechanisms about how the stimulus is received by HK. One is that the extracellular signal is sensed through the periplasmic input domain of a histidine kinase. In this case, the sensor domain locates in the periplasm and the kinase domain locates in the cytoplasm. They are connected through the cell membrane (53-55). Second one is that the stimulus is perceived by membrane helixes and then transduced to the cytoplasmic domain (56, 57). The third way is that a cytoplasmic signal is sensed by a soluble protein that it can associate with HK (58-60).

1.3.2 Histidine kinase dimerization and autophosphorylation

The majority of HKs exist as stable homodimers for function. HKs harbor a coiled-coil structure formed by the DHp four-helix bundle as described above. The autophosphorylation reaction on histidine kinase (phosphortransfer from ATP to a histidine side chain) plays a central role in the whole signal transduction process. The core length of histidine kinase is around 350 amino acids and is involved in ATP binding and kinase phosphorylation (61, 62). Either the Nδ1 or the Nε2 atom on histidine residues imidazole ring can receive phosphoryl group (63, 64). Phosphoramidate bond of phosphohistidine is with high energy to transfer the phosphoryl group to

other molecules, therefore the half-life of this reaction is quite short, ranging from around a few seconds or several minutes (65). Autophosphorylation can occur *in cis* (autophosphorylation in each monomer) (66, 67) or *in trans* (each monomer forms a dimer, phosphorylates the other monomer) (68).

1.3.3 Cofactor for autokinase activity of histidine kinase

Kinases utilize metal cofactors in active sites to coordinate phosphate group binding, especially for those ATP-dependent enzymes. Cofactor performs the function as follow: (i) mediate to bind ATP in the catalytic pocket of enzyme; (ii) act as a Lewis acid with high charge density (69). Usually, autokinase activity of HK is Mg^{2+}-dependent. Mn^{2+} is a necessary for some HKs from plants and some serine/tyrosine kinases (70, 71). In bacteria, only histidine kinase FrzE from *Myxococcus xanthus* is known that it needs Mn^{2+} for autokinase activity (72).

1.3.4 Phosphoryl transfer

After HK is phosphorylated, the phosphoryl group will be transferred to a conversed aspartate residue on the RR, since the high-energy phosphoramidate bond is quite unstable. In this process, the RR interacts with DHp, CA domain and the linker between DHp and CA domain for phosphoryl transfer. For example, the HK:RR interface has some loose interactions between polar amino acids and overall poor surface complementarities, which will form slippery interfaces between HK and RR, providing enough space which allows some changes but without affecting binding capacity (66, 73, 74). Besides, RR can also interact with a loop that acts as an ATP cover (ATP-lid) for phosphoryl transfer, as observed in the *T. maritima* HK853:RR468 structure (66, 75).

1.3.5 Dephosphorylation of response regulator

In many cases, histidine kinase also functions as phosphatase to dephosphorylate the RR and stop the signaling transduction process (76). Dephosphorylation is caused by water molecule nucleophilic attack on the phosphoryl group of the RR (77). Up to now, four different RR phosphatase families were identified: CheC/CheX (78), CheZ (79), Rap (80) and Spo0E (81). The mechanisms of the first three families are similar even through the structures of those RRs are different. Those RR phosphatases insert an amide-side-chain amino acid into RR to mediate nucleophilic attack of a water molecule on the phosphoryl group (82). As for last family of RRs, lysine residue and acidic amino acids in RRs active center form a salt bridge for dephosphorylation (83).

1.3.6 LytS/LytTR-like two-component systems

TM domain harboring with at least 5 helices is a feature for LytS histidine kinase family (84). This domain is followed with a C-terminal intracellular GAF domain and a histidine catalysis domain. Instead, 5TM domain is combined with intracellular GGDEF (diguanylate cyclase catalytic) domains in the YhcK-type of protein, which belongs to 5TMR-LYT family (5 transmembrane receptors of the LytS-YhcK type). Signal peptide exists in all proteins of 5TMR-LYT family, which means there is topology similarity in 5TMR-LYT family and 7TMRs. N-terminus of these proteins is located towards periplasmic and C-terminus locates towards cytoplasm. There are some different features for the sequence of TM domain of 5TMR-LYT family, e.g., residues with small sized functional groups (glycine and proline) are always enriched in the

second helix, there is a glycine in the middle of helix-5 and an NXR motif in the loop connecting helix-1 and helix-2 (84).

RRs in LytTR family are characterized by a LytTR-like effector domain and a receiver domain. The effector domain consists of about 96 amino acids posing with different conformations based on the intracellular response, normally some LytR-type RRs have a 10-stranded ß-fold DNA-binding domain according to the predictions (32).

1.3.7 The BtsS/BtsR two-component system of *Escherichia coli*

There are 30 TCSs in *Escherichia coli*. BtsS/BtsR (85, 86) and YpdA/YpdB (87) [namely PyrS/PyrR (88)], are two LytS/LytTR-type systems. BtsS/BtsR is responsible for pyruvate sensing and it is broadly distributed in γ-proteobacteria (89, 90). The architecture of BtsS is composed with an input domain (5TMR_LYT domain (pfam07694) and cytoplasmic GAF domain, DHp domain and CA domain (86) (FIG 3). BtsR is the regulator belongs to LytR family. It consists of a Che-Y like receiver domain and a DNA-binding domain with 10-stranded ß-fold (91, 92). Previous studies found that BtsS is a sensor for pyruvate with high affinity (K_d =58.6 µM). After binding pyruvate, BtsS/BtsR will trigger the expression of *btsT*, which encodes another transporter for pyruvate and H^+ (93) (FIG 3). Expression of *btsT* is under regulated by the cyclic AMP (cAMP) receptor protein (CRP) (CRP-cAMP) (86) and carbon storage regulator A (CsrA) at the posttranscriptional level (94). Additionally, the transcription of btsT is positively regulated by YpdA/YpdB and YhjX (95).

Different bacteria have unequal numbers of TCSs for pyruvate sensing. *E. coli* has two different systems (BtsS/BtsR and PyrS/PyrR) and three pyruvate transporters (BtsT, YhjX and CstA) for pyruvate sensing (96). *Salmonella enterica* serovar Typhimurium has only one BtsS/BtsR system and two transporters (BtsT and CstA) (97) for pyruvate sensing. *Vibrio campbellii* has one BtsS/BtsR system and only transporter (BtsU) (98) for pyruvate sensing. These bacteria also behave differently in phenotypes when pyruvate sensing process is affected (99).
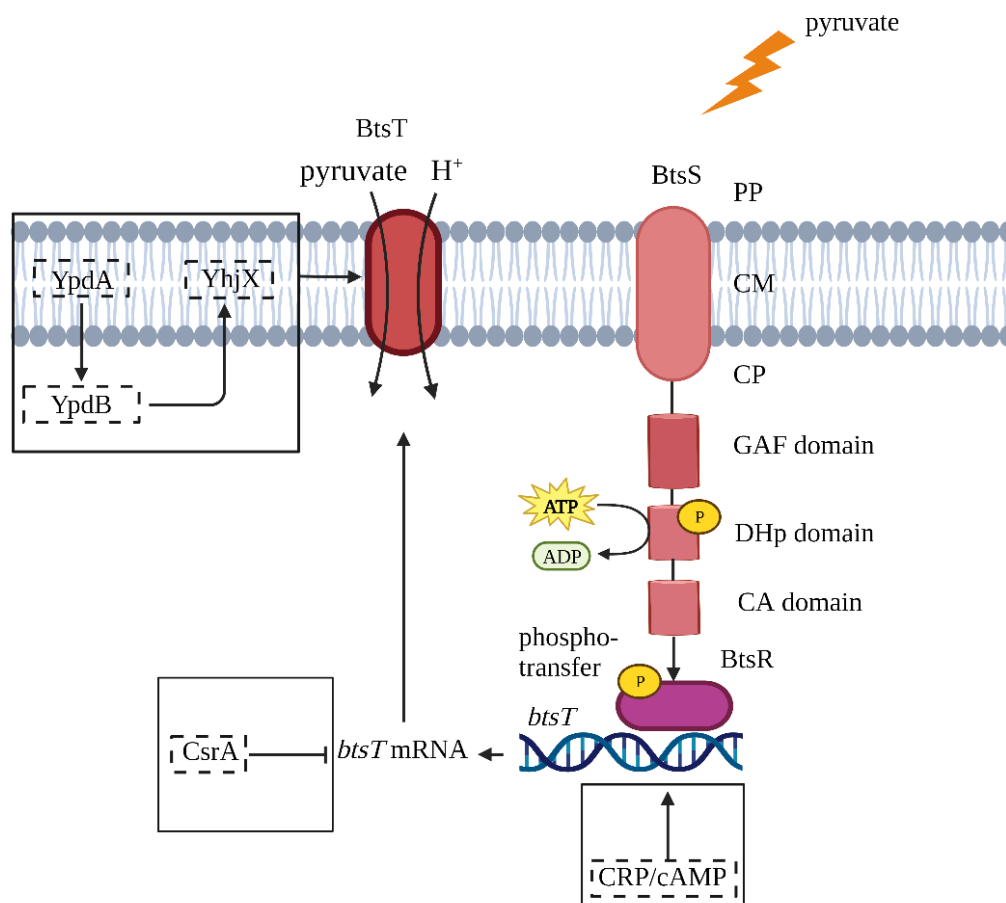
FIG 1.3 Two-component system BtsS/BtsR in *E. coli* for pyruvate sensing. BtsS is a 5TM LYT (LytS-YhcK) type histidine kinase has sensor, GAF, DHp and CA domains. BtsR consists of a CheY-like receiver domain and a LytTR-type DNA-binding domain. The phosphorylation sites are indicated (H, His; D, Asp). Expression of *btsT* is upregulated by YpdA/YpdB. It is also regulated by the cAMP/CRP complex and Csr regulatory circuit in transcriptional level. PP

- periplasm, CM - cytoplasmic membrane, CP - cytoplasm. Figure was cited from publication: Jin Qiu, Ana Gasperotti, Nathalie Sisattana, Martin Zacharias, and Kirsten Jung. The LytS-type histidine kinase BtsS is a 7-transmembrane receptor that binds pyruvate. mBio. doi: 10.1128/mbio.01089-23. Online ahead of print.

1.4 Lactate biosensor and its application

Lactate is quite a common product in the anaerobic metabolic pathway. It is used for monitoring of human health (100) and physical performance (101). In the absence of oxygen, lactate concentration increases and it is dangerous for life, such as lactate acidosis and respiratory failure (101, 102). Additionally, the concentration of lactate can also affect the flavor and quality of food (103). Thus, lactate level detection in a fast and accurate way is important for many application fields. It is also necessary to monitor lactate level of bacteria in biotechnological cultivation processes (102).

1.5 Scope of this thesis

BtsS/BtsR is one of LytS/LytTR-type HK/RR systems in *Escherichia coli* that can sense extracellular pyruvate. Upon perception of pyruvate, this system will activate *btsT* expression, which encodes another symporter for H^+ and pyruvate. But how a response is triggered by pyruvate binding on molecular level is still unknown. Determination of which amino acids form pyruvate binding pocket in BtsS and how pyruvate binding affects the signaling transduction are the targets of this thesis, as well as convertion the BtsS into a lactate sensor.

To answer questions for the first part, BtsS sequence was analyzed and model was predicted by Alphafold2.0. Location of BtsS N-terminus was determined by fusion expression with MalE. By performaing alanine scanning mutagenesis and differential radial capillary action of ligand assay, four amino acids were identified to form pyruvate binding site. Interactions between BtsS and pyruvate was further explained by the auto docking. Their effects on autophosphorylation was

clarified. BtsS was found to prefer Mn^{2+}-ATP instead of Mg^{2+}-ATP. BtsS dimerization was also detected *in vivo*.

Besides, it was clarified BtsS-Ser25, located on the first helix, kept the BtsS in an ON state after replaced with alanine or valine. BtsS-Arg192, located on the seventh helix, affected the *btsT* expression by preventing interaction between BtsS and BtsR. BtsS-Cys15, located on the first helix, is likely involved in the formation of a disulfide bridge, but this is not essential for signal transduction *in vivo* under the conditions tested.

The second part of this thesis was to convert BtsS into a lactate sensor. Two strategies were applied: site-directed mutagenesis and random mutagenesis. First, variants BtsS-E117Q/R72E and BtsS-E151Q/Q154E were constructed since hydroxyl group of lactate requires a strong H-bond acceptor meanwhile to maintain the environment for binding. But neither of them showed lactate response activity (see [results]). Besides, two good error-prone PCR conditions were set up with suitable mutation ratio. The condition can also be used for other proteins engineering.

2 Materials and Methods

2.1 Materials

2.1.1 Chemicals

Table 1 Chemicals used in this thesis

Material	Manufacturer
Acetic acid	Carl Roth, Germany
Agarose	Serva, Germany Roth, Germany
Arabinose	Roth, Germany
Ammonium Persulfate (APS)	Roth, Germany
Ampicillin	Roth, Germany
Alanine	Sigma-Aldrich, Germany

Aspartate	Sigma-Aldrich, Germany
Asparagine	Sigma-Aldrich, Germany
Arginine	Sigma-Aldrich, Germany
Bovine serum Albumin (BSA)	Sigma-Aldrich, Germany
Copper sulfate	Sigma-Aldrich, Germany
Chloroform	Roth, Germany
Color Prestained Protein Standard	New England Biolabs, Germany
Dodecyl-beta-D-maltosid (DDM)	Sigma-Aldrich, Germany
Dithiothreitol (DTT)	Sigma-Aldrich, Germany
DNA oligonucleotides	Sigma-Aldrich, Germany
DNA standard (2-Log DNA-Ladder)	New England Biolabs, Germany
dNTPs (deoxynucleotide triphosphates)	Invitrogen, Germany
First anti-mouse Flag-tag antibody	Thermo Fisher, USA
First anti-mouse His-tag antibody	Thermo Fisher, USA
Fructose	Sigma-Aldrich, Germany
Folin-Ciocalteus Phenol	Merck, Germany
Gamma-^{32}P-ATP	Hartmann Analytic GmbH, Germany
Glucose	Roth, Germany
Glycerol	Roth, Germany
Glycine	Sigma-Aldrich, Germany
Gentamycin	Roth, Germany
Hi Yield Plasmid Mini Kit	Süd-Laborbedarf GmbH, Germany
Hi Yield PCR Clean-Up & Gel-Extraction Kit	Süd-Laborbedarf GmbH, Germany
Imidazole	Roth, Germany
Iodine	Sigma-Aldrich, Germany
Isopropyl-β-D-thiogalactopyranoside (IPTG)	Roth, Germany
Kanamycin	Roth, Germany
L-lactate	Roth, Germany
Lysine	Sigma-Aldrich, Germany
Maltose	Roth, Germany

Magnesium chloride	Sigma-Aldrich, Germany
Manganese chloride	Sigma-Aldrich, Germany
Mannose	Sigma-Aldrich, Germany
N, N, N′, N′-Tetramethylethylenediamine	Roth, Germany
Nitrocellulose membrane	GE Healthcare, Germany
PCRBIO VeriFi™ Polymerase	PCR Biosystems, UK
Potassium chloride	Sigma-Aldrich, Germany
Potassium sodium tartrate	Sigma-Aldrich, Germany
Pyruvate	Roth, Germany
Q5 High-Fidelity DNA Polymerase	New England Biolabs, Germany
Q5 site-directed Mutagenesis Kit	New England Biolabs, Germany
Restriction Nuclease	New England Biolabs, Germany
Serine	Sigma-Aldrich, Germany
Sodium chloride	Roth, Germany
Sodium carbonate	Sigma-Aldrich, Germany
Sodium dodecyl sulphate (SDS)	Roth, Germany
Sodium-Deoxycholate	Sigma-Aldrich, Germany
Secondary anti-mouse antibody conjugated to alkaline phosphatase	Thermo Fisher, USA
Succinate	Roth, Germany
Taq DNA Polymerase	New England Biolabs, Germany
Tryptone	Sigma-Aldrich, Germany
T4-DNA ligase	New England Biolabs, Germany
Trichloroacetic acid	Sigma-Aldrich, Germany
Tris (hydroxymethyl) aminomethane	Sigma-Aldrich, Germany
$(1,10\text{-phenanthroline})_3$	Sigma-Aldrich, Germany
Tris (2-carboxyethyl) phosphine hydrochloride	Sigma-Aldrich, Germany
Yeast extract	Sigma-Aldrich, Germany
$3\text{-}^{14}C$ pyruvate	Biotrend, Germany

2.1.2 Primers

Table 2 Primers used in this thesis

Primer	Sequence from 5' to 3'	T_m (°C)
R72H-F	TGCCAATACCCATGCGATAGGCG	68
R72H-R	ATAGAATCGTCAATGTGCAACCCAAAC	69
R72E-F	TGCCAATACCGAAGCGATAGGCG	58
R72E-R	ATAGAATCGTCAATGTGC	62
R72Q-F	TGCCAATACCCAAGCGATAGGCG	61
R72Q-R	ATAGAATCGTCAATGTGCAAC	58
R72K-F	TGCCAATACCAAGGCGATAGGCG	57
R72K-R	ATAGAATCGTCAATGTGC	62
R99H-F	GGCTTACATCACTATTCGATGGGGGGCATGACC	69
R99H-R	GCCGGTCAGCCCAACCAG	67
R99E-F	CGGCTTACATGAATATTCGATGGGGGGC	70
R99E-R	CCGGTCAGCCCAACCAGC	68
R99Q-F	GGCTTACATCAGTATTCGATGGGGGGCATGACC	68
R99Q-R	GCCGGTCAGCCCAACCAG	67
R99K-F	CGGCTTACATGAATATTCGATGGGGGGC	70
R99K-R	CCGGTCAGCCCAACCAGC	68
C110G-F	CGCGTTAAGTGGCATGATCTCG	65
C110G-R	GTCATGCCCCCCATCGAA	63
C110S-F	GCGTTAAGTTCCATGATCTCGACCATC	66
C110S-R	GGTCATGCCCCCCATCGA	63
C110V-F	CGCGTTAAGTGTCATGATCTCGACCATC	65
C110V-R	GTCATGCCCCCCATCGAA	63
S113T-F	TTGCATGATCACGACCATCGTTG	64
S113T-R	CTTAACGCGGTCATGCCC	62
S113V-F	TTGCATGATCGTGACCATCGTTGAAGGATTAC	63
S113V-R	CTTAACGCGGTCATGCCC	62
S113G-F	TTGCATGATCGGGACCATCGTTGAAGGATTAC	64
S113G-R	CTTAACGCGGTCATGCCC	62
T114S-F	ATGATCTCGAGCATCGTTGAAG	62

T114S-R	GCAACTTAACGCGGTCAT	58
T114V-F	CATGATCTCGGTCATCGTTGAAGG	61
T114V-R	CAACTTAACGCGGTCATG	58
T114G-F	CATGATCTCGGGCATCGTTGAAGG	63
T114G-R	CAACTTAACGCGGTCATG	58
R192H-F	CTGTTTATGCATATATTGCTCGATAAACGCGCG	71
R192H-R	CGCCGCGCCGACGGTATT	71
R192Q-F	CTGTTTATGCAGATATTGCTCGATAAACGCGCG ATGTTTGAAAAATAC	72
R192Q-R	CGCCGCGCCGACGGTATT	71
R192K-F	GCTGTTTATGAAGATATTGCTCGATAAACGCGC GATG	69
R192K-R	GCCGCGCCGACGGTATTG	71
R192E-F	CTGTTTATGCAGATATTGCTCGATAAACGCGCG ATGTTTGAAAAATAC	72
R192E-R	CGCCGCGCCGACGGTATT	69
S25T-F	ATGGTTAATGTGTAAAACGCC	56
S25T-R	GCAATGACTAAAAAAACGC	57
S25V-F	ATGGTTAATGGTTAAAACGCCATTATTCATAC	55
S25V-R	GCAATGACTAAAAAAACGC	57
S25W-F	ATGGTTAATGTGGAAAACGCCATTATTC	60
S25W-R	GCAATGACTAAAAAAACGC	57
R192E-F	CTGTTTATGCATATTGCTCGATAAACGCGCGAT GTTTGAAAAATAC	71
R192E-R	CGCCGCGCCGACGGTATT	65
C15A-F	TCAGCAGATGGCCGTTTTTTTAGTCATTGCATG	64
C15A-R	AGCAGCAGCAACACCAGA	60
C15S-F	TCAGCAGATGAGCGTTTTTTTAGTCATTG	65
C15S-R	AGCAGCAGCAACACCAGA	60
C15E-F	TCAGCAGATGGAAGTTTTTTTAGTCATTGCATG GTTAAG	63

C15E-R	AGCAGCAGCAACACCAGA	60
C15D-F	TCAGCAGATGGACGTTTTTTAGTCATTGCATG	65
C15D-R	AGCAGCAGCAACACCAGA	60
C15K-F	TCAGCAGATGAAGGTTTTTTAGTCATTGCATGG	63
C15K-R	AGCAGCAGCAACACCAGA	60
E117Q-F	GACCATCGTTCAAGGATTACTC	59
E117Q-R	GAGATCATGCAACTTAACG	59
E151Q-F	GTTCGTCGCTCAAATGGTGCAAATGCTG	68
E151Q-R	GTGACGGCACCGGCGGTA	62
Q154E-F	TGAAATGGTGGAAATGCTGATCATCCTTG	71
Q154E-R	GCGACGAACGTGACGGCA	66
R72A-F	TGCCAATACCGCCGCGATAGGCG	57
R72A-R	ATAGAATCGTCAATGTGC	55
R99A-F	CGGCTTACATGCATATTCGATGGGGGG	66
R99A-R	CCGGTCAGCCCAACCAGC	68
C110A-F	CGCGTTAAGTGCCATGATCTCGACCATC	65
C110A-R	GTCATGCCCCCCATCGAA	63
S113A-F	TTGCATGATCGCGACCATCGTTG	66
S113A-R	CTTAACGCGGTCATGCCC	61
T114A-F	CATGATCTCGGCCATCGTTGA	62
T114A-R	CAACTTAACGCGGTCATG	60
R192A-F	GCTGTTTATGGCTATATTGCTCGATAAACGCGGATGTTTGAAAAATACAC	70
R192A-R	GCCGCGCCGACGGTATTG	65
S25A-F	ATGGTTAATGGCAAAAACGCCATTATTC	60
S25A-R	GCAATGACTAAAAAAACGC	56
K26A-F	GTTAATGAGTGCAACGCCATTATTC	56
K26A-R	CATGCAATGACTAAAAAAACG	58
K26R-F	GTTAATGAGTCGAACGCCATTATTC	56
K26R-R	CATGCAATGACTAAAAAAACG	58
K43A-F	TCTGCCGCATGCATTTCTCTGC	61

K43A-R	CGAACCGTGACCTGCATT	62
K43R-F	TCTGCCGCATCGATTTCTCTGC	61
K43R-R	CGAACCGTGACCTGCATT	62
R39H-F	GTCACGGTTCATCTGCCGCAT	63
R39H-R	CTGCATTAACGGTATGAATAATGG	60
R39E-F	GGTCACGGTTGAACTGCCGCATA	63
R39E-R	TGCATTAACGGTATGAATAATG	60
R39Q-F	GTCACGGTTCAGCTGCCGCATA	61
R39Q-R	CTGCATTAACGGTATGAATAATG	60
R39K-F	GGTCACGGTTAAACTGCCGCATA	61
R39K-R	TGCATTAACGGTATGAATAATG	60
T27A-F	AATGAGTAAAGCACCATTATTCATACCG	58
T27A-R	AACCATGCAATGACTAAAAAAC	56
T37A-F	AATGCAGGTCGCAGTTCGTCTGC	61
T37A-R	AACGGTATGAATAATGGCG	60
H42A-F	TCGTCTGCCGGCAAAATTTCTCTGCTAC	59
H42A-R	ACCGTGACCTGCATTAAC	56
T94A-F	GGTTGGGCTGGCAGGCGGCTTAC	72
T94A-R	AGCCCACCGACGACCGGA	68
H98A-F	CGGCGGCTTAGCACGATATTCGATGGGGGGC	72
H98A-R	GTCAGCCCAACCAGCCCA	68
Y100A-F	CTTACATCGAGCATCGATGGGGGGCATGACCGCGTTAAGTTG	72
Y100A-R	CCGCCGGTCAGCCCAACC	68
S101A-F	ACATCGATATGCAATGGGGGGCATGACCGC	66
S101A-R	AAGCCGCCGGTCAGCCCA	65
T106A-F	GGGGGGCATGGCAGCGTTAAGTT	66
T106A-R	ATCGAATATCGATGTAAGCCGC	65
N70A-F	TTCTATTGCCGCCACCCGTGCGATAG	62
N70A-R	TCGTCAATGTGCAACCCA	60
R72A-F	TGCCAATACCGCCGCGATAGGCG	57

R72A-R	ATAGAATCGTCAATGTGC	58
V86D-F	CGGCGGTCCGGACGTCGGTGGGC	72
V86D-R	AGTAAGCCGCCCATTACCGCGC	68
V86N-F	CGGCGGTCCGAACGTCGGTGGGC	72
V86N-R	AGTAAGCCGCCCATTACCGC	68
G96N-F	GCTGACCGGCAATTACATCGATATTCGATGGGG	68
G96N-R	CCAACCAGCCCACCGACG	66
G96E-F	GCTGACCGGCGAATTACATCGATATTCGATGG	68
G96E-R	CCAACCAGCCCACCGACG	66
G96D-F	GCTGACCGGCGATTTACATCGATATTCGATGG	69
G96D-R	CCAACCAGCCCACCGACG	66
R130A-F	CATCCTGATCGCCCGCGGGCGC	67
R130A-R	CTGTGTACCAGGCCACCG	65
R131A-F	CCTGATCCGCGCCGGGCGCACT	67
R131A-R	ATGCTGTGTACCAGGCCA	65
R133A-F	CCGCCGCGGGGCCACTGATAAA	62
R133A-R	ATCAGGATGCTGTGTACC	60
R192A-F	GCTGTTTATGGCTATATTGCTCGATAAACGCGCGATGTTTGAAAAATACAC	70
R192A-R	GCCGCGCCGACGGTATTG	68
R198A-F	GCTCGATAAAGCCGCGATGTTTGAAAAATAC	56
R198A-R	AATATACGCATAAACAGC	52
K136A-F	GCGCACTGATGCAGTCTTTAACCCCATTACC	69
K136A-R	CCGCGGCGGATCAGGATG	62
R131H-F	CTGATCCGCCACGGGCGCACT	70
R131H-R	GATGCTGTGTACCAGGCCAC	69
R131K-F	CCTGATCCGCAAGGGGCGCACTG	65
R131K-R	ATGCTGTGTACCAGGCCA	66
R131Q-F	CTGATCCGCCAGGGGCGCACTG	66
R131Q-R	GATGCTGTGTACCAGGCC	62

R131E-F	CCTGATCCGCGAGGGGCGCACTG	64
R131E-R	ATGCTGTGTACCAGGCCA	62
R198K-F	GCTCGATAAAAAGGCGATGTTTGAAAAATAC	56
R198K-R	AATATACGCATAAACAGC	54
R198H-F	CTCGATAAACACGCGATGTTTG	58
R198H-R	CAATATACGCATAAACAGC	56
R198Q-F	CTCGATAAACAGGCGATGTTTGAAAAATAC	58
R198Q-R	CAATATACGCATAAACAGC	56
R198E-F	GCTCGATAAAGAGGCGATGTTTGAAAAATAC	56
R198E-R	AATATACGCATAAACAGC	54
R133H-F	CGCCGCGGGCACACTGATAAA	66
R133H-R	GATCAGGATGCTGTGTACCAG	64
R133E-F	CCGCCGCGGGGAGACTGATAAAG	62
R133E-R	ATCAGGATGCTGTGTACC	60
R133K-F	CCGCCGCGGGAAAACTGATAAAG	62
R133K-R	ATCAGGATGCTGTGTACC	60
R133Q-F	CCGCCGCGGGCAAACTGATAAAG	65
R133Q-R	ATCAGGATGCTGTGTACCAG	60
K136H-F	GCGCACTGATCACGTCTTTAACCCCATTACC	66
K136H-R	CCGCGGCGGATCAGGATG	68
K136E-F	GCGCACTGATGAAGTCTTTAACCCC	68
K136E-R	CCGCGGCGGATCAGGATG	66
R136Q-F	GCGCACTGATCAAAGTCTTTAACCCCATTACC	68
R136Q-R	CCGCGGCGGATCAGGATG	66
malEc-pBAD24-btsSR-F	GGGCTAGCAGGAGGAATTCATGAAAATCGAAG AAGGTAAACTGG	57
malEc-pBAD24-btsSR-R	GCAACACCAGATTAAAATCGTACAT	59
pBAD24-malEc-btsSR-F	ATGTACGATTTTAATCTGGTGTTGC	58
pBAD24-malEc-btsSR-R	CCAGTTTACCTTCTTCGATTTTCATGAATTCCTC CTGCTAGCCC	59

malEp-pBAD24-btsSR-F	GGGCTAGCAGGAGGAATTCATGAAATAAAAAC AGGTGCACGC	60
malEp-pBAD24-btsSR-R	GCAACACCAGATTAAAATCGTACAT	58
pBAD24-malEp-btsSR-F	ATGTACGATTTTAATCTGGTGTTGC	59
pBAD24-malEp-btsSR-R	GCGTGCACCTGTTTTATTTTCATGAATTCCTCCT GCTAGCCC	59
btsS-pUT18-F	TGCCTGCAGGTCGACTCTAGAATGTACGATTTT AATCTGGTGTTG	56
btsS-pUT18-R	AATTCGAGCTCGGTACCCGGGGATCGTGGTGGT GGTGGTGGTG	58
pUT18-btsS-F	CACCACCACCACCACCACGATCCCCGGGTACCG AGCT	62
pUT18-btsS-R	CCAGATTAAAATCGTACATTCTAGAGTCGACCT GCAGGCA	63
btsS-pUT25-F	GCTGCAGGGTCGACTCTAGAATGTACGATTTTA ATCTGGTGTTG	56
pUT25-btsS-R	GGTCGACTCTAGAATGTACGATTTTAATCTGG	58
R39A-F	GGTCACGGTTGCTCTGCCGCATAAATTTC	68
R39A-R	TGCATTAACGGTATGAATAATG	62
R99A-F	CGGCTTACATGCATATTCGATGGGGGG	68
R99A-R	CCGGTCAGCCCAACCAGC	62
R163A-F	TGCGATCGCCGCACCTTATGAAG	61
R163A-R	AGGATGATCAGCATTTGC	62
R190A-F	AGATGCGGTGGCTCTGGTGAGTAATATTGC	61
R190A-R	TCATAAGGTCGGGCGATC	62
IF	CTCACGAATTCTCATTTTTCTGCAAGAGTT	60
IR	AAGGATGATCAGCATTTGCACCATTTCA	56
VF	GCAGCAACACCAGATTAAAATCGTACAT	60
VR	GCCAATGATGGTCACCAATACCGTC	56

2.1.3 Strains and plasmids

Table 3 Strains and plasmid used in this thesis

Strain or plasmid	Genotype or description	Reference
E. coli strains		
DH5α	F⁻ λ⁻ *endA1 glnV44 thi-1 recA1 relA1 gyrA96 deoR nupG* φ80d *lacZ* ΔM15 Δ(*lacZYA-argF*) *U169 hsdR17*(r$_K^-$ m$_K^+$)	(104)
MG1655 Δ*btsSR*	F⁻ λ⁻ *ilvG rfb50 rph-1* Δ*btsSR*	(105)
MG1655 Δ*btsSR*Δ*ypdABC*	F⁻ λ⁻ *ilvG rfb50 rph-1* Δ*btsSR*Δ*ypdABC*	(98)
BTH101	F⁻ *cyaA-99 araD139 galE15 galK16 rpsL1 hsdR2 mcrA1 mcrB1*	(106)
TKR2000	Δ*kdpFABCDE trkA405 trkD1 atp706 nagA thi rha lacZ*	(107)
MM39	*araD lacI* Δ*U1269 malE*444, Str^r	(108)
Plasmids		
pBBR-*btsT-lux*	P$_{btsT}$-212/+88 cloned in the BamHI and EcoRI sites of pBBR1-MCS5-TT-RBS-*lux*; Gm^r	(105)
pBBR-*btsT-lacZ*	P$_{btsT}$-212/+88 cloned in the BamHI and EcoRI sites of pBBR1-MCS5-TT-RBS-*lacZ*; Gm^r	This work
pBAD24	Arabinose-inducible P$_{BAD}$ promoter, pBR322 ori; Amp^r	(109)
pBAD24-*btsS*-6His	*btsS*-6His cloned into the EcoRI and XbaI sites of pBAD24; Amp^r	(105)
pBAD24-*btsS*-S25A-6His	replacement of S25A in pBAD24-*btsS*-6Hi*s*; Amp^r	This work
pBAD24-*btsS*-R72A-6His	replacement of R72A in pBAD24-*btsS*-6Hi*s*; Amp^r	This work
pBAD24-*btsS*-R99A-6His	replacement of R99A in pBAD24-*btsS*-6Hi*s*; Amp^r	This work
pBAD24-*btsS*-C110A-6His	replacement of C110A in pBAD24-*btsS*-6Hi*s*; Amp^r	This work
pBAD24-*btsS*-S113A-6His	replacement of S113A in pBAD24-*btsS*-6Hi*s*; Amp^r	This work
pBAD24-*btsS*-R192A-6His	replacement of R192A in pBAD24-*btsS*-6Hi*s*; Amp^r	This work
pBAD24-*btsS*-H382Q-6His	replacement of H382Q in pBAD24-*btsS*-6Hi*s*; Amp^r	(105)
pBAD24-*btsS/R*	*btsS*-Flag/*btsR*-6His cloned into the EcoRI and XbaI sites of pBAD24; Amp^r	This work
pBAD24-*btsS*-S25A/*btsR*	replacement of S25A in pBAD24-*btsS/R*; Amp^r	This work
pBAD24-*btsS*-S25W/*btsR*	replacement of S25W in pBAD24-*btsS/R*; Amp^r	This work
pBAD24-*btsS*-S25T/*btsR*	replacement of S25T in pBAD24-*btsS/R*; Amp^r	This work
pBAD24-*btsS*-S25V/*btsR*	replacement of S25V in pBAD24-*btsS/R*; Amp^r	This work
pBAD24-*btsS*-K26A/*btsR*	replacement of K26A in pBAD24-*btsS/R*; Amp^r	This work
pBAD24-*btsS*-K26R/*btsR*	replacement of K26R in pBAD24-*btsS/R*; Amp^r	This work
pBAD24-*btsS*-K26H/*btsR*	replacement of K26H in pBAD24-*btsS/R*; Amp^r	This work
pBAD24-*btsS*-K26E/*btsR*	replacement of K26E in pBAD24-*btsS/R*; Amp^r	This work
pBAD24-*btsS*-R39A/*btsR*	replacement of R39A in pBAD24-*btsS/R*; Amp^r	This work

pBAD24-*btsS*-R39K/*btsR*	replacement of R39K in pBAD24-*btsS/R*; Amp^r	This work
pBAD24-*btsS*-R39H/*btsR*	replacement of R39H in pBAD24-*btsS/R*; Amp^r	This work
pBAD24-*btsS*-K43A/*btsR*	replacement of K43A in pBAD24-*btsS/R*; Amp^r	This work
pBAD24-*btsS*-R72A/*btsR*	replacement of R72A in pBAD24-*btsS/R*; Amp^r	This work
pBAD24-*btsS*-R72E/*btsR*	replacement of R72E in pBAD24-*btsS/R*; Amp^r	This work
pBAD24-*btsS*-R72H/*btsR*	replacement of R72H in pBAD24-*btsS/R*; Amp^r	This work
pBAD24-*btsS*-R72K/*btsR*	replacement of R72K in pBAD24-*btsS/R*; Amp^r	This work
pBAD24-*btsS*-R72Q/*btsR*	replacement of R72Q in pBAD24-*btsS/R*; Amp^r	This work
pBAD24-*btsS*-R99A/*btsR*	replacement of R99A in pBAD24-*btsS/R*; Amp^r	This work
pBAD24-*btsS*-R99E/*btsR*	replacement of R99E in pBAD24-*btsS/R*; Amp^r	This work
pBAD24-*btsS*-R99Q/*btsR*	replacement of R99Q in pBAD24-*btsS/R*; Amp^r	This work
pBAD24-*btsS*-R99H/*btsR*	replacement of R99H in pBAD24-*btsS/R*; Amp^r	This work
pBAD24-*btsS*-R99K/*btsR*	replacement of R99K in pBAD24-*btsS/R*; Amp^r	This work
pBAD24-*btsS*-C110A/*btsR*	replacement of C110A in pBAD24-*btsS/R*; Amp^r	This work
pBAD24-*btsS*-C110V/*btsR*	replacement of C110V in pBAD24-*btsS/R*; Amp^r	This work
pBAD24-*btsS*-C110G/*btsR*	replacement of C110G in pBAD24-*btsS/R*; Amp^r	This work
pBAD24-*btsS*-C110S/*btsR*	replacement of C110S in pBAD24-*btsS/R*; Amp^r	This work
pBAD24-*btsS*-S113A/*btsR*	replacement of S113A in pBAD24-*btsS/R*; Amp^r	This work
pBAD24-*btsS*-S113T/*btsR*	replacement of S113T in pBAD24-*btsS/R*; Amp^r	This work
pBAD24-*btsS*-S113V/*btsR*	replacement of S113V in pBAD24-*btsS/R*; Amp^r	This work
pBAD24-*btsS*-S113G/*btsR*	replacement of S113G in pBAD24-*btsS/R*; Amp^r	This work
pBAD24-*btsS*-T114A/*btsR*	replacement of T114A in pBAD24-*btsS/R*; Amp^r	This work
pBAD24-*btsS*-T114V/*btsR*	replacement of T114V in pBAD24-*btsS/R*; Amp^r	This work
pBAD24-*btsS*-T114G/*btsR*	replacement of T114G in pBAD24-*btsS/R*; Amp^r	This work
pBAD24-*btsS*-T114S/*btsR*	replacement of T114S in pBAD24-*btsS/R*; Amp^r	This work
pBAD24-*btsS*-R130A/*btsR*	replacement of R130A in pBAD24-*btsS/R*; Amp^r	This work
pBAD24-*btsS*-R131A/*btsR*	replacement of R131A in pBAD24-*btsS/R*; Amp^r	This work
pBAD24-*btsS*-R131E/*btsR*	replacement of R131E in pBAD24-*btsS/R*; Amp^r	This work
pBAD24-*btsS*-R131Q/*btsR*	replacement of R131Q in pBAD24-*btsS/R*; Amp^r	This work
pBAD24-*btsS*-R133A/*btsR*	replacement of R133A in pBAD24-*btsS/R*; Amp^r	This work

pBAD24-*btsS*-K136A/*btsR*	replacement of K136A in pBAD24-*btsS/R*; Amp[r]	This work
pBAD24-*btsS*-R163A/*btsR*	replacement of R163A in pBAD24-*btsS/R*; Amp[r]	This work
pBAD24-*btsS*-R170A/*btsR*	replacement of R170A in pBAD24-*btsS/R*; Amp[r]	This work
pBAD24-*btsS*-R192A/*btsR*	replacement of R192A in pBAD24-*btsS/R*; Amp[r]	This work
pBAD24-*btsS*-R192H/*btsR*	replacement of R192H in pBAD24-*btsS/R*; Amp[r]	This work
pBAD24-*btsS*-R192K/*btsR*	replacement of R192K in pBAD24-*btsS/R*; Amp[r]	This work
pBAD24-*btsS*-R192Q/*btsR*	replacement of R192Q in pBAD24-*btsS/R*; Amp[r]	This work
pBAD24-*btsS*-R197A/*btsR*	replacement of R197A in pBAD24-*btsS/R*; Amp[r]	This work
pBAD24-*btsS*-R198A/*btsR*	replacement of R198A in pBAD24-*btsS/R*; Amp[r]	This work
pBAD24-*btsS*-N70A/*btsR*	replacement of N70A in pBAD24-*btsS/R*; Amp[r]	This work
pBAD24-*btsS*-T71A/*btsR*	replacement of T71A in pBAD24-*btsS/R*; Amp[r]	This work
pBAD24-*btsS*-T94A/*btsR*	replacement of T94A in pBAD24-*btsS/R*; Amp[r]	This work
pBAD24-*btsS*-Y100A/*btsR*	replacement of Y100A in pBAD24-*btsS/R*; Amp[r]	This work
pBAD24-*btsS*-S101A/*btsR*	replacement of S101A in pBAD24-*btsS/R*; Amp[r]	This work
pBAD24-*btsS*-T106A/*btsR*	replacement of T106A in pBAD24-*btsS/R*; Amp[r]	This work
pBAD24-*btsS*-E151Q/Q154E/*btsR*	replacement of E151Q/Q154E in pBAD24-*btsS/R*; Amp[r]	This work
pBAD24-*btsS*-E117Q/R72E/*btsR*	replacement of E117Q/R72E in pBAD24-*btsS/R*; Amp[r]	This work
pKT25N	vector of the bacterial two-hybrid system. Carries T25 fragment (720 bp) of *cyaA*, Kan[r]	(106)
pUT18	vector of the bacterial two-hybrid system. Carries T15 fragment ((616 bp) of *cyaA*, Amp[r]	(111)
pUT18-*btsS*-6His	*btsS*-6His cloned in XbaI and BamHI sites of pUT18 resulting in C-terminal CyaA-T18-protein fusions, Kan[r]	This work
pKT25N-*btsS*-6His	*btsS*-6His cloned in XbaI and BamHI sites of pKT25N resulting in C-terminal CyaA-T25-protein fusions, Amp[r]	This work
pUT18-zip	Expression vector, Amp[r]	(106)
pKT25N-zip	Expression vector, Kan[r]	(106)
pUT18-*btsS*-S25A-6His	replacement of S25A in pUT18-*btsS*-6His; Amp[r]	This work
pUT18-*btsS*-R72A-6His	replacement of R72A in pUT18-*btsS*-6His; Amp[r]	This work

pUT18-*btsS*-R99A-6His	replacement of R99A in pUT18-*btsS*-6His; Amp[r]	This work
pUT18-*btsS*-C110A-6His	replacement of C110A in pUT18-*btsS*-6His; Amp[r]	This work
pUT18-*btsS*-S113A-6His	replacement of S113A in pUT18-*btsS*-6His; Amp[r]	This work
pUT18-*btsS*-T114A-6His	replacement of S113A in pUT18-*btsS*-6His; Amp[r]	This work
pBAD24-*btsS*-S25A-6His	replacement of S25A in pKT25N-*btsS*-6His; Kan[r]	This work
pKT25N-*btsS*-R72A-6His	replacement of R72A in pKT25N-*btsS*-6His; Kan[r]	This work
pKT25N-*btsS*-R99A-6His	replacement of R99A in pKT25N-*btsS*-6His; Kan[r]	This work
pKT25N-*btsS*-C110A-6His	replacement of C110A in pKT25N-*btsS*-6His; Kan[r]	This work
pKT25N-*btsS*-S113A-6His	replacement of S113A in pKT25N-*btsS*-6His; Kan[r]	This work
pKT25N-*btsS*-T114A-6His	replacement of S113A in pKT25N-*btsS*-6His; Kan[r]	This work
pMAL-p2X	Expression vector encoding MBP, Amp[r]	New England Biolabs
pMAL-c2X	Expression vector, encoding MBP without signal peptide, Amp[r]	New England Biolabs
pMALp-*btsS*	*btsS* cloned in BamHI and HindIII sites of pMAL-p2X resulting in the fusion of MalEp to the N-terminus of BtsS, Amp[r]	This work
pMALc-*btsS*	*btsS* cloned in BamHI and HindIII sites of pMAL-c2X resulting in the fusion of MalEc to the N-terminus of BtsS, Amp[r]	This work
pBAD24-pMALp-*btsS/R*	*malE*p-*btsS/R* cloned into the EcoRI and XbaI sites of pBAD24; Amp[r]	This work
pBAD24-pMALc-*btsS/R*	*malE*c-*btsS/R* cloned into the EcoRI and XbaI sites of pBAD24; Amp[r]	This work
pBAD24-*btsS/R*-RM	Random mutagenesis for BtsS transmembrane domain in pBAD24-*btsS/R*; Amp[r]	This work

2.2 Methods

2.2.1 Construction of *btsS* variants

All the variants were constructed using the Q5 site-directed mutagenesis kit (New England

BioLabs) or following the prolonged overlap extension PCR (POE-PCR) protocols (110) , in which

epPCR for BtsS transmembrane domain gene amplification was performed with Taq DNA polymerase. A HiYield plasmid mini kit (Suedlaborbedarf) was used for plasmid DNAs isolation. DNA fragments were purified from agarose gels using a HiYield PCR cleanup and gel extraction kit (Suedlaborbedarf). Restriction enzymes were purchased from company New England BioLabs and used according to the protocol.

2.2.2 Use of MalE as reporter protein for BtsS N-terminus location determination

Cited from publication: Jin Qiu, Ana Gasperotti, Nathalie Sisattana, Martin Zacharias, and Kirsten Jung. The LytS-type HK BtsS is a 7-transmembrane receptor that binds pyruvate. mBio. doi: 10.1128/mbio.01089-23. Online ahead of print.

E. coli MM39 was transformed with plasmid pMAL-c2X, pMAL-p2X, pMALc-*btsS* or pMALp-*btsS*. Cells were plated and incubated on LB agar plates supplemented with antibiotics ampicillin (100 µg/ml) and streptomycin (50 µg/ml). Positive control *E. coli* MG1655 and negative cintrol MM39 were also streaked on LB agar plates. Single colony were re-streaked on M9 minimal medium agar plates supplemented with 0.1% (w/v) maltose and incubated for 36 h at 37°C (108).

The *in vivo* expression of *btsT* triggered by BtsS/BtsR was measured (85). *E. coli* MG1655Δ*btsSR* was co-transformed with pBBR-*btsT-lux* and pBAD24-pMALp-*btsS/R* or pBAD24-pMALc-*btsS/R* or pBAD24-*btsS/R* (positive control) or pBAD24 (negative control) at the same time. Cells were transferred after overnight inoculation from LB medium to M9 minimal medium containing 5 mM pyruvate, L-lactate and succinate, respectively, supplemented with 15 mM succinate and incubated in a plate reader (BMG Labtech CLARIOstar, Germany) at 37°C. OD_{600} for growth and luminescence were detected continuously. Luminescence was determined as relative light units (RLU counts s^{-1}) related to the OD_{600}.

2.2.3 *In vivo* signal transduction assay of BtsS

E. coli MG1655Δ*btsSR* was co-transformed with pBBR-*btsT-lux* and pBAD24-*btsS*/*R* or pBBR-*btsT-lux* and pBAD24-*btsS*/*R* variants. Colony was inoculated in 5 mL LB medium with antibiotics (50 µg/ml gentamycin and100 µg/ml ampicillin) after overnight incubation and cells were grown at 37 °C until OD_{600} reached 0.05. Then they were transferred to M9 minimal medium containing 5 mM pyruvate or succinate or lactate (supplymented with 15 mM succinate to have a 20 mM whole carbon concentration) and incubated at 37 °C. Luminescence and growth (OD_{600}) were assayed every 10 min in a luminescence reader (BMG Labtech CLARIOstar, Germany). Using the same protocol, pyruvate concentration dependency for *btsT* expression was tested by using 5 mM, 10 mM, 20 mM and 50 mM pyruvate as the C source. The total carbon concentration was kept constant at 50 mM by adding succinate. Additionally, overnight incubated cells were transferred to 0.1x LB medium and after 1 h (time point 0) incubation and different concentrations of pyruvate were added (111). Luminescence were determined for each condition and were calculated as RLU in counts per second per OD_{600}. Flag-tagged BtsS or variants were detected by Western blot using an anti-Flag primary antibody and a secondary anti-mouse antibody conjugated to alkaline phosphatase (Thermo Fisher, USA).

2.2.4 Overproduction and purification of BtsS-6His and BtsS-S25A-6His

E. coli TKR2000 was transformed with pBAD24-*btsS*-6His or pBAD24-*btsS*-S25A-6His. After inoculation in KML medium [0.5% (w/v) yeast extract, 1% (w/v) tryptone and [1% (w/v) KCl] (OD_{600}=0.05), cells were grown at 37°C to an OD_{600} of 0.5 and induced by the addition of 0.2% (w/v) arabinose for overproduction. Cells were harvested after 3 hours of induction and then collected with centrifugation with the speed of 5 000 rpm for 20 min. Cells were lysed with buffer

20 mM Tris HCl, pH 8.0, 250 mM NaCl, 1 mM DTT and 10% glycerol. The pellet was solubilized by adding 1.5% (w/v) DDM in the same buffer and incubation for 30 min at 4 °C. Supernatant was collected after ultracentrifugation conditions. BtsS-6His and BtsS-S25A-6His was purified with Ni-NTA affinity purification. Resins were equilibrated with 30 mM imidazole, 20 mM Tris HCl, pH 8.0, 250 mM NaCl, 1 mM DTT, 10% glycerol and 0.02% (w/v) DDM. Protein was eluted with elution buffer which component was the same as above but with 100 mM, 200 mM, 300 mM or 500 mM imidazole. Every fraction was collected and checked by SDS-PAGE.

2.2.5 Nano differential scanning fluorimetry assay for BtsS-6His and BtsS-S25A-6His

Nano differential scanning fluorimetry (NanoDSF) was performed using Prometheus NT.48 equipped with backreflection mode (NanoTemper Technologies, München, Germany). 2.5 mg/ml purified BtsS-6His or BtsS-S25A-6His were mixed with 0 mM, 0.5 mM, 1 mM, 10 mM, 50 mM or 250 mM pyruvate and lactate, then loaded in nanoDSF grade standard capillaries (NanoTemper Technologies GmbH, München, Germany) and exposed at thermal stress from 40 °C to 80 °C by thermal ramping rate of 1.5 °C/min. Fluorescence emission from tryptophan after UV excitation at 280 nm was collected at 330 nm and 350 nm with dual-UV detector. Thermal stability parameter melting temperature, T_m, was calculated with ThermControl software (NanoTemper Technologies, München, Germany).

2.2.6 Autokinase assay

E. coli TKR2000 was transformed with pBAD24-*btsS*-6His or variants and cells were inoculated with KML medium supplemented with 100 µg/ml ampicillin. 0.2% (w/v) arabinose was added when OD_{600} reached 0.5 and cells were inoculated at 18 °C overnight. Cells were harvested by centrifugation with speed of 5 000 rpm and membrane vesicles were prepared as described (112). Membrane vesicles of 2 mg protein/ml containing BtsS or variants were incubated at 25 °C

in phosphorylation buffer [250 mM NaCl, 5 % glycerol (v/v), 25 mM Tris HCl, pH 7.5, 5 mM MgCl$_2$ or 5 mM MnCl$_2$, 2 mM DTT, 0 μM, 50 μM, 100 μM, 200 μM, 500 μM or 1 mM pyruvate]. Phosphorylation was initiated after adding 20 μM [γ-^{32}P] ATP (2.38 Ci/mmol). 20 μl aliquots were removed at corresponding time points and the reaction was stopped by mixing with 5 μl of 5-fold SDS sample buffer (113). To detect the kinase activity under oxidizing or reducing condition, Mn^{2+}-BtsS kinase activity assayed under reducing or oxidizing condition containing 5 mM Cu (II) (1,10-phenanthroline)$_3$, or 1 mM iodine or 10 mM TCEP mixed with BtsS in the presence of 5 mM Mn^{2+}. After incubation at 25 °C for 20 min, 20 μM [γ-^{32}P] ATP (2.38 Ci/mmol) was added. Reactions were stopped at the time indicated. All samples were checked by SDS-PAGE. Proteins were transferred to a nitrocellulose membrane, and phosphorylated proteins were detected by exposure of the membrane on a Storage Phosphor Screen. Phosphorylated proteins were quantified by image analysis using Image Quant® software (GE Healthcare, Freiburg, Germany). For each gel, a standard was loaded and set to 100 % (= 1), which was phosphorylated BtsS incubated in the presence of 50 μM pyruvate, 5 mM MnCl$_2$ for 5 min.

2.2.7 *In vivo* dimerization studies using bacterial adenylate cyclase two-hybrid assay

Cited from publication: Jin Qiu, Ana Gasperotti, Nathalie Sisattana, Martin Zacharias, and Kirsten Jung. The LytS-type histidine kinase BtsS is a 7-transmembrane receptor that binds pyruvate. mBio. doi: 10.1128/mbio.01089-23. Online ahead of print.

The bacterial adenylate cyclase two-hybrid assay (BACTH) was performed to test dimerization of BtsS and the variants *in vivo* (106). *E. coli* BTH101 was transformed with pKT25N and pUT18 derivatives. Leucine zipper protein dimerization was used as a positive control. Cells were incubated in LB medium supplemented with 0.5 mM IPTG overnight at 37 °C, and transferred to 0.1xLB medium (nutrient limitation) (114) plus 0.05 mM IPTG and the indicated pyruvate

concentrations. Cells were harvested until OD_{600} reached 0.3 to 0.35 and β-galactosidase activity was determined and expressed in Miller units (106). Production of BtsS hybrid proteins were detected by Western blot analysis using a monoclonal anti-His antibody and a secondary anti-mouse antibody conjugated to alkaline phosphatase (Thermo Fisher, USA).

2.2.8 Differential radial capillary action of ligand assay (DRaCALA)

Binding of pyruvate to BtsS was determined and quantified with differential radial capillary action of ligand assay (DRaCALA) (115) as previously described (111). *E. coli* MG1655 Δ*btsSR*Δ*ypdABC* was transformed with plasmids pBAD24 (negative control), pBAD24-*btsS*-6His (positive control), pBAD24-*btsS*-R72A-6His, pBAD24-*btsS*-R99A-6His, pBAD24-*btsS*-C110A-6His, pBAD24-*btsS*-S113A-6His. 15 µM radiolabeled (3-^{14}C) pyruvate (55 mCimmol^{-1}, Biotrend) was mixed with membrane vesicles containing control vesicles from empty vector (EV) or BtsS or variants and incubated for 20 min at room temperature. Triplicate 5-µl aliquots were loaded on a nitrocellulose membrane, dried, and visualized by a PhosphorImager. Radioactive signal intensities were quantified by using ImageJ. The equation $F_B=(I_{inner}-I_{background})/I_{total}$ was used to calculate fraction bound (F_B) (115). Increasing concentrations of cold pyruvate (0 µM to 500 µM) were added to the mixture to determine the K_d value. 50 mM cold pyruvate was also used and the fraction bound was assayed to reach the saturation. Competition efficiency (CE) was calculated as follows: $CE=(F_{B(NC)}-F_{B(pyr)})/F_{B(NC)}$. $F_{B(NC)}$ was calculated when there was no cold pyruvate, and $F_{B(pyr)}$ were values calculated from the samples containing a mixture of ^{14}C-pyruvate and different concentrations of cold pyruvate. The negative control value got from empty vector (EV) was subtracted for all F_B values. 25 mg/ml of membrane vesicle containing approximately 7% BtsS-

6His or variants was used in this experiment.

2.2.9 Structural modeling of BtsS in complex with pyruvate

AlphaFold2.0 was used to generate the structural model of a BtsS dimer and pyruvate docking was performed by using the best ranked model. In the model, the four residues Arg72, Arg99, Cys110 and Ser113 found critical for binding were forming part of a pocket of BtsS. Crystal structure of pyruvate formate-lyase in *E. coli* with bound pyruvate can be found in the PDB: 1MZO entry and the residues arrangement is similar to the geometry of BtsS. Pyruvate was first manually placed in the putative binding pocket in the BtsS model (close to the critical residues) based on 1MZO structure and it was used to derive the upper bound distance restraints between side chain of the four critical residues and pyruvate. An energy minimization (2500 steps) to remove sterical overlap in the start structure using the Amber20 molecular modeling package was performed for modeling and pyruvate docking. In the next step, Molecular Dynamics (MD) simulations were performed by employing an implicit Generalized Born solvent model (igb=5 option in Amber) and including positional restraints on all heavy atoms (force constant: 0.05 kcal mol^{-1}Å^{-2}) but not on the residues in close vicinity of the bound pyruvate. Besides, the distance restraints between these four critical residues in the binding region and pyruvate was included in the simulations. MD simulations were continued for 10 ns and resulted in a stable binding geometry that was again energy minimized for 2,500 steps to obtain a structural model of the complex.

2.2.10 Conversion BtsS into a lactate sensor by random mutagenesis

Random mutagenesis is a well applied strategy for directed evolution. To generate a variant

library, the template plasmid pBAD24-*btsS/R* was mutated by error-prone PCR (epPCR). DNA fragment gene *btsS*-TM (600 bp) encoding BtsS transmembrane domain was amplified using epPCR conditions as follows:10 mM Tris HCl, pH 8.3, 50 mM KCl, 100 pg, 200 pg and 500 pg template plasmid, 0.2 mM dATP, 0.2 mM dGTP, 1 mM dCTP, 1 mM dTTP, 5 mM $MgCl_2$, 0.4 mM, 1 mM and 2 mM $MnCl_2$, 0.05 U/µL Taq polymerase, 0.2 µM IF primer and 0.2 µM IR primer in a total volume of 50 µL. The PCR reaction was done according to the Taq polymerase amplification protocol. PCR products of vector backbone and insert fragment were cleaned up by using a HiYield PCR cleanup and gel extraction kit (Suedlaborbedarf). Vector backbone pBAD24-*btsS/R-rm* (6.5 kb, pBAD24 with *btsS/R* fragment except for *btsS*-TM gene) was amplified with VF and VR primers using a Q5 high-fidelity polymerase and PCR condition was as follows: 98 °C denaturation, 30 s; 30 cycles of 98 °C denaturation, 30 s, 60°C annealing, 30 s, extension at 72 °C, 3 min; and 2-min extension at 72 °C. To generate the DNA multimers by POE-PCR, the PCR solution was prepared as follows: 1× Q5 buffer, 0.2 mM dNTP mixtures, 5 ng/µL vector pBAD24-*btsS/R-rm*, equimolar amount of DNA fragment *btsS*-TM gene and 0.02 U/µL Q5 DNA polymerase. POE-PCR was conducted as follows: 98 °C denaturation, 30 s; 30 cycles of 98 °C denaturation, 30 s, 60°C annealing 30 s, extension at 72 °C, 4 min; 2-min extension at 72 °C. *E. coli* DH5α was transformed with DNA multimers and 8 colonies were randomly picked and sequenced to check library diversity.

After the library was set up, the colonies on the plate were washed with LB medium. These cells were inoculated overnight at 37°C and the plasmids were extracted. MG1655Δ*btsSR*Δ*lacZ* was co-transformed with mixture of of pBAD24-*btsS/R*-RM and plasmid pBBR-*btsT-lacZ*, plating and incubating on LB-Agar medium. Colonies were re-streaked on M9 minimal medium agar plate supplemented with 50 mM lactate or pyruvate plus 50 µg/ml X-gal, then incubated at 37°C for 48 h to screen by the blue and white color. The mutants turn blue on the lactate plate but turns white

on pyruvate plate are the promising ones to be converted into a lactate biosensor.

3 Results

3.1 Pyruvate-sensing of BtsS/BtsR signaling cascade of *Escherichia coli*

3.1.1 Periplasmic location of the N-terminus of BtsS

BtsS is a LytS-type HK. 5TMR-LYT domain is a feature for proteins in the LytS-type family, suggesting that there are at least five transmembrane helices in BtsS TM domain. However, transmembrane helix formed by the first 36 amino acids of BtsS does not belong to this domain (FIG 3.1.1A). At the beginning of this study, two different models for the membrane topology of BtsS were found. Transmembrane helices prediction based on hydrophobicity [with software TMHMM-2.0 (116, 117), ProtScale (118) and PsiPred (119), (FIGs 3.1.1B-D)] predicted a BtsS model that has six transmembrane helices and the N-terminus was located towards the cytoplasm (FIG 3.1.2A, right panel, see below). Another model predicted by AlphaFold2.0 (120) showed BtsS has seven transmembrane helices and N-terminus is positioned to the periplasm (FIGs 3.1.2A, left panel, see below). AlphaFold2.0 produces a per-residue confidence score (pLDDT9) with a score from 0-100. This score was very high (>90) for most amino acids forming the transmembrane helices and connecting loops starting at amino acid Val47. For the N-terminal part, a confident score (90 > pLDDT > 70) was found. Therefore, it was necessary to experimentally determine the localization of the N-terminus.

A

BtsS

input domain | transmitter domain

36 aa | LytS-YhcK | G A F | DHp domain | CA domain

B

TMHMM posterior probabilities for WEBSEQUENCE

probability

1.2
1
0.8
0.6
0.4
0.2
0

100   200   300   400   500

transmembrane ——   inside ——   outside ——

C

ProtScale output for user_sequence

Hydropath. / Kyte & Doolittle ——

Score

3
2
1
0
-1
-2
-3

0   100   200   300   400   500

Position

D

```
          10          20          30          40          50
  1  M Y D F N L V L L L L Q Q M C V F L V I A W L M S K T P L F I P L M Q V T V R L P H K F L C Y I V F  50
 51  S I F C I M G T W F G L H I D D S I A N T R A I G A V M G G L L G G P V V G G L V G L T G G L H R Y  100
101  S M G G M T A L S C M I S T I V E G L L G G L V H S I L I R R G R T D K V F N P I T A G A V T F V A  150
151  E M V Q M L I I L A I A R P Y E D A V R L V S N I A A P M M V T N T V G A A L F M R I L L D K R A M  200
201  F E K Y T S A F S A T A L K V A A S T E G I L R Q G F N E V N S M K V A Q V L Y Q E L D I G A V A I  250
251  T D R E K L L A F T G I G D D H H L P G K P I S S T Y T L K A I E T G E V V Y A D G N E V P Y R C S  300
301  L H P Q C K L G S T L V I P L R G E N Q R V M G T I K L Y E A K N R L F S S I N R T L G E G I A Q L  350
351  L S A Q I L A G Q Y E R Q K A M L T Q S E I K L L H A Q V N P H F L F N A L N T I K A V I R R D S E  400
401  Q A S Q L V Q Y L S T F F R K N L K R P S E F V T L A D E I E H V N A Y L Q I E K A R F Q S R L Q V  450
451  N I A I P Q E L S Q Q Q L P A F T L Q P I V E N A I K H G T S Q L L D T G R V A I S A R R E G Q H L  500
501  M L E I E D N A G L Y Q P V T N A S G L G M N L V D K R L R E R F G D D Y G I S V A C E P D S Y T R  550
551  I T L R L P W R D E A                                                                                561
          10          20          30          40          50
```

Strand | Helix | Coil | Disordered
Disordered, protein binding | Putative Domain Boundary | Membrane Interaction | Transmembrane Helix
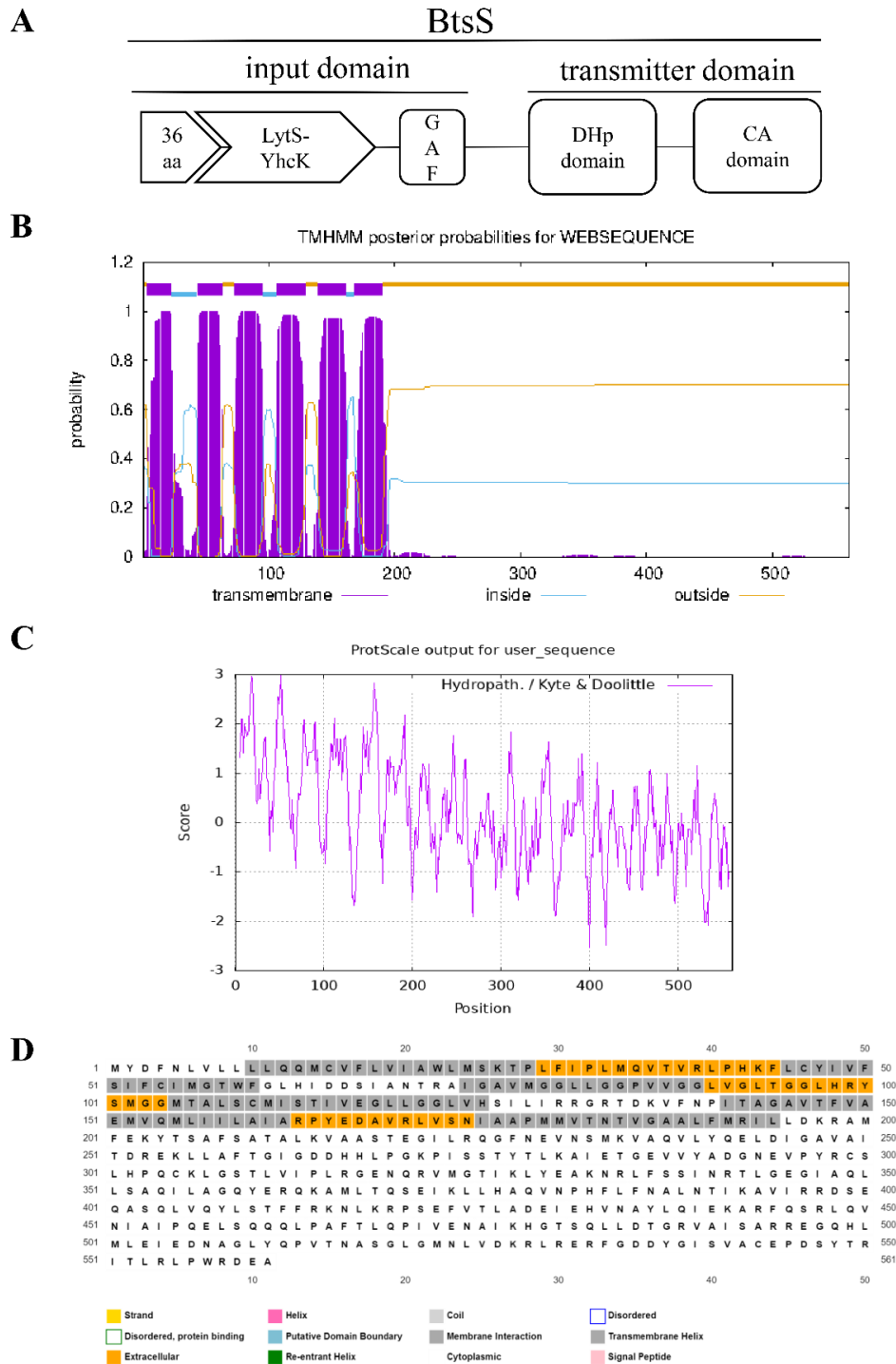Extracellular | Re-entrant Helix | Cytoplasmic | Signal Peptide

FIG 3.1.1 Domain structure of BtsS and the hydrophobicity analysis of BtsS. (A) BtsS is a HK composed of an input domain and a transmitter domain. The input domain of BtsS consists of the 5TMR-LYT domain and a GAF domain. The transmitter domain consists of a DHp domain and a CA domain. (B) Transmembrane structure prediction using TMHMM-2.0 (117, 118). (C) Hydrophilicity plot using ProtScale (119). (D) BtsS structure analysis using

To address this question, a MalE fusion strategy was applied in this study. This method previously determined that the N-terminus of the quorum-sensing hybrid HK LuxN of *Vibrio harveyi* located towards the periplasmic site (108). Periplasmic binding protein, MalE, binds maltose and higher maltodextrins which can be imported by the ABC transporter complex MalEFGK. Wild-type MalE contains a signal peptide to translocate the protein through the cytoplasmic membrane, which is encoded by the vector pMAL-p2X and named as MalEp. MalEc, the same MalE protein but without signal peptide, is a cytoplasmic protein encoded by pMAL-c2X (121). Both *malE* variants were fusion expressed with the 5' end of *btsS* and hybrid proteins were supposed to be either periplasmically localized (MalEp-BtsS) or cytoplasmically localized (MalEc-BtsS) maltose binding-protein (MBP) (FIG 3.1.2A). A complementation of a Δ*malE* mutant (*E. coli* MM39) was used to test the position of MalE in the hybrid proteins. The *E. coli* MM39 has a deletion of the *malE* gene and it cannot grow with maltose as the sole carbon source (C source) (FIG 3.1.2B). *E. coli* MM39 was transformed with plasmids pMAL-p2X (control) or pMALp-*btsS* encoding periplasmic MalEp or the hybrid MalEp-BtsS, respectively. Both strains were able to grow when maltose was used as a C source, indicating MalE was functional active. In contrast, *E. coli* MM39 transformed with pMAL-c2X or pMALc-*btsS* encoding MalE without signal peptide (MalEc) or the hybrid MalEc-BtsS, did not grow on maltose-containing plates (FIG 3.1.2B).

In vivo BtsS/BtsR signal transduction was detected to test the function of each MBP-BtsS construct. Only the hybrid protein with the N-terminus of BtsS on the correct side of the membrane is functional. The MBP-BtsS constructs were tested with the RR BtsR for complementation of reporter strain lacking the *btsS/R* genes and expressing a *btsT* promoter-luciferase fusion

(P$_{btsT}$::*luxCDABE*). Strains were cultivated in minimal medium supplemented with 5 mM pyruvate and 15 mM succinate, a condition that induces *btsT* expression (85, 111). MalEp-BtsS mediated pyruvate-dependent activation of *btsT* expression behaved similarily as wild-type BtsS, although it showed a 5.1-fold reduced induction (FIG 3.1.2C). In contrast, *btsT* expression cannot be induced by MalEc-BtsS (FIG 3.1.2C). It indicated that only fusion of the sequence encoding MalE with a signal peptide to the 5'-end of *btsS* resulted in a hybrid protein with a functional MalE in the periplasm and a signaling active BtsS. In contrast, hybrid protein MalEc-BtsS resulted in a location that MalE was towards to the cytoplasm and an inactive BtsS (FIG 3.1.2C). These results supported a periplasmic location of the N-terminus of BtsS, which means that BtsS is anchored in the cytoplasmic membrane and it has seven transmembrane helices (FIG 3.1.2A, left panel).
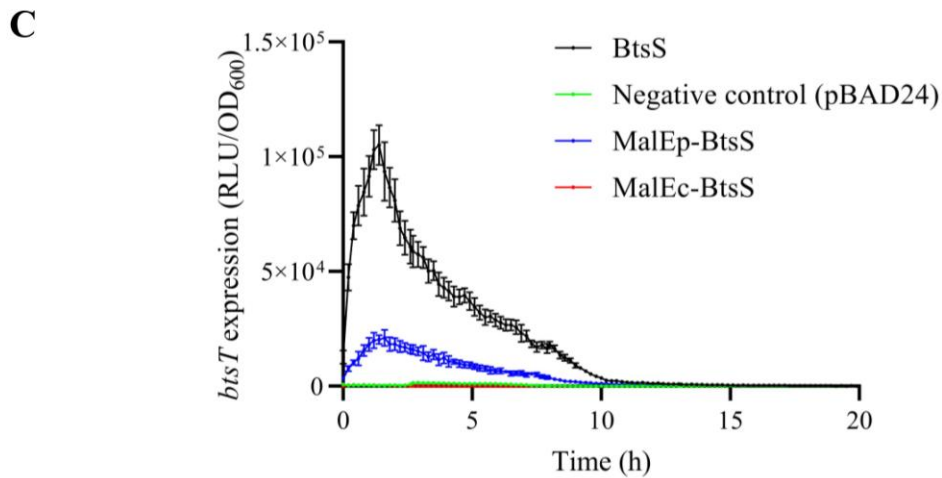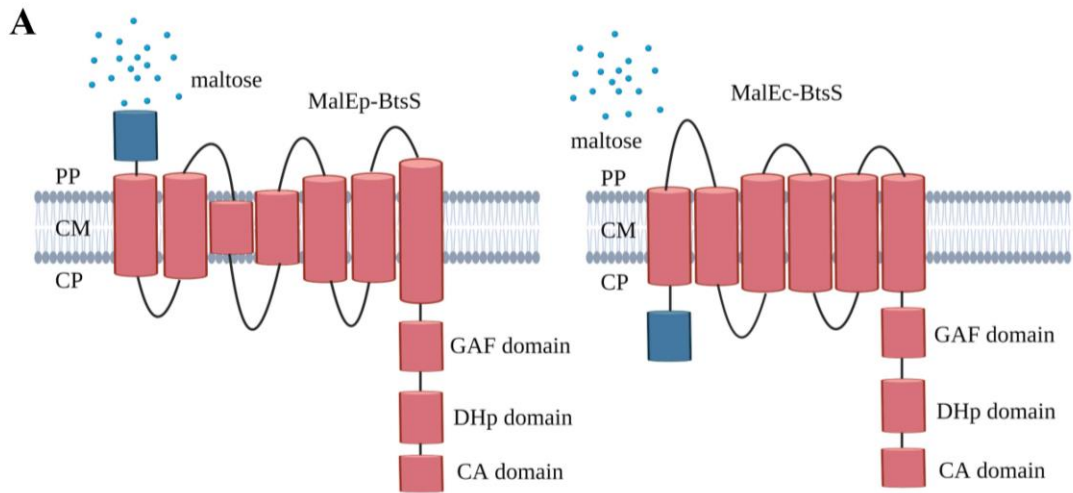
FIG 3.1.2 Periplasmic location of the N-terminus of BtsS. (A) Schematic illustration of the use of maltose-binding protein MalE (blue-labeled domain) as reporter protein to test the location of the N-terminus of BtsS. MalE is a periplasmic protein that binds maltose, which is imported by the ABC transporter complex MalEFGK. See text for more details. (B) Growth of *E. coli* MM39 (Δ*malE*) after complementation with different MalE and MalE-BtsS variants on maltose as sole C source compared to *E. coli* MG1655 (*malE*⁺) and MM39 (Δ*malE*) (C) Functionality of MalE-

BtsS variants was tested using the reporter strain MG1655Δ*btsSR*/pBBR-*btsT-lux* transformed either with pBAD24 as a negative control, pBAD24-*btsS/R* as a positive control, pBAD24-pMALp-*btsS/R* or pBAD24-pMALc-*btsS/R*. Cells of an overnight culture were inoculated in M9 minimal medium containing pyruvate (5 mM) and succinate (15 mM) as C source and grown at 37°C in a microplate reader. OD_{600} and luminescence were measured, and data were relative light units (RLU) in counts per second per OD. All experiments were performed as biological triplicates (n = 3), and representative plates and curves (standard deviation <10%) are shown. Figure was cited from publication: Jin Qiu, Ana Gasperotti, Nathalie Sisattana, Martin Zacharias, and Kirsten Jung. The LytS-type histidine kinase BtsS is a 7-transmembrane receptor that binds pyruvate. mBio. doi: 10.1128/mbio.01089-23. Online ahead of print.

3.1.2 Screening for amino acids involved in pyruvate sensing by alanine scanning mutagenesis

Previous study has shown that BtsS is pyruvate sensor with high affinity (K_d = 58.6 µM) and pyruvate binds to the extracellular side of the transmembrane domain (111). Pyruvate has a carboxyl group. Study on KinD (a protein can bind pyruvate) (122) or pyruvate formate lyase (123) showed carboxyl group of pyruvate is in contact with positively charged amino acids. The goal in this thesis was to identify the pyruvate-binding site of BtsS.

There are four lysines and ten arginines in the input domain of BtsS. In order to detect which amino acid is for pyruvate binding, each of them was replaced with alanine. Then, wild-type BtsS and variants were tested with complementation of reporter strain lacking the *btsS/R* genes and expressing a *btsT* promoter-luciferase fusion (P*btsT*::*luxCDABE*) (85, 111). Among the 14 tested variants, *btsT* could not be induced by six of them, which were BtsS-K26A, BtsS-R39A, BtsS-R72A, BtsS-R99A, BtsS-R131A and BtsS-R192A (FIG 3.1.3A). All BtsS variants except BtsS-R131A were produced (FIG 3.1.3B). Although the *btsT* expression level was significantly reduced for variant BtsS-R198A, it was still dependent on pyruvate concentration (FIG 3.1.3C). The production and integration of all BtsS variants was tested by SDS-PAGE and Western blot. The

first-round screening indicated that Lys26, Arg39, Arg72, Arg99 and Arg192 might be involved in
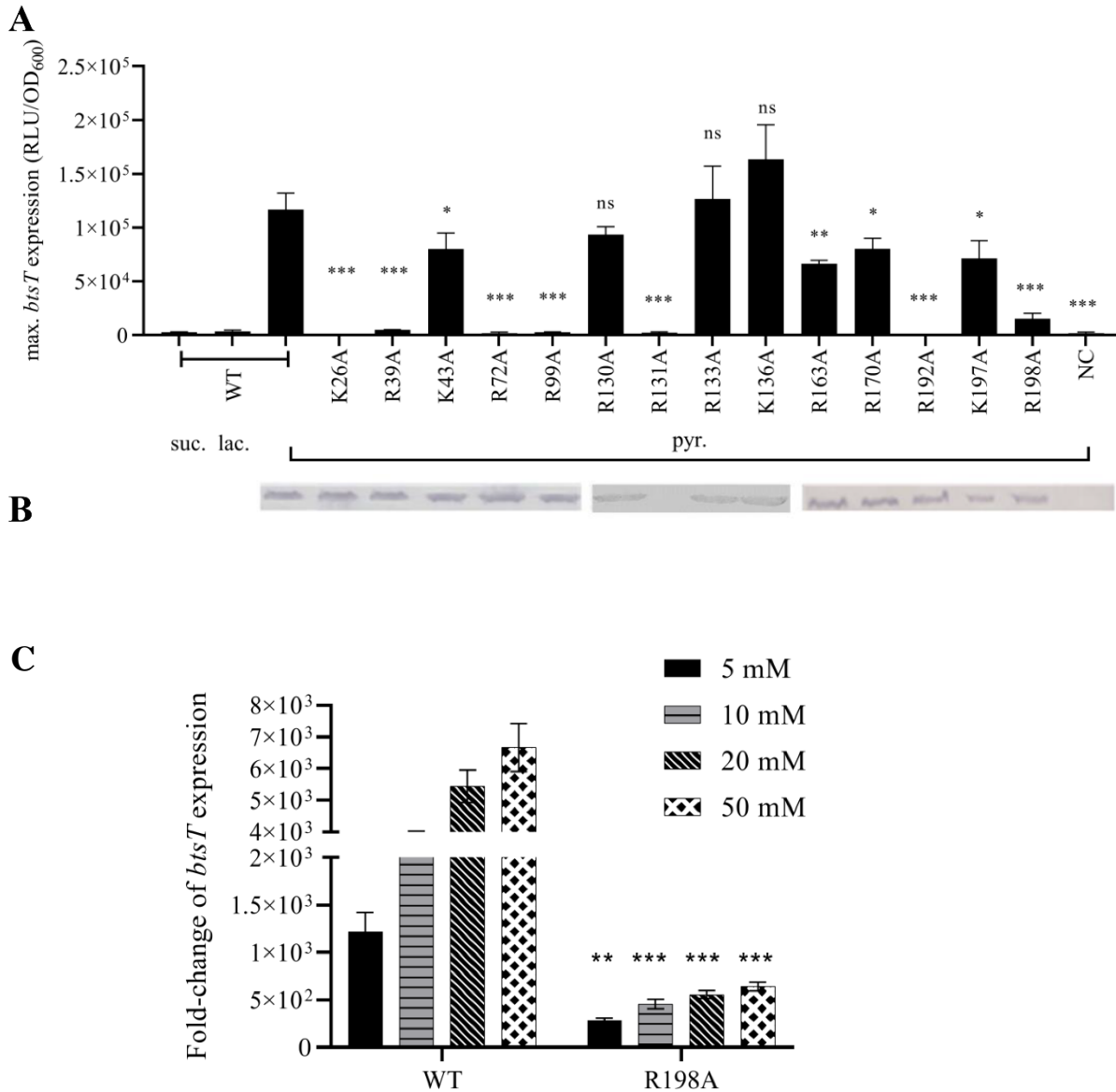
pyruvate-sensing and/or signaling of BtsS.

FIG 3.1.3 Screening for amino acids involved in pyruvate sensing in BtsS. (A) Reporter strain MG1655Δ*btsSR*

encoding the promoter fusion P*btsT::luxCDABE* was transformed either with plasmid pBAD24 as a negative control

(NC), pBAD24-*btsS/R* (WT) as a positive control, or pBAD24-*btsS/R* encoding BtsS variants. The response to pyruvate

(pyr.) was tested as described in FIG 2. As negative controls, the response of WT to succinate (suc.) and lactate (lac.)

was tested. The maximal luciferase activity (RLU) normalized to an optical density (OD$_{600}$) of 1 served as the measure

of *btsT* expression. All experiments were performed as biological triplicates (n = 3), and the error bars represent the standard deviation of the means. (B) Verification of production and integration of BtsS variants in the cytoplasmic membrane of *E. coli*. Cells were disrupted and fractionated, 25 µg protein of the membrane fraction was analyzed by SDS-PAGE and Western blotting. BtsS was detected by a monoclonal mouse antibody against the Flag tag and an alkaline phosphatase-coupled secondary antibody. (C) Reporter strain MG1655Δ*btsSR*/pBBR-*btsT-lux* was transformed either with pBAD24-*btsS/R* (WT) as a positive control, or pBAD24-*btsS*-R198A/*btsR*. Cells were grown with different concentrations of pyruvate (5 mM, 10 mM, 20 mM and 50 mM) as the C source, with the total C concentration kept constant at 50 mM in each case by addition of succinate, and BtsS/BtsR-mediated *btsT* expression (measured as P$_{btsT}$::*luxCDABE* and reported in relative light units) was measured over time. Maximum luciferase activity (RLU), normalized to an optical density (OD$_{600}$) of 1 are reported. Fold-change values were calculated using the succinate control. Statistics: Student's unpaired two-sided t-test (*** $p < 0.001$; ** $p < 0.01$; *$p < 0.05$; ns $p > 0.05$). Figure was cited from publication: Jin Qiu, Ana Gasperotti, Nathalie Sisattana, Martin Zacharias, and Kirsten Jung. The LytS-type histidine kinase BtsS is a 7-transmembrane receptor that binds pyruvate. mBio. doi: 10.1128/mbio.01089-23. Online ahead of print.

3.1.3 Arg72, Arg99, Cys110 and Ser113 are involved in pyruvate sensing

Not only the charged side chain was removed but also the size was reduced after those positively charged amino acids were replaced with alanine. Therefore, amino acids that can maintain the charge (Arg, Lys, His) and size (Gln) or even have the opposite charged (Glu) side chain were further chosen to replace with those five amino acids which were important for BtsS/BtsR. All corresponding BtsS-Arg72 and BtsS-Arg99 variants prevented *btsT* induction after they were replaced by any other amino acid (FIG 3.1.4A). These amino acids are likely to be essential for stimulus perception or signal transduction of BtsS. In contrast, variants were able to respond to pyruvate after replacement of BtsS-Lys26, BtsS-Arg39, BtsS-Arg131, and BtsS-Arg192 with other amino acids (FIG 3.1.4A and FIG 3.3.1). Therefore, these four amino acids were not

further studied.

Amino acids that might interact with pyruvate hydroxyl group were then studied, especially the amino acids that were located close to Arg72 and Arg99 in BtsS model. Therefore, Asn70, Thr71, Thr94, Tyr100, Ser101, Thr106, Cys110, Ser113, and Thr114 in BtsS were then replaced with Ala. Variants BtsS-C110A, BtsS-S113A, and BtsS-T114A prevented *btsT* expression (FIG 3.1.4A), whereas variants BtsS-N70A, BtsS-T71A, BtsS-T94A, BtsS-Y100A, BtsS-S101A, BtsS-T106A (FIG 3.1.4B) induced *btsT* expression and it was pyruvate-dependent. Then BtsS-Cys110, BtsS-Ser113, and BtsS-Thr114 were replaced with other amino acids. All BtsS-Cys110 and BtsS-Ser113 variants (C110V, C110G, C110S, S113V, S113G, S113T) prevented *btsT* expression when pyruvate was used as sole C source (FIG 3.1.4A). In contrast, the replacements of BtsS-Thr114 by Ser, Val and Gly allowed *btsT* expression (FIG 3.1.4A). All variants were produced as membrane-integrated proteins and was verified by SDS-PAGE and Western blotting. These results indicated that Cys110 and Ser113 were also essential for BtsS to sense pyruvate.

In vivo activity determination of the BtsS variants was done in complemented reporter strain by adding 5 mM pyruvate as a C source. To test whether the affinity of BtsS variants for pyruvate was changed, *btsT* induction was tested in two additional *in vivo* assays containing different pyruvate concentrations. Cells were cultivated in M9 minimal medium with pyruvate concentrations ranging from 5 to 50 mM and the total carbon concentration (50 mM) was kept constant by adding succinate. Results of concentration-dependent *btsT* expression for BtsS-R72A, BtsS-R99A, BtsS-C110A, and BtsS-S113A showed they did not induce *btsT* expression under any condition (FIG 3.1.4C). Another assay was based on previous work (85) which showed that starving *E. coli* cells exposed to very low pyruvate concentrations (10 µM to 1 mM) induced *btsT* expression in a concentration-dependent manner. BtsS-R72A, BtsS-R99A, BtsS-C110A, and BtsS-S113A variants showed not only an approximately 100-fold lower response compared with wild

type, but also a slight shift to higher pyruvate concentrations (FIG 3.1.4D). In conclusion, BtsS-Arg72, BtsS-Arg99, BtsS-Cys110, and BtsS-Ser113 are involved in pyruvate sensing.
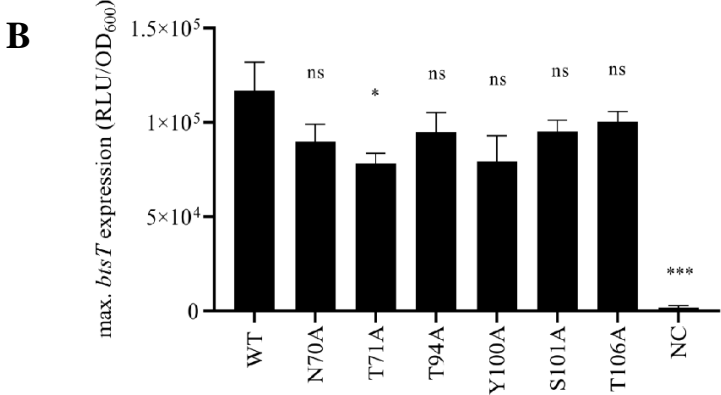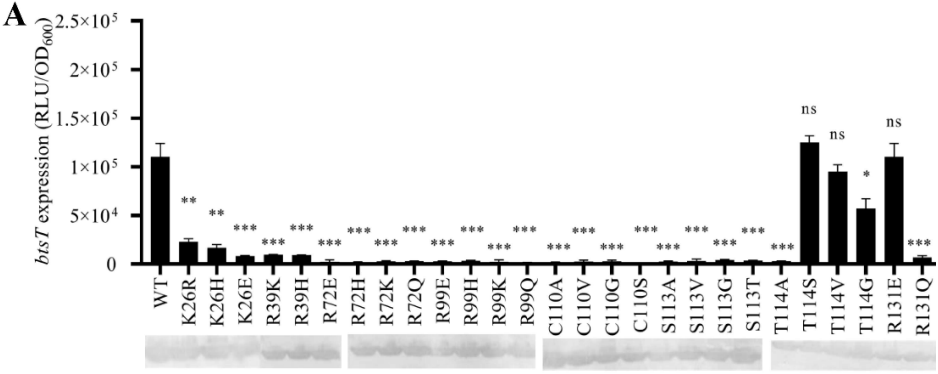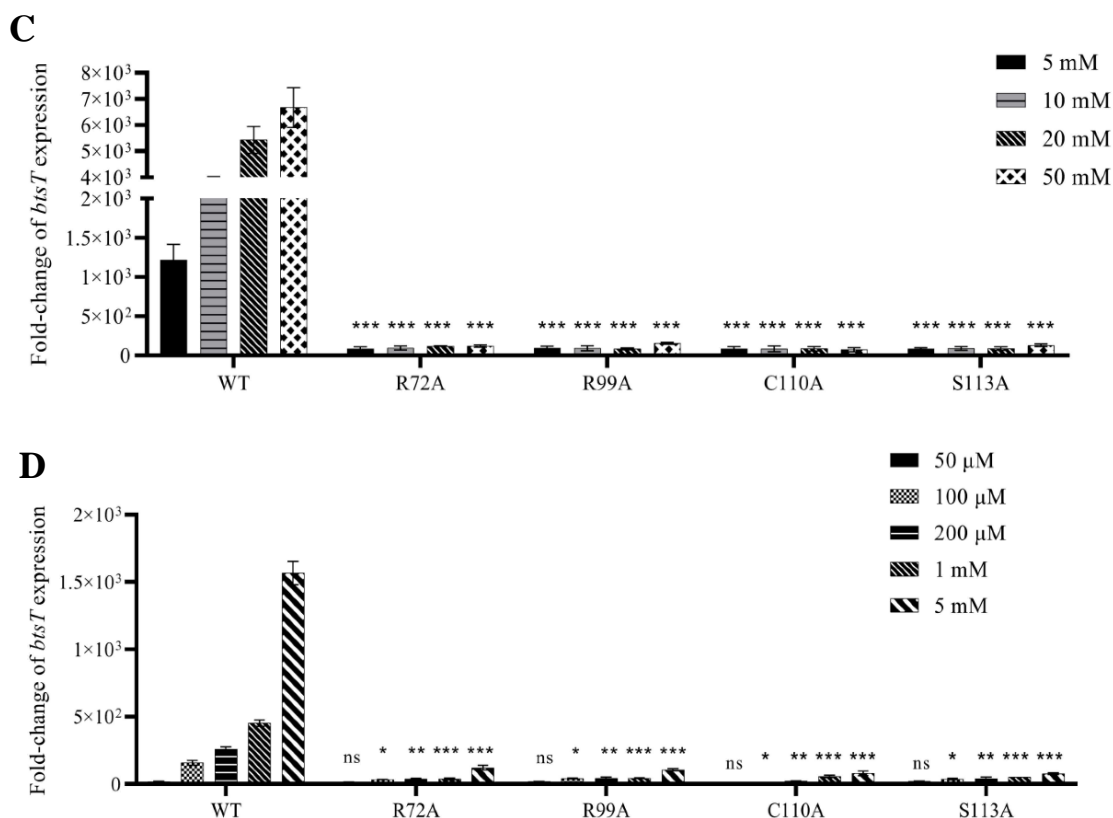
FIG 3.1.4 Arg72, Arg99, Cys110, and Ser113 are essential for pyruvate sensing in BtsS. (A) Reporter strain MG1655Δ*btsSR*/pBBR-*btsT-lux* was transformed with either plasmid pBAD24 as a negative control, pBAD24-*btsS/R* as a positive control, or pBAD24-*btsS/R* encoding the indicated BtsS variants. The response to 5 mM pyruvate (supplemented with succinate for a total of 20 mM C source) was tested as described in FIG 2. Maximum luciferase activity (RLU), normalized to an optical density (OD_{600}) of 1, served as a measure of *btsT* expression. (B) The same experimental approach as in A was used, but strains were grown in M9 minimal medium containing different concentrations of pyruvate (supplemented with succinate, total 50 mM C source). Fold-change values were calculated using the succinate control. (C) Reporter strains as in A and B were cultivated in 0.1x LB medium to establish starvation conditions. After 1 hour, the indicated concentration of pyruvate or water (negative control) was added. Cells immediately induced *btsT* expression. Fold-change values were calculated using the water control. (D) The same experimental approach as in A was used. All experiments were performed as biological triplicates (n = 3), and the error bars represent the standard deviation of the means. Statistics: Student's unpaired two-sided t-test (*** $p < 0.001$; ** p

3.1.4 Arg72, Arg99, Cys110 and Ser113 form a pyruvate-binding site

The ability of the BtsS variants with replacements at position Arg72, Arg99, Cys110 and Ser113 for altered affinities to bind pyruvate was investigated *in vitro*. DRaCALA was used here (115), which had previously used to identify BtsS and pyruvate interactions (85). A radiolabeled ligand is used in this assay. The principle of DRaCALA is based on the immobilization of the protein-ligand complex on a nitrocellulose membrane, while the unbound ligand diffuses radially with the buffer due to the capillary action of the membrane. Thus, both protein-bound ligand and total ligand are detected. The fraction of ligand bound to protein, defined as F_B, is calculated from the signal intensity of the area with protein (inner circle) and the signal intensity of the whole area (outer circle). Membrane vesicles prepared from the *E. coli ΔbtsSRΔypdABC* mutant after overproduction of BtsS (WT) or BtsS-R72A, BtsS-R99A, BtsS-C110A, BtsS-S113A were used and equal amounts of protein was incubated with increasing concentrations of pyruvate, each containing 15 µM radiolabeled ^{14}C-pyruvate. The mixture was dropped onto a nitrocellulose membrane (FIG 3.1.5A). Migration of the ligand by capillary action was detected after exposure of the membrane to a phosphoscreen followed by image analysis. As a negative control, membrane vesicles of the *E. coli ΔbtsSRΔypdABC* mutant was used, in which no pyruvate-binding proteins should be found (EV) (FIG 3.1.5A). Dark inner circles were detected for the wild type that were not seen in the negative control, indicating binding of ^{14}C-pyruvate and resulting in an F_B value of 0.198. To determine pyruvate affinity, the total pyruvate concentration was steadily increased by adding cold pyruvate, which resulted in less pronounced dark rings due to competition between cold and radiolabeled pyruvate. K_d values were calculated after background (EV) was subtracted

for all concentrations. For wild-type BtsS, a K_d value of 67.3±10.6 μM was determined, consistent with previous measurements (85). For the BtsS variants with amino acid substitutions that affected pyruvate sensing, the K_d values were: BtsS-R72A K_d =107.2±12.3 μM; BtsS-R99A K_d =245.4±10.1 μM; BtsS-C110A K_d = 375.2±21.2 μM and BtsS-S113A K_d =283.6±8.0 μM (FIG 3.1.5B). These results indicate that replacement of BtsS-Arg72, BtsS-Arg99, BtsS-Cys110, and BtsS-Ser113 with alanine decreases the affinity of BtsS for pyruvate, suggesting that these amino acids may be part of the pyruvate-binding site.
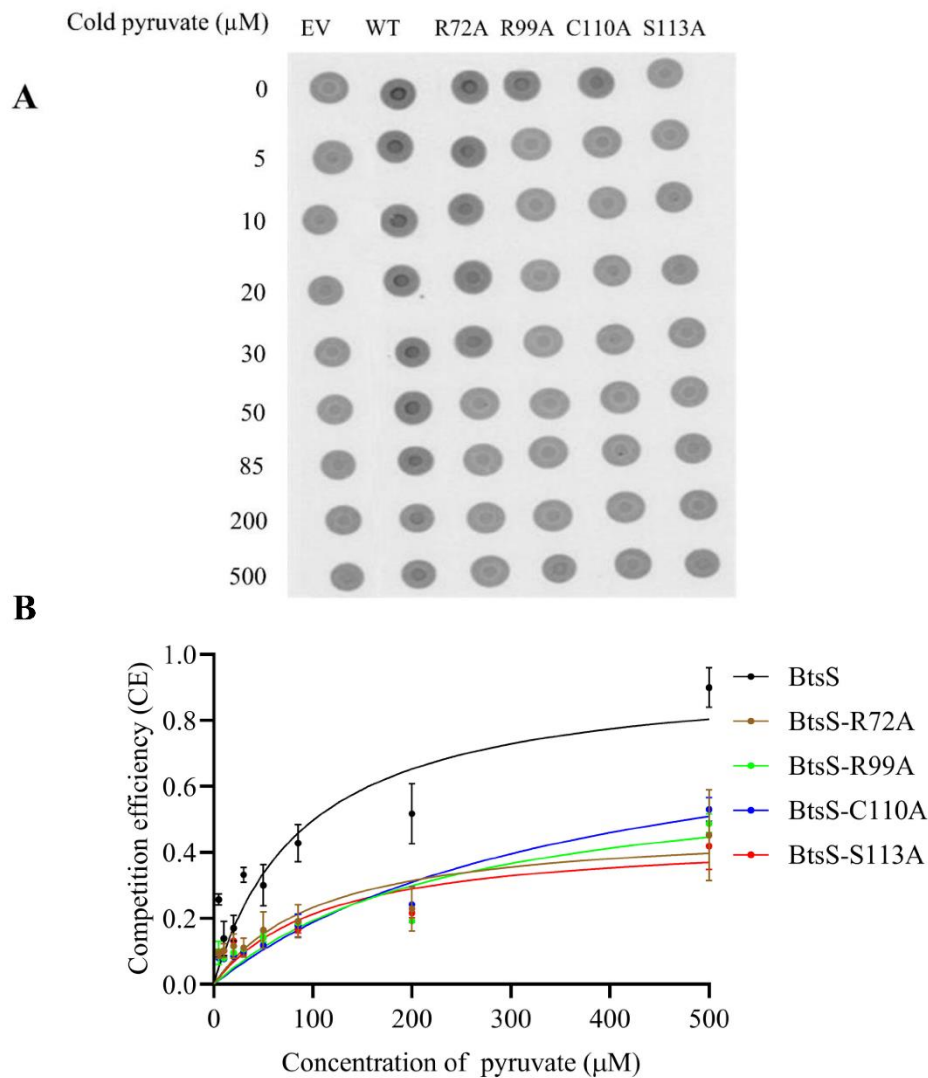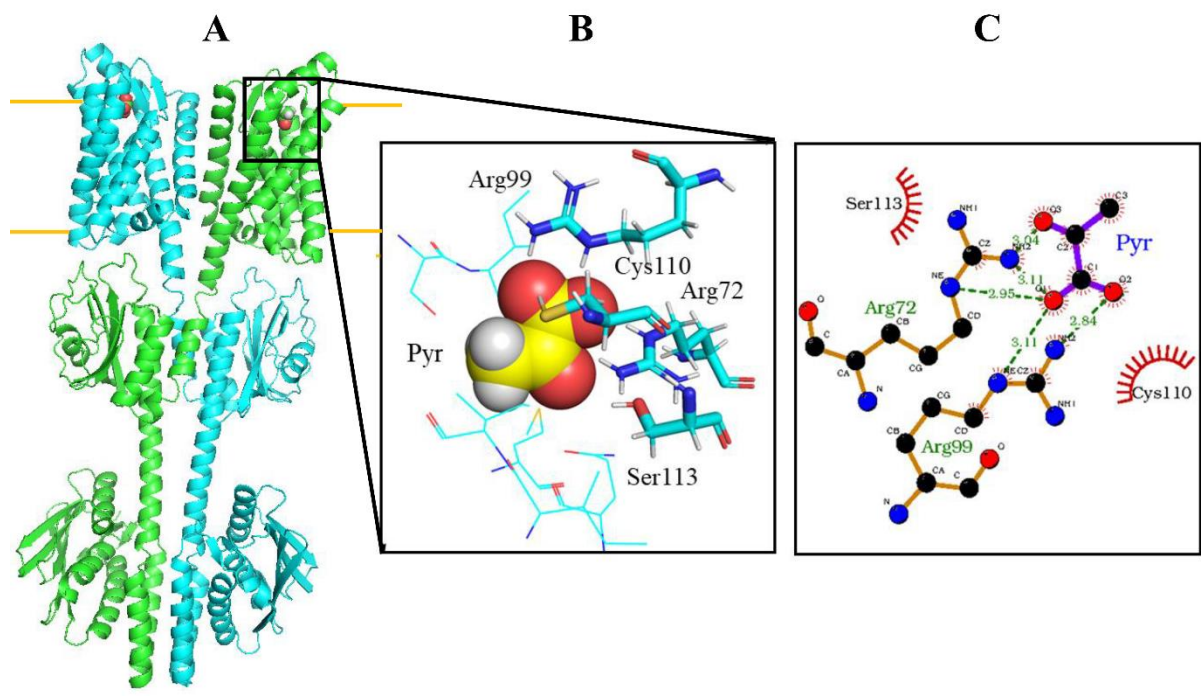

FIG 3.1.5 *In vitro* binding assay of pyruvate to BtsS. (A) DRaCALA image of interactions between pyruvate and BtsS (WT) or BtsS-R72A, BtsS-R99A, BtsS-C110A, BtsS-S113A, or no BtsS (EV) in membrane vesicles of *E. coli*

$\Delta btsSR\Delta ypdABC$. Protein-ligand (15 µM radiolabeled ^{14}C-pyruvate) mixtures were spotted on a nitrocellulose membrane, allowed to dry before imaging using a PhosphoImager. (B) Determination of the dissociation constant (K_d) for the receptor-pyruvate complex for the BtsS variants compared with wild type. Competition efficiency (CE) CE=($F_{B(NC)}$−$F_{B(pyr)}$)/$F_{B(NC)}$ (see Materials and Methods for details) was plotted as a function of pyruvate concentration. The CE value reached 1.0 in the presence of 50 mM cold pyruvate. The best-fit curves were determined by nonlinear regression using the equation y=B_{max}*x/(K_d+x). K_d values were determined in n=3 independent experiments, and the error bars represent the standard deviation of the means. K_d of BtsS, BtsS-R72A, BtsS-R99A, BtsS-C110A and BtsS-S113A is 67.3±10.6 µM, 107.2±12.3 µM, 245.4±10.1 µM, 375.2±21.2 µM and 283.6±8.0 µM, respectively. Figure was cited from publication: Jin Qiu, Ana Gasperotti, Nathalie Sisattana, Martin Zacharias, and Kirsten Jung. The LytS-type histidine kinase BtsS is a 7-transmembrane receptor that binds pyruvate. mBio. doi: 10.1128/mbio.01089-23. Online ahead of print.

3.1.5 Model of the 3D-structure of BtsS and the pyruvate binding site

Based on structural modeling information and MD-based autodocking pyruvate with BtsS (FIGs 3.1.6A-C), Cys110 was in close contact with pyruvate (but does not form hydrogen bonds), however pyruvate formed stable hydrogen bonds with Arg72 and Arg99. The geometry of pyruvate binding was stable during MD simulation (FIG 3.1.6D). The two oxygen atoms of the pyruvate carboxyl group formed hydrogen bonds with the guanidinium group of Arg99, and the guanidinium group of Arg72 formed a bifurcated hydrogen bond with the carbonyl oxygen of pyruvate. Additionally, there was no direct hydrogen bond was formed although Ser113 was located close to pyruvate. But a close H-bond contact between Ser113 and Arg72 was observed in the model structure. Therefore, Ser113 might play an important role in placing and stabilizing the position of the guanidinium group of Arg72, allowing close contact with pyruvate. The positively charged Arg72 and Arg99 provide strong and favorable electrostatic interactions to stabilize the complex since pyruvate is negatively charged.
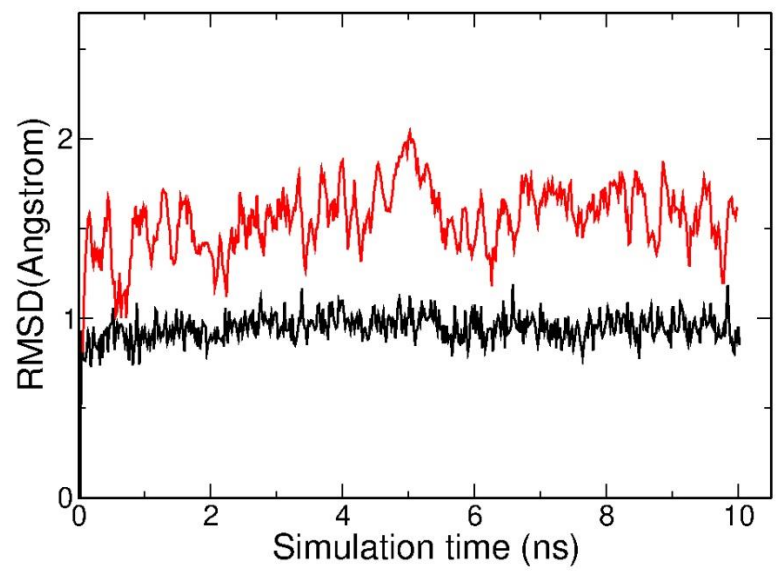
FIG 3.1.6 AlphaFold2.0 based structural model of the BtsS dimer with bound pyruvate. (A) AlphaFold2.0 based

structural model of the BtsS dimer with bound pyruvate. Each BtsS monomer is represented as a green or light blue

cartoon and the membrane boundaries are indicated by yellow lines. (B) The putative pyruvate (Pyr) binding geometry

(pyruvate in van der Waals representation) is shown enlarged in the right panel, including the arrangement of residues

important for binding as stick model. (C) Schematic 2D contact view of pyruvate binding to BtsS. Hydrogen bonds between Arg72/99 and pyruvate as well as direct contacts to Cys110 are indicated. Ser113 contacts and stabilizes the Arg72 placement. (D) Root-mean-square deviation (RMSD) of protein backbone atoms (black line, pyruvate binding domain, residues 1-202) during MD simulation of the complex of BtsS with pyruvate from the starting structure. The simulation included positional restraints on the protein (force constant: 0.05 kcal mol-1Å-2). The RMSD of the pyruvate ligand (after best superposition of the pyruvate binding domain on the start structure) is also shown (red line). Figure was cited from publication: Jin Qiu, Ana Gasperotti, Nathalie Sisattana, Martin Zacharias, and Kirsten Jung. The LytS-type histidine kinase BtsS is a 7-transmembrane receptor that binds pyruvate. mBio. doi: 10.1128/mbio.01089-23. Online ahead of print.

3.1.6 Binding of pyruvate affects autokinase activity of BtsS

After the stimulus is perceived by HKs, this information will be transduced into an intracellular signal by initiating a phosphorylation cascade (112). Autokinase activity of BtsS was not able to be detected previously (85). This was not surprising at first, because BtsS belongs to the LytS-type HKs and proteins in this family have several unique features (124): In the H-box, the conserved histidine is preceded by a proline, and followed by a phenylalanine instead of the usual acidic residue. The F-box is not conserved, there is an unusual signature sequence in the N-box, and the distance between the H- and X-box is reduced.

In this study, the autophosphorylation activity of BtsS was tested again *in virto* and results showed that the cofactor makes a difference. When assayed in the presence of Mg^{2+}-ATP, only very weak BtsS autophosphorylation activity was detectable (FIG 3.1.7A). However, the autophosphorylation activity of BtsS was about 10-fold higher when Mn^{2+} was used as a cofactor instead of Mg^{2+} (FIG 3.1.7A). The predicted phosphorylation site at His382 was also confirmed, as the variant BtsS-H382Q could not be phosphorylated (FIG 3.1.7B).

To identify whether BtsS autophosphorylation was stimulated by pyruvate binding, autophosphorylation activity of wild-type BtsS and all pyruvate-insensitive BtsS variants were determined under the condition that contains different concentrations of pyruvate. Autophosphorylation initial rate of wild-type BtsS showed a 1.6-fold increase in the presence of 25 µM pyruvate. The initial rate was also increased when assayed with 50 and 100 µM pyruvate, (FIG 3.1.7B). But it was not further stimulated in the presence of even higher concentrations of pyruvate (200, 500, 1000 µM) (FIG 3.1.7B). In contrast, initial rates of variants BtsS-R72A, BtsS-R99A, BtsS-C110A and BtsS-S113A were quite lower and it was not dependent on pyruvate concentration (FIGs 3.1.7B and 3.1.8-3.1.11). Initial rates were 2.3 to 3.6-fold lower compared to wild-type BtsS. BtsS-T114A was used as a control to show the effects on BtsS autokinase was due to pyruvate binding instead of amino acid substitution (FIG 3.1.12).
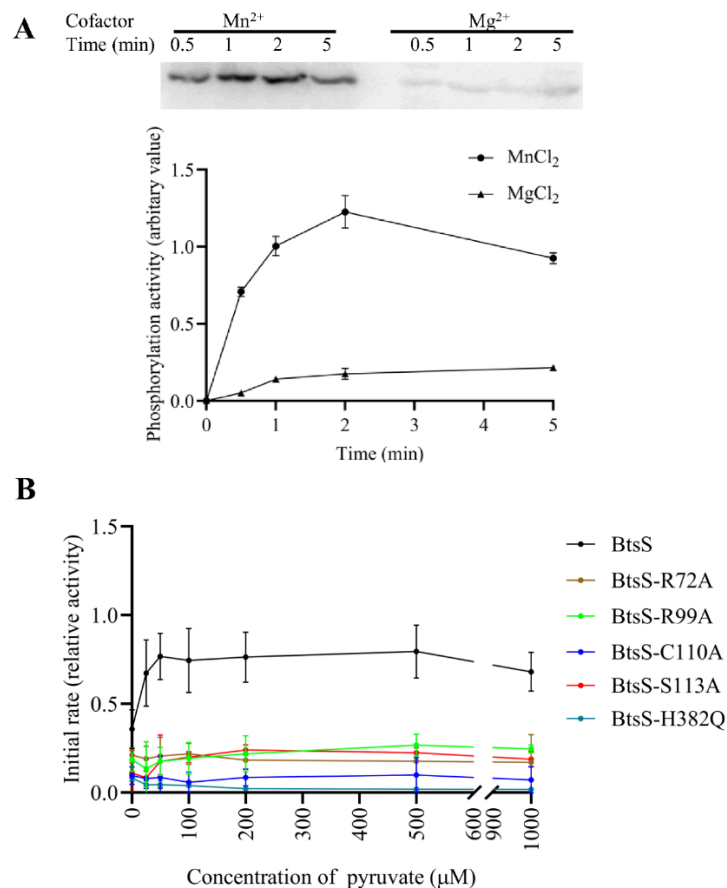
FIG 3.1.7 Autophosphorylation activity of BtsS and its variants. (A) Time-dependent autophosphorylation of BtsS in the presence of Mg^{2+} and Mn^{2+}. Membrane vesicles from *E. coli* TKR2000 producing BtsS-6His were incubated in the presence of 50 µM pyruvate. At time zero, 20 µM [γ-^{32}P] ATP (2.38 Ci/mmol) and either 5 mM $MgCl_2$ or $MnCl_2$ was added. Reactions were stopped at the indicated time point, and phosphorylated proteins were separated by SDS-PAGE, followed by phosphoimage analysis. Upper panel - phosphoimages of representative gels, lower panel - quantified values of radiolabeled BtsS using ImageQuant. Shown are the relative values normalized to the phosphorylation level of wild-type BtsS after incubation with 50 µM pyruvate and 5 mM $MnCl_2$ for 5 min (value of 1.0). (B) The effect of increasing pyruvate concentrations on the initial rate of autophosphorylation of BtsS, BtsS-R72A, BtsS-R99A, BtsS-C110A, BtsS-S113A, and BtsS-H382Q. Samples were processed and data were calculated as described in A. Figure was cited from publication: Jin Qiu, Ana Gasperotti, Nathalie Sisattana, Martin Zacharias, and Kirsten Jung. The LytS-type histidine kinase BtsS is a 7-transmembrane receptor that binds pyruvate. mBio. doi: 10.1128/mbio.01089-23. Online ahead of print.
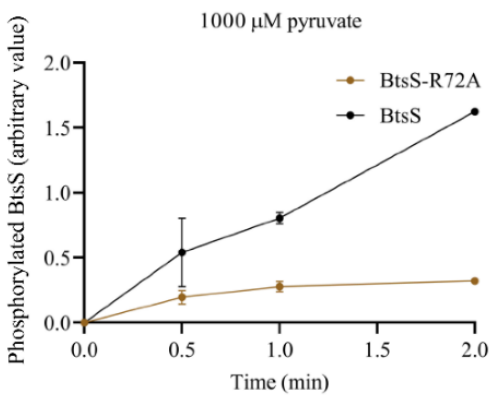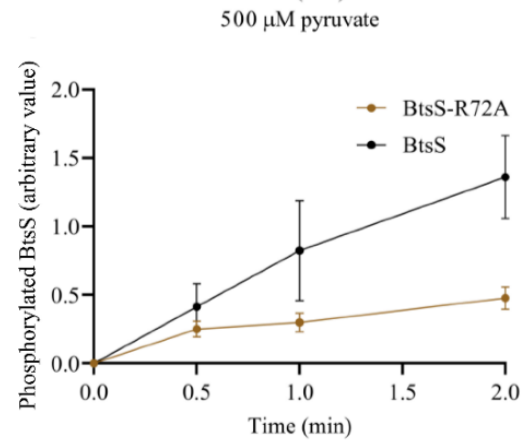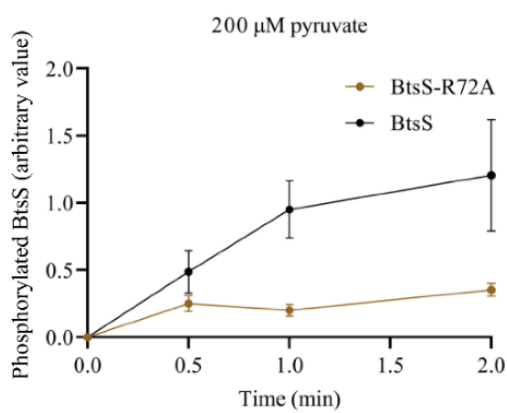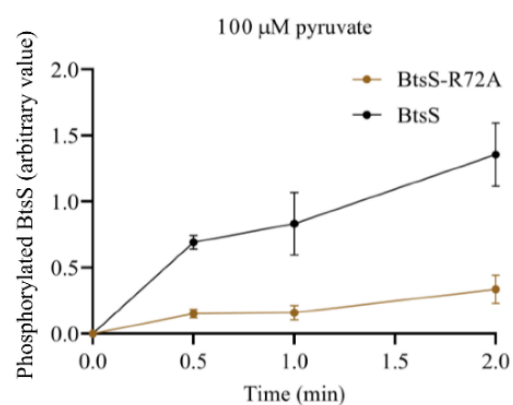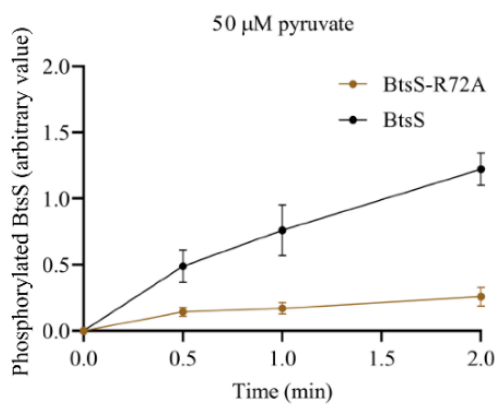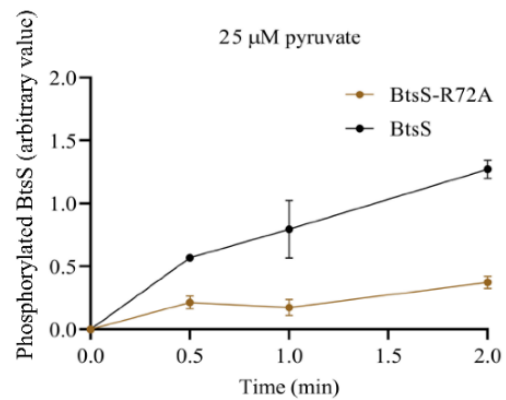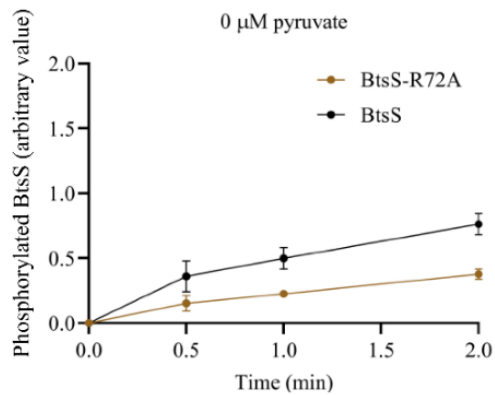
FIG 3.1.8 Influence of increasing pyruvate concentrations on the autophosphorylation activity of BtsS-R72A compared to wild-type BtsS. Membrane vesicles (2 mg/mL) were incubated in the presence of the indicated pyruvate concentrations. At time zero, 20 µM [γ-^{32}P] ATP (2.38 Ci/mmol) was added. Reactions were stopped at the indicated time points, and phosphorylated proteins were separated by SDS-PAGE, followed by phosphoimage analysis. Values are normalized to the phosphorylation level of wild-type BtsS after incubation with 50 µM pyruvate and 5 mM MnCl$_2$ for 5 min (value of 1.0). Figure was cited from publication: Jin Qiu, Ana Gasperotti, Nathalie Sisattana, Martin Zacharias, and Kirsten Jung. The LytS-type histidine kinase BtsS is a 7-transmembrane receptor that binds pyruvate. mBio. doi: 10.1128/mbio.01089-23. Online ahead of print.

FIG 3.1.9 Influence of increasing pyruvate concentrations on the autophosphorylation activity of BtsS-R99A compared to wild-type BtsS. The same experimental approach as in FIG 3.1.8 was used. Figure was cited from publication: Jin Qiu, Ana Gasperotti, Nathalie Sisattana, Martin Zacharias, and Kirsten Jung. The LytS-type histidine kinase BtsS is a 7-transmembrane receptor that binds pyruvate. mBio. doi: 10.1128/mbio.01089-23. Online ahead of print.

FIG 3.1.10 Influence of increasing pyruvate concentrations on the autophosphorylation activity of BtsS-C110A compared to wild-type BtsS. The same experimental approach as in FIG 3.1.8 was used. Figure was cited from publication: Jin Qiu, Ana Gasperotti, Nathalie Sisattana, Martin Zacharias, and Kirsten Jung. The LytS-type histidine kinase BtsS is a 7-transmembrane receptor that binds pyruvate. mBio. doi: 10.1128/mbio.01089-23. Online ahead of print.
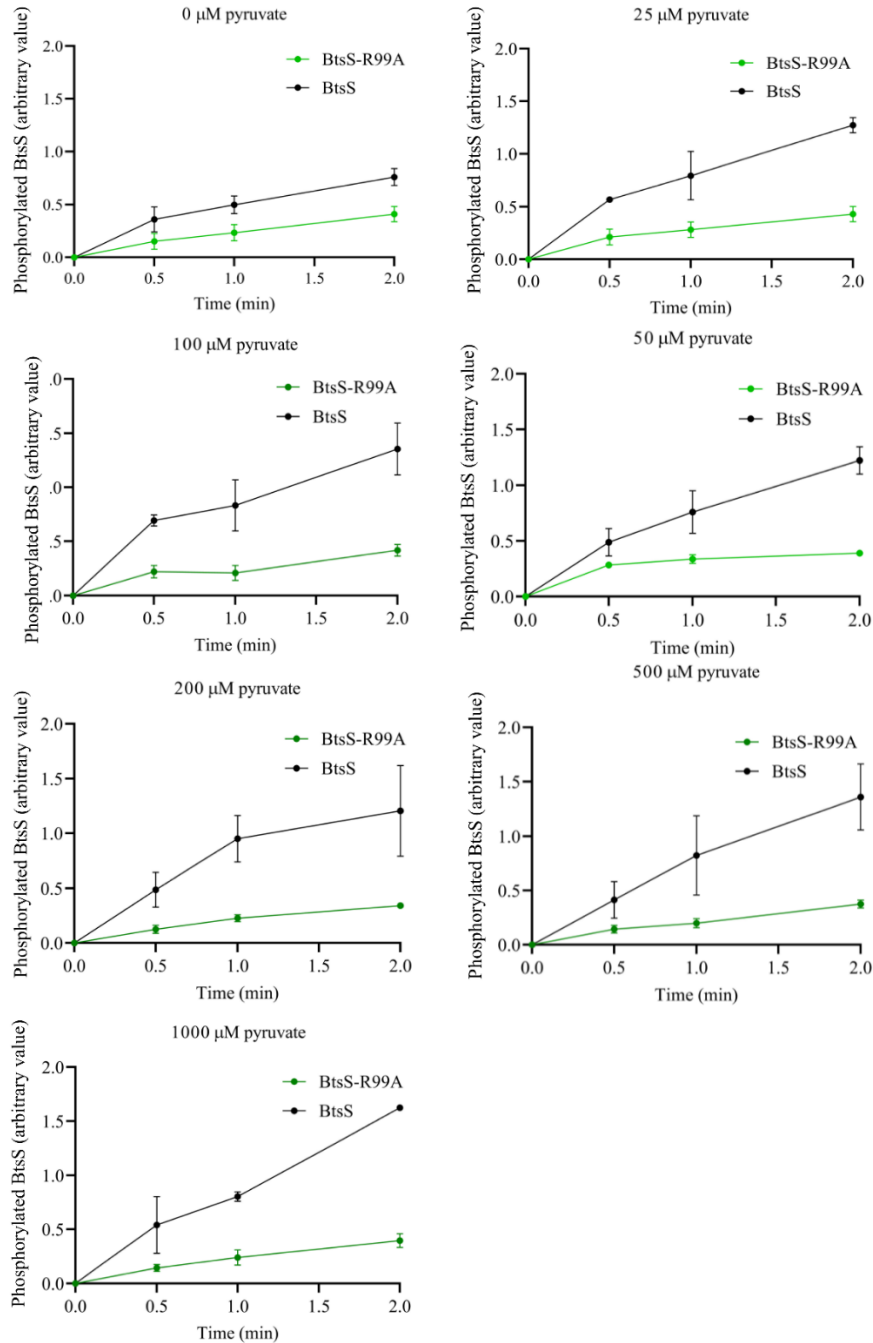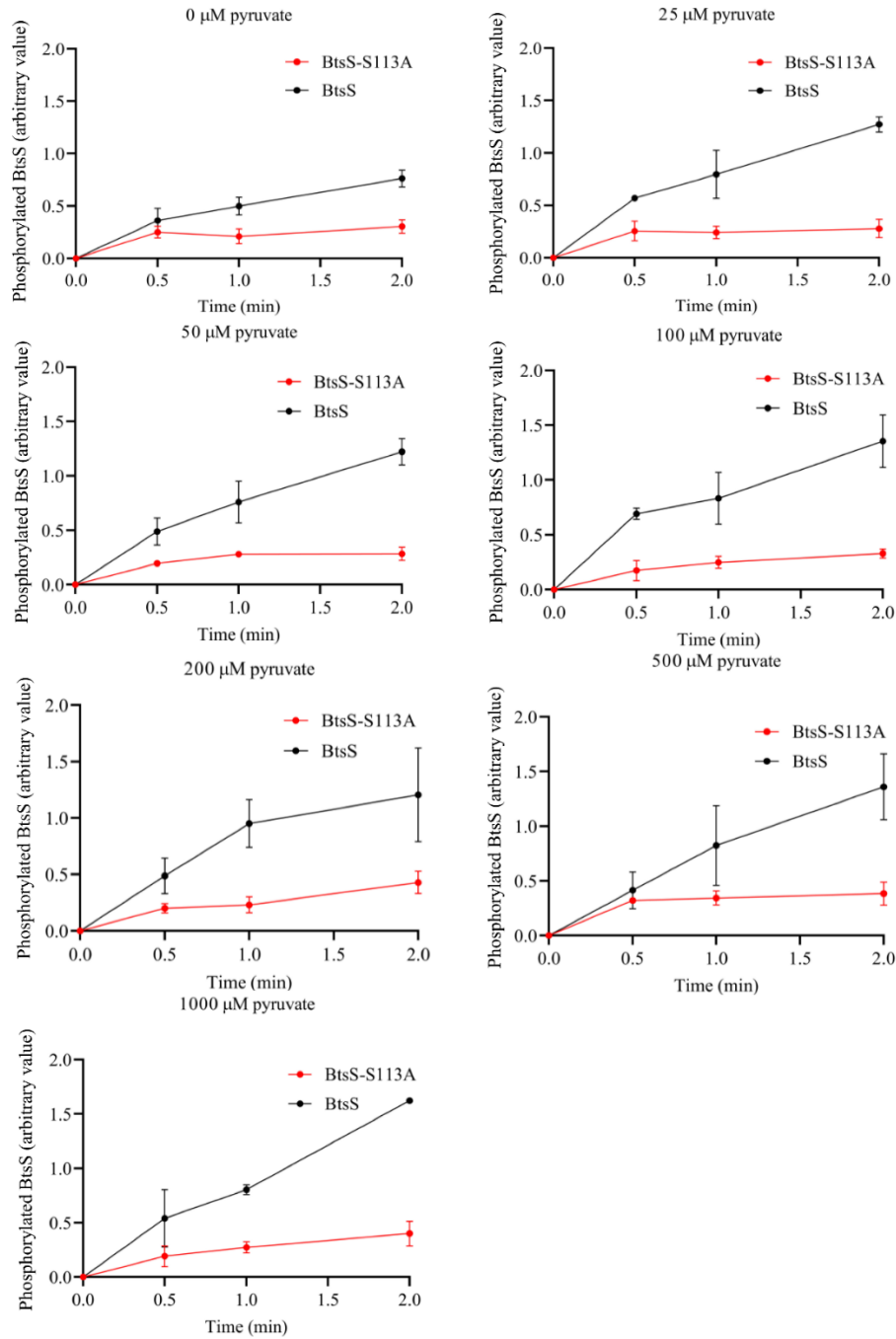
FIG 3.1.11 Influence of increasing pyruvate concentrations on the autophosphorylation activity of BtsS-S113A compared to wild-type BtsS. The same experimental approach as in FIG 3.1.8 was used. Figure was cited from publication: Jin Qiu, Ana Gasperotti, Nathalie Sisattana, Martin Zacharias, and Kirsten Jung. The LytS-type histidine kinase BtsS is a 7-transmembrane receptor that binds pyruvate. mBio. doi: 10.1128/mbio.01089-23. Online ahead of print.
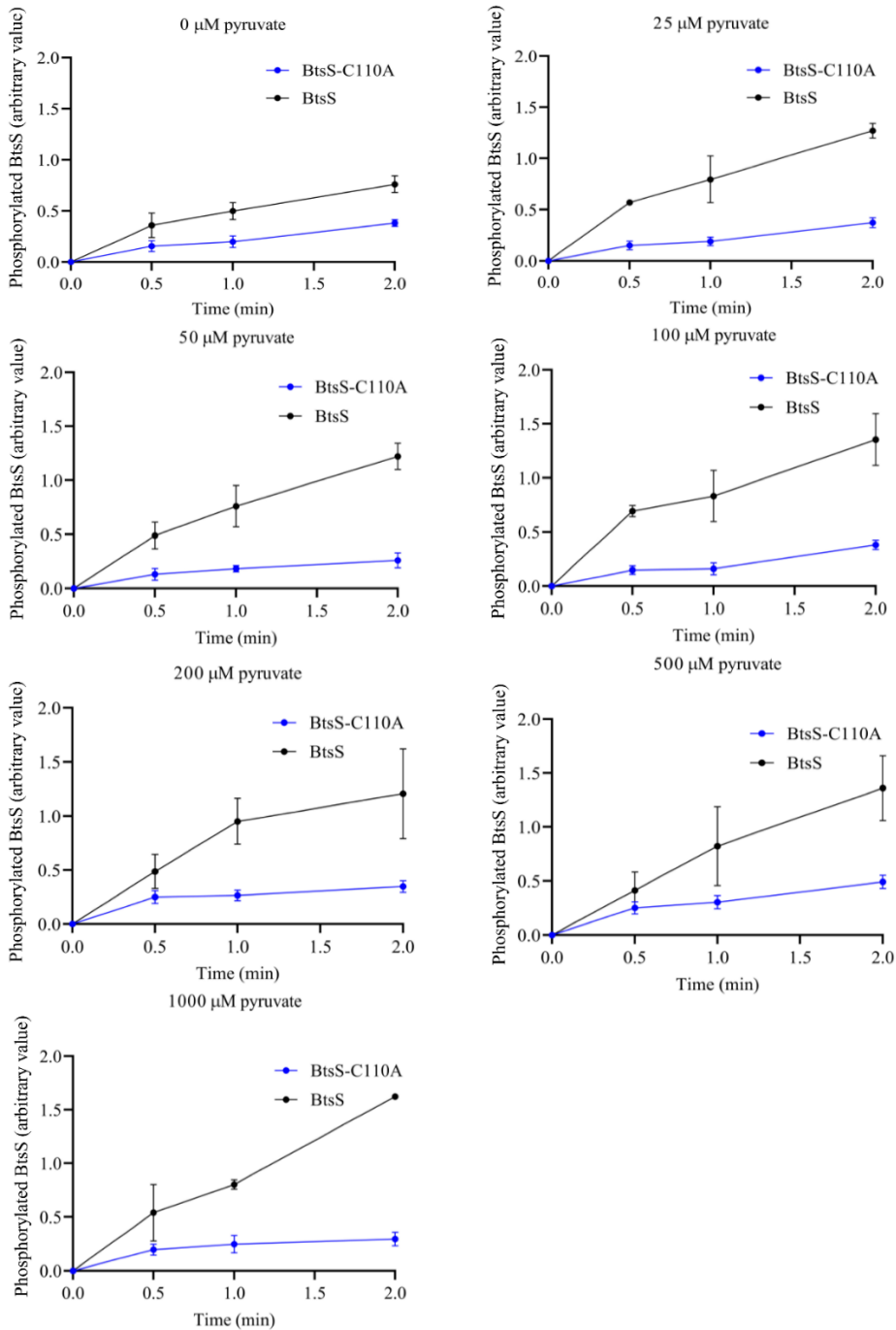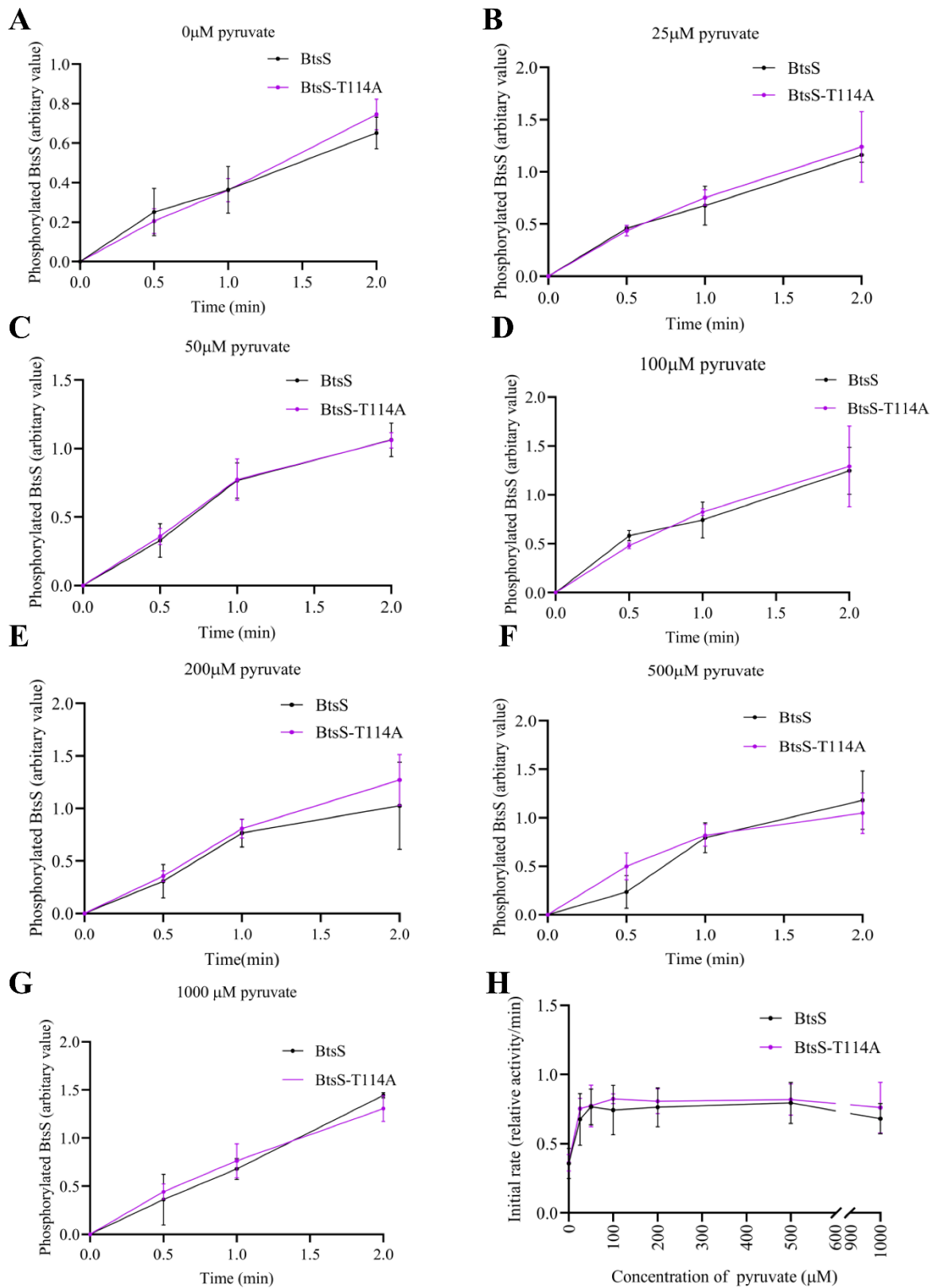
FIG 3.1.12 Influence of increasing pyruvate concentrations on the autophosphorylation activity of BtsS-T114A compared to wild-type BtsS. (A-G) Pyruvate concentration dependency of autokinase activity. (H) The effect of increasing pyruvate concentrations on the initial rate of autophosphorylation BtsS and BtsS-T114AThe same experimental approach as in FIG 3.1.8 was used. Figure was cited from publication: Jin Qiu, Ana Gasperotti, Nathalie Sisattana, Martin Zacharias, and Kirsten Jung. The LytS-type histidine kinase BtsS is a 7-transmembrane receptor that binds pyruvate. mBio. doi: 10.1128/mbio.01089-23. Online ahead of print.

3.2 Insights into BtsS dimerization

3.2.1 BtsS forms dimer for kinase function

Dimerization is necessary for HKs to mediate autophosphorylation by ATP either *in trans* or *in cis* (125). In addition to measuring the autophosphorylation activity, the dimerization of BtsS and its variants were also determined *in vivo*. Bacterial adenylate cyclase based two-hybrid system was used here (106). Previous study showed wild-type BtsS is dimerized in the presence of pyruvate (95), which was indicated by a high β-galactosidase activity that was in the same range as leucine zipper protein GCN4 (positive control) (FIG 3.2.1A). In contrast, individual replacement of amino acids BtsS-Arg72, BtsS-Arg99, BtsS-Cys110 and BtsS-Ser113 with alanine prevented dimerization, which were indicated by very low β-galactosidase activities that were almost in the same range as the value of the negative control. As a control, dimerization of the variant BtsS-T114A was tested and it behaved like the wild-type (FIG 3.2.1A). Variants BtsS-R72A, BtsS-R99A, BtsS-C110A, and BtsS-S113A were produced as intact hybrid proteins which were confirmed by SDS-PAGE and immunodetection (FIGs 3.2.1B-C).
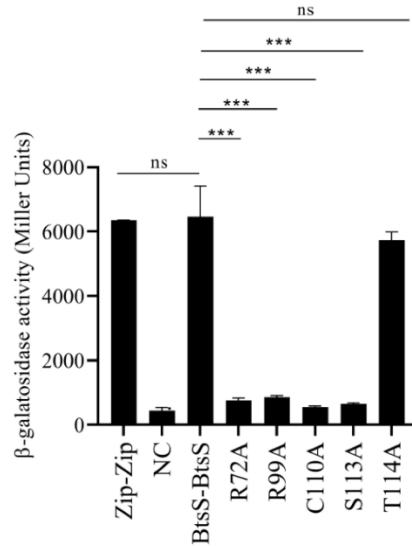
FIG 3.2.1 BACTH-based reporter assay to detect the dimerization of BtsS and its variants. *E. coli* BTH101 was co-transformed with plasmid pairs encoding the C-terminal T18 and C-terminal T25 hybrids. Cells were grown in 0.1 x LB medium supplemented with 0.5 mM IPTG and 100 µM pyruvate at 37°C overnight. The activity of the reporter enzyme β-galactosidase was determined and served as a measure of the strength of the interaction. Dimerization of yeast leucine zipper protein GCN4 (Zip-Zip) was used as a positive control. The pUT18 and pKT25N vectors served as negative control (NC). All experiments were performed in triplicate, and error bars indicate standard deviation of the means. Statistics: Student's unpaired two-sided t-test (*** $p < 0.001$; ** $p < 0.01$; *$p < 0.05$; ns $p > 0.05$). (B)Verification of production and integration of BtsS-T18 and (C) BtsS-T25 variants in the cytoplasmic membrane of *E. coli* BTH101. Cells were disrupted and fractionated, 25 µg protein of the membrane fraction was analyzed by SDS-PAGE and Western blotting. BtsS was detected by a monoclonal mouse antibody against the His tag and an alkaline phosphatase-coupled secondary antibody. Figure 3.1.2A was cited from publication: Jin Qiu, Ana Gasperotti, Nathalie Sisattana, Martin Zacharias, and Kirsten Jung. The LytS-type histidine kinase BtsS is a 7-transmembrane receptor that binds pyruvate. mBio. doi: 10.1128/mbio.01089-23. Online ahead of print.

Under reducing conditions, disulfide bond in dimer can be destroyed. BtsS autokinase activity displayed pyruvate concentration dependency from 0 to 100 mM pyruvate when there was no reducing or oxidizing catalyst added (FIG 3.1.7B). However, autokinase activity was reduced dramatically after treatment with oxidizing or reducing agent (FIG 3.2.2). In conclusion, BtsS functions as a dimer in BtsS/BtsR two-component system.
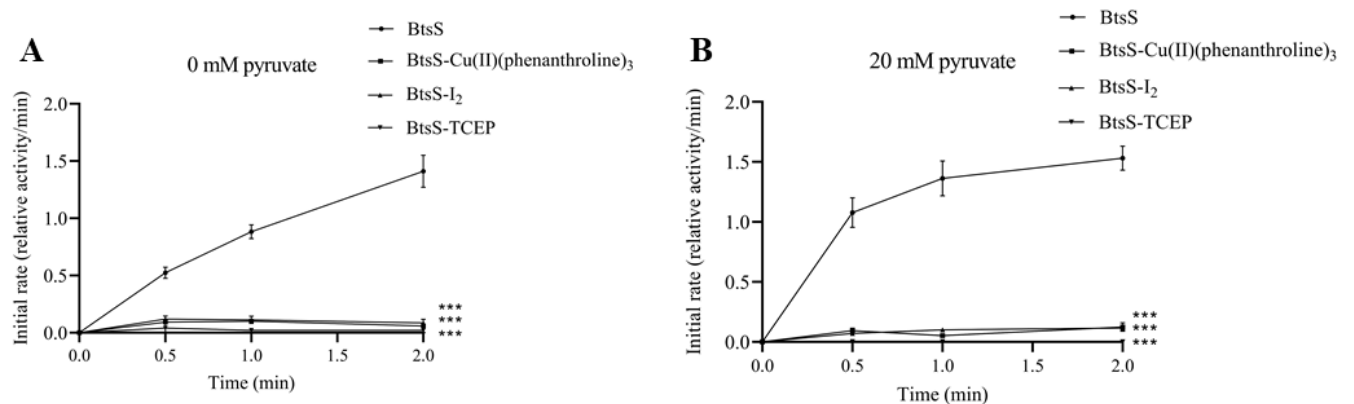
FIG 3.2.2 Autophosphorylation activity detection for BtsS under oxidizing or reducing condition. (A) Time-dependent autophosphorylation of BtsS assayed with no pyruvate. Membrane vesicles from *E. coli* TKR2000 producing BtsS-6His were incubated with either 0.5 mM Cu (II) (1,10-phenanthroline)$_3$, 1 mM iodine or 10 mM TCEP. At time zero, 20 μM [γ-^{32}P] ATP (2.38 Ci/mmol) and 5 mM MnCl$_2$ was added. Reactions were stopped at the indicated time point, and phosphorylated proteins were separated by SDS-PAGE, followed by phosphoimage analysis. BtsS autokinase activity was quantified using ImageQuant. Shown are the relative values normalized to the phosphorylation level of wild-type BtsS after incubation with 50 μM pyruvate and 5 mM MnCl$_2$ for 5 min (value of 1.0). (B) Time-dependent autophosphorylation of BtsS assayed with 20 mM pyruvate. Same protocol was used as (A). All experiments were performed in triplicate, and error bars indicate standard deviation of the means. Statistics: Student's unpaired two-sided t-test (*** $p < 0.001$; ** $p < 0.01$; * $p < 0.05$; ns $p > 0.05$).

3.2.2 BtsS-Cys15 is likely to form disulfide bond but it is not essential for signal transduction

Although the dimerization of BtsS was determined, what was still unclear is which Cys is responsible for dimerization. There are seven cysteine amino acids in BtsS. When looking into the model of BtsS predicted by Alphafold2.0, Cys15, located in first helix of transmembrane domain, might be involved in dimerization formation of BtsS since it was in the interface of each monomer. To verify this hypothesis, site-directed mutagenesis was done for Cys15. Initially, it was replaced by alanine to abolish the functional group, followed by replacement with negative charged aspartate and glutamate, positive charged lysine and similar sized serine to determine if Cys15 was necessary for BtsS/BtsR system. Subsequently, these variants and wild type were tested by complementation of reporter strain lacking the *btsS/R* genes and expressing a *btsT* promoter-luciferase fusion (P$_{btsT}$::*luxCDABE*). Fold-change of *btsT* expression for wild type and variants BtsS-C15A, BtsS-C15D, BtsS-C15K and BtsS-C15S were 487.60±108.2, 75.79±20.30, 36.95±7.14, 91.94±23.04, respectively, when pyruvate was used as a C source. Expression level of *btsT* was decreased after BtsS-Cys15 was replaced with these four amino acids. Variant BtsS-C15D, BtsS-C15K and BtsS-C15S showed almost no *btsT* induction with all indicated concentrations of pyruvate (FIG 3.2.3A). But variant BtsS-C15A and BtsS-C15E showed pyruvate concentration dependence (FIG 3.2.3B), even though induction level of *btsT* expression was lower than wild type, which means BtsS-C15A/BtsR and BtsS-C15E/BtsR could still sense pyruvate. Besides, all the variants were produced successfully (FIG 3.2.3C). Thus, BtsS-Cys15 is likely to form disulfide bond since BtsS formed dimer for function and one Cys15 on one monomer is close to the other Cys15 on another monomer, but it is not essential for signal transduction function *in vivo*.
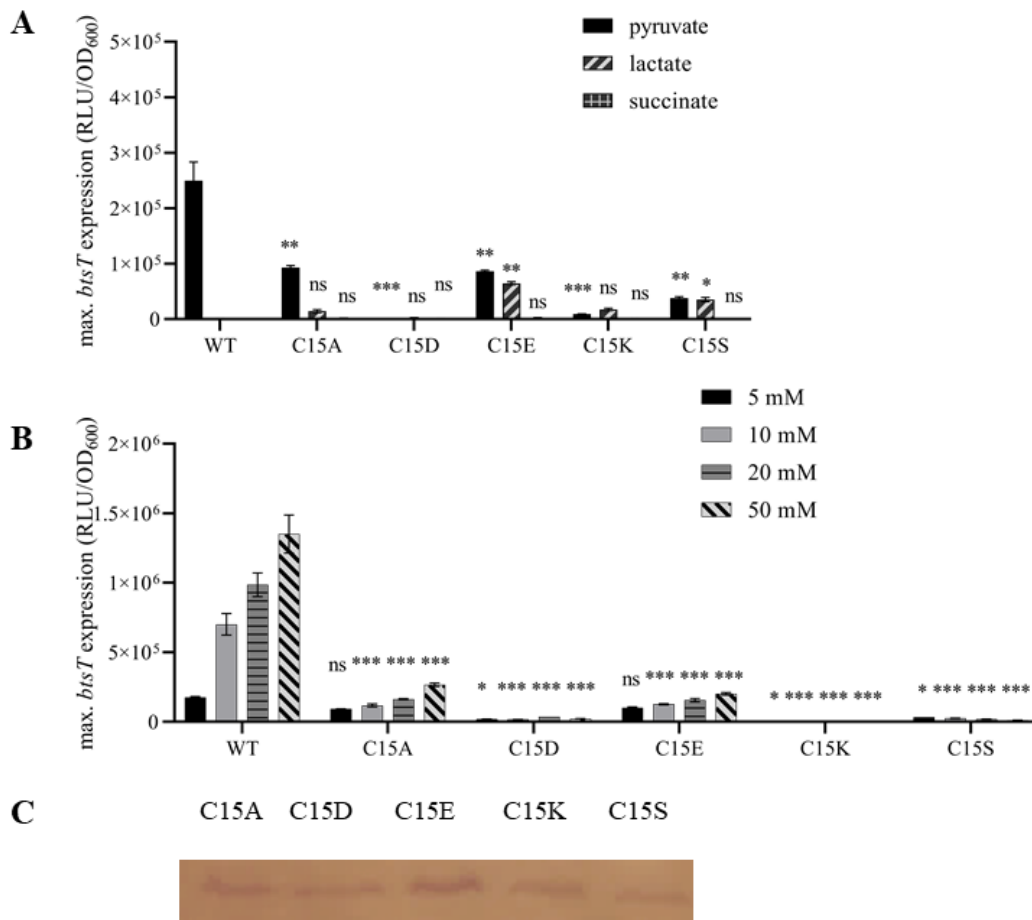
FIG 3.2.3 BtsS-Cys15 is not necessary for BtsS/BtsR system to sense pyruvate. pBAD24-*btsS/R* or variants were transformed with *E. coli* MG1655Δ*btsSR*/pBBR-*btsT-lux*. Growth and the activity of the reporter enzyme luciferase were determined. (A) Cells were grown in M9 minimal medium plus 5 mM pyruvate, lactate or succinate supplemented with 15 mM succinate. (B) Cells were grown in M9 minimal medium plus indicated concentration of pyruvate supplemented with succinate to make the total carbon sources constant. Growth and luciferase activity were monitored continuously. The maximal luciferase activity normalized to an optical density of 1 (RLU/OD$_{600}$) was used as a measure of the degree of induction of *btsT*. All experiments were performed at least three times, and the error bars indicate the standard deviations of the means. Statistical analysis was performed by using unpaired t-test/Assuming Gaussian distribution. Statistics: Student's unpaired two-sided t-test (*** $p < 0.001$; ** $p < 0.01$; *$p < 0.05$; ns $p >$

0.05). (C) Verification of production and integration of BtsS variants in the cytoplasmic membrane of *E. coli*. Cells were disrupted and fractionated, 25 µg protein of the membrane fraction was analyzed by SDS-PAGE and Western blotting. BtsS was detected by a monoclonal mouse antibody against the Flag tag and an alkaline phosphatase-coupled secondary antibody.

3.3 BtsS-Arg192 plays an important role in BtsS and BtsR interaction

3.3.1 BtsS-Arg192 affects pyruvate response for BtsS/BtsR system

When screening which amino acids were involved in pyruvate sensing by alanine scanning mutagenesis, BtsS-Arg192 was found to affect *btsT* expression based on *in vivo* expression results (FIG 3.3.1). With the same mutagenesis strategy, BtsS-Arg192 was replaced with alanine. *In vivo btsT* expression was assayed as described before and results showed that variant BtsS-R192A was not able to induce *btsT* expression (FIG 3.3.1A). Besides, there was almost no *btsT* expression when assayed with 5 mM, 10 mM, 20 mM or 50 mM pyruvate (FIG 3.3.1B). Furthermore, to identify if BtsS-Arg192 was necessary for BtsS/BtsR system, it was replaced with amino acids which is similarly charged (histidine and lysine), opposite charged (glutamate) or similar sized (glutamine). Wild type and variants were tested with the same complementation reporter strain as described. Results showed that variant BtsS-R192H, BtsS-R192K, BtsS-R192Q and BtsS-R192E induced *btsT* expression, even though the expression level was lower than wild type (FIG 3.3.1C). The production and integration of all BtsS variants into the cytoplasmic membrane of *E. coli* was tested by resolving the proteins of the membrane fractions by SDS-PAGE and Western blot detection. All BtsS variants were produced successfully (FIG 3.3.1D). The conclusion is BtsS-

Arg192 is somehow involved in pyruvate response, but this amino acid is not a necessary amino acid for BtsS/BtsR system.
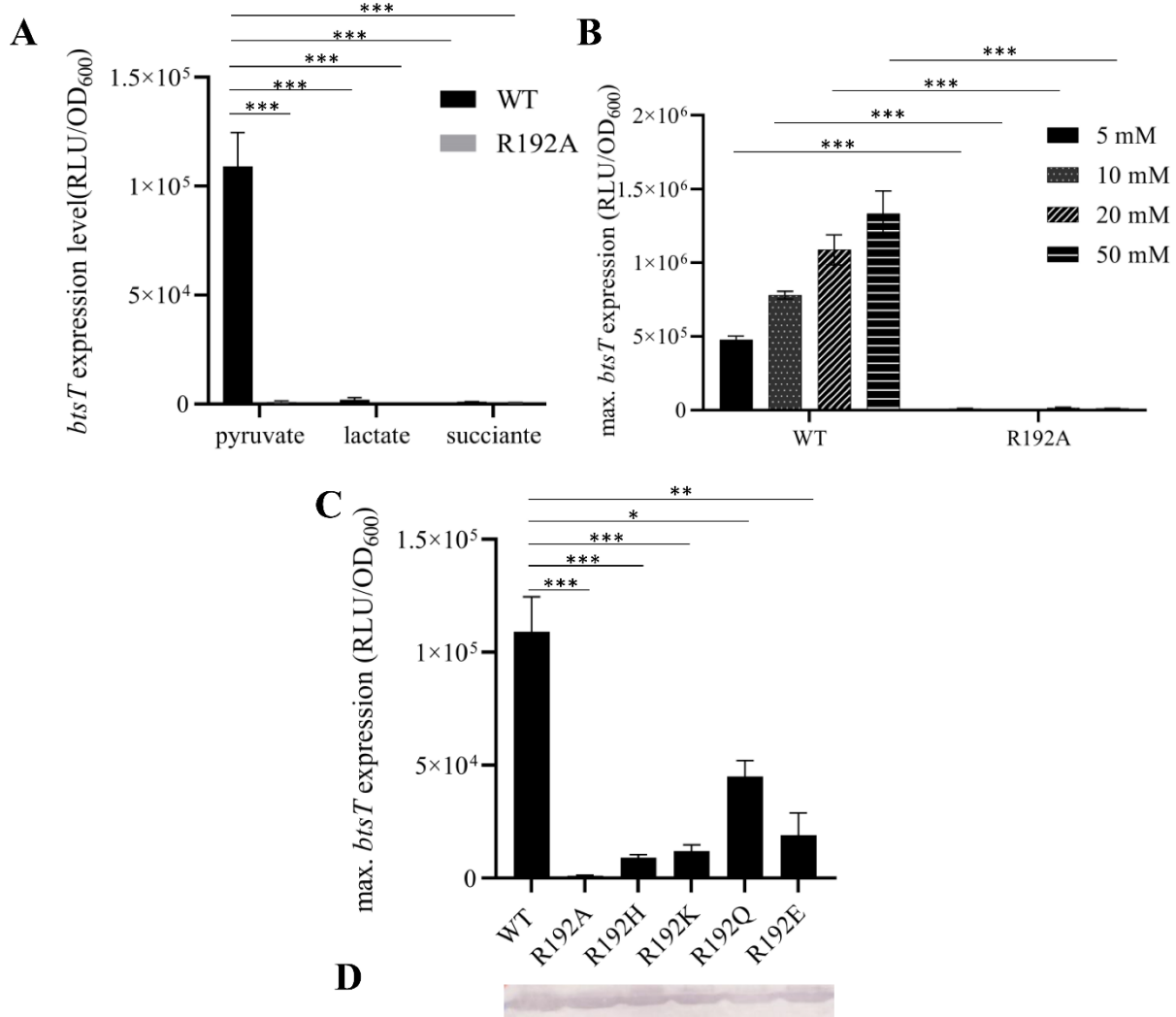
FIG 3.3.1 BtsS-Arg192 affects the BtsS/BtsR system for sensing pyruvate. pBAD24-*btsS/R* or variants were transformed with *E. coli* MG1655Δ*btsSR*/pBBR-*btsT-lux*. Growth and the activity of the reporter enzyme luciferase were determined. (A) Cells were grown in M9 minimal medium plus 5 mM pyruvate, lactate or succinate supplemented with 15 mM succinate. (B) Cells were grown in M9 minimal medium plus indicated concentration of pyruvate supplemented with succinate to make the total carbon sources constant. Growth and luciferase activity were monitored continuously. The maximal luciferase activity normalized to an optical density of 1 (RLU/OD$_{600}$) was used as a

measure of the degree of induction of *btsT*. All experiments were performed at least three times, and the error bars indicate the standard deviations of the means. Statistical analysis was performed by using unpaired t-test/Assuming Gaussian distribution. Statistics: Student's unpaired two-sided t-test (*** $p < 0.001$; ** $p < 0.01$; *$p < 0.05$; ns $p > 0.05$). Figure was cited from publication: Jin Qiu, Ana Gasperotti, Nathalie Sisattana, Martin Zacharias, and Kirsten Jung. The LytS-type histidine kinase BtsS is a 7-transmembrane receptor that binds pyruvate. mBio. doi: 10.1128/mbio.01089-23. Online ahead of print.

3.3.2 BtsS-R192A affects the interaction between BtsS and BtsR

Paragraph below was cited from publication: Jin Qiu, Ana Gasperotti, Nathalie Sisattana, Martin Zacharias, and Kirsten Jung. The LytS-type histidine kinase BtsS is a 7-transmembrane receptor that binds pyruvate. mBio. doi: 10.1128/mbio.01089-23. Online ahead of print.

To identify how BtsS-Arg192 affects *btsT* expression, autophosphorylation of BtsS and BtsS-R192A was tested under the same conditions as described before, which contains 0 µM, 50 µM, 100 µM, 200 µM, 500 µM or 1 mM pyruvate and 5 mM $MnCl_2$ as the cofactor. The activity and initial rate of BtsS-R192A autophosphorylation was in the same level as wild type, which means pyruvate binding, BtsS dimerization and autophosphorylation of BtsS were still functional after replacement of BtsS-Arg192 with alanine (FIG 3.3.2). Thus, these processes did not get affected by the amino acid substitution.
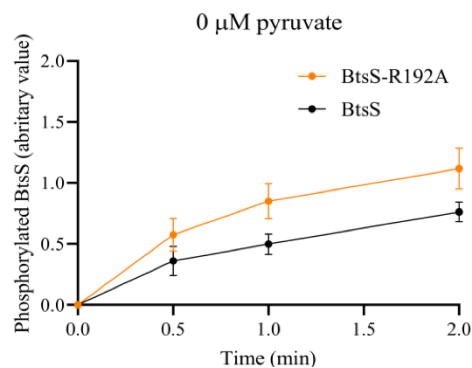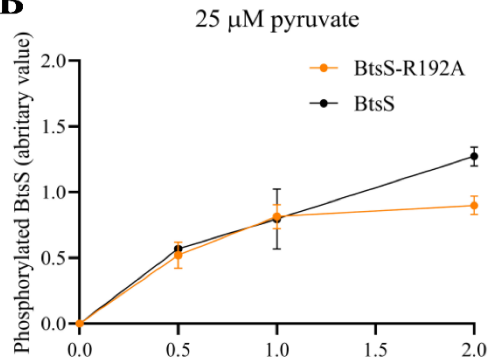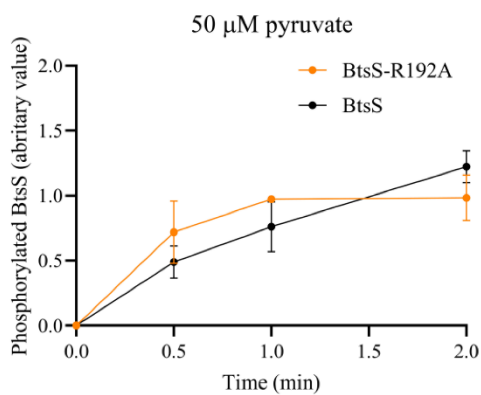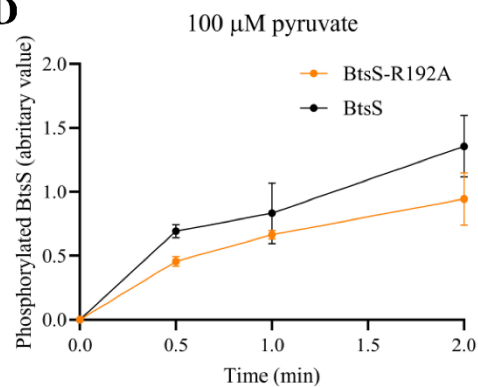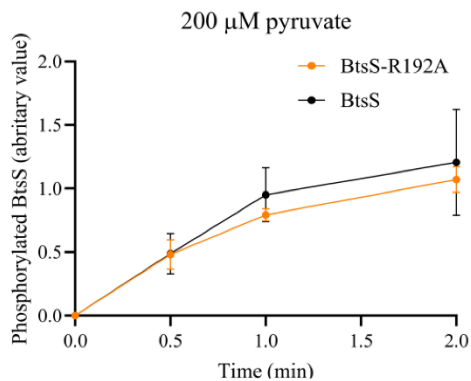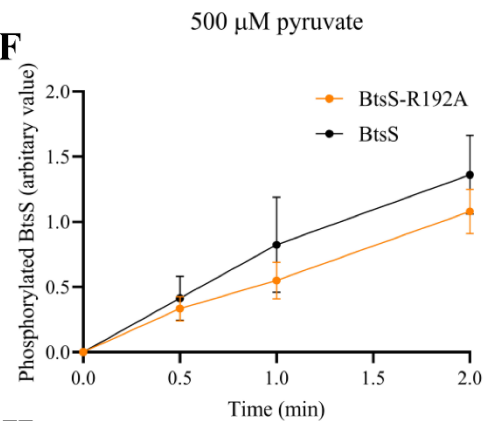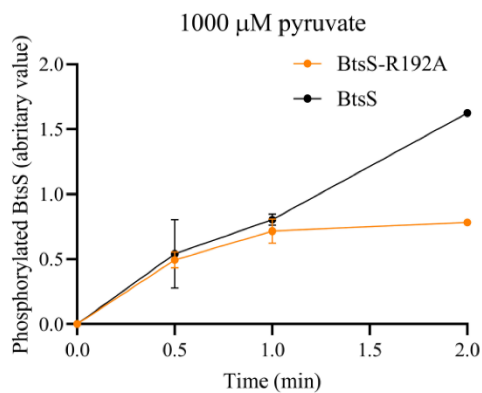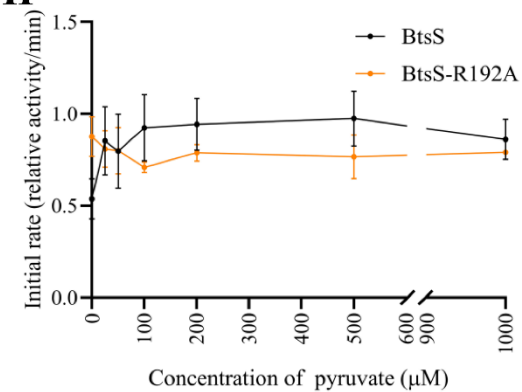
FIG 3.3.2 Influence of increasing pyruvate concentrations on the autophosphorylation activity of BtsS-R192A compared to wild-type BtsS. (A-G) Autophosphorylation activity of BtsS, BtsS-R192A. 2 mg/mL membrane vesicles prepared from *E. coli* TKR2000 producing BtsS-6His and BtsS-S25A-6His were incubated with 20 µM [γ-^{32}P] ATP (2.38 Ci/mmol) and indicated concentration cold pyruvate. Reactions were stopped after 0.5, 1 and 2-min incubation. Wild type membrane vesicles incubated for 5 min with 50 µM cold pyruvate was used as a standard. Phosphorylated proteins were separated on 12.5% SDS-PAGE and radioactivity was detected by autoradiography after overnight exposure. Phosphorylation initial rate was quantified with ImageQuant. Activity of the standard is considered as 100%.). (H) The effect of increasing pyruvate concentrations on the initial rate of autophosphorylation of BtsS, BtsS-R192A. Samples were processed and data were calculated as described in A-G. Figure was cited from publication: Jin Qiu, Ana Gasperotti, Nathalie Sisattana, Martin Zacharias, and Kirsten Jung. The LytS-type histidine kinase BtsS is a 7-transmembrane receptor that binds pyruvate. mBio. doi: 10.1128/mbio.01089-23. Online ahead of print.

In addition to detecting the autophosphorylation activity, interactions of BtsS and BtsR for wild-type BtsS and R192A variant were determined using bacterial adenylate cyclase based two-hybrid system (23). The results showed wild-type BtsS interacted with BtsR as indicated by a high β-galactosidase activity that was in the same range as the positive control (leucine zipper protein GCN4) (FIG 3.3.3). In contrast, replacement of BtsS-Arg192 with alanine prevented interaction between BtsS and BtsR, as indicated by very low β-galactosidase activities that were almost in the same range as the value of the negative control. These hybrid proteins variants were all produced as confirmed by SDS-PAGE and immunodetection.
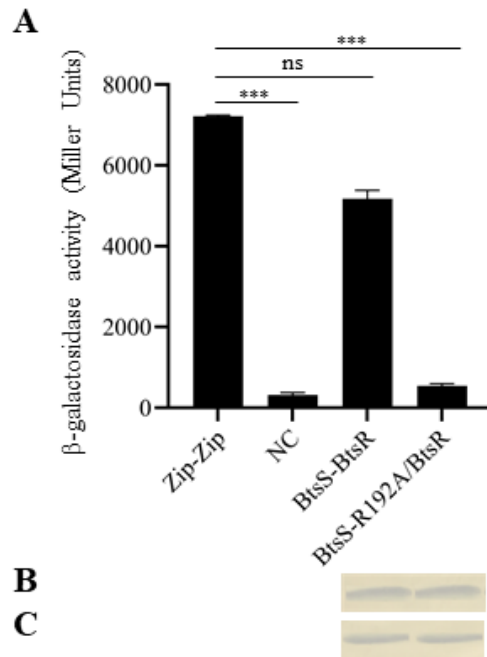
FIG 3.3.3 Determination of BtsS/BtsR or BtsS-R192A/BtsR interaction by β-galactosidase assay. (A) A two-hybrid assay based on fragmented bacterial adenylate cyclase (Cya) was used to identify BtsS-BtsS dimerization *in vivo*. For this purpose, fragments T18 and T25 of Bordetella pertussis CyaA were fused to BtsS or mutants as indicated, while fusions to yeast leucine zipper fragments were used as a positive control (Zip-Zip) (7,000 Miller units). *E. coli* BTH101 was co-transformed with plasmid pairs encoding the C-terminal T18 and C-terminal T25 hybrids. Cells were grown under aerobic conditions in 0.1×LB medium supplemented with 0.5 mM IPTG and 100 µM pyruvate at 37°C overnight. The activity of the reporter enzyme β-galactosidase was determined and served as a measure of the interaction strength. The experiment was performed in triplicate, and error bars indicate standard deviations of the means. Statistical analysis was performed by using unpaired t-test/Assuming Gaussian distribution. Statistics: Student's unpaired two-sided t-test (*** $p < 0.001$; ** $p < 0.01$; *$p < 0.05$; ns $p > 0.05$). (B) Verification of production and integration of BtsS or BtsS-R192A of *E. coli*. Cells were disrupted and fractionated, 15 µg protein of the membrane fraction was analyzed by SDS-PAGE and Western blotting. BtsS or BtsS-R192A variant were detected by a monoclonal mouse antibody against the His tag and an alkaline phosphatase-coupled secondary antibody.

3.4 Replacement BtsS-Ser25 with alanine or valine keeps BtsS in an ON state

3.4.1 Replacement BtsS-Ser25 with alanine or valine induces *btsT* expression

Ser25 is located at end of the first helix of BtsS. After it was replaced with alanine, expression of *btsT* could be induced when assayed with different compounds (FIG 3.4.1A). As for wild type, *btsT* was induced when pyruvate was used as sole C source. Serine could also trigger the expression of *btsT* since serine is the first conversion product from pyruvate. Induction was significantly reduced when cells were grown in minimal medium supplemented with amino acids (Ala, Asn, Asp, Arg, Lys) as sole C source. Growth on typical phosphotransferase system (PTS) sugars, e.g., glucose, galactose, mannose, mannitol, and fructose, barely activated *btsT* expression. However, BtsS-S25A/BtsR showed different patterns under each condition. Expression of *btsT* could be induced by most of those compounds (except for alanine, aspartate, asparagine and LB) and the level was much higher than that wild type. Cells grew very slow in M9 minimal medium plus alanine, aspartate or asparagine. All these results showed that replacement BtsS-Ser25 with alanine might block BtsS kinase in an ON state (FIG 3.4.1A).

To verify the function of alanine in this position, BtsS-Ser25 was replaced by other amino acids (valine, threonine and tryptophan). Here, valine is polar as alanine, threonine is similar as serine. The functional group of tryptophan is big which will occupy more space and might also block the kinase. Results of *in vivo* assay showed that BtsS-S25V/BtsR could induce *btsT* expression when those compounds were added in the medium, while BtsS-S25T/BtsR behaved like wild type. BtsS-S25W/BtsR couldn't response to any tested compound because protein BtsS-S25W was not produced by checking with Western blot (FIGs 3.4.1B and C). Here, the hypothesis is alanine or valine in 25th amino acid position could keep BtsS in an ON state resulting in a response to all compounds tested.
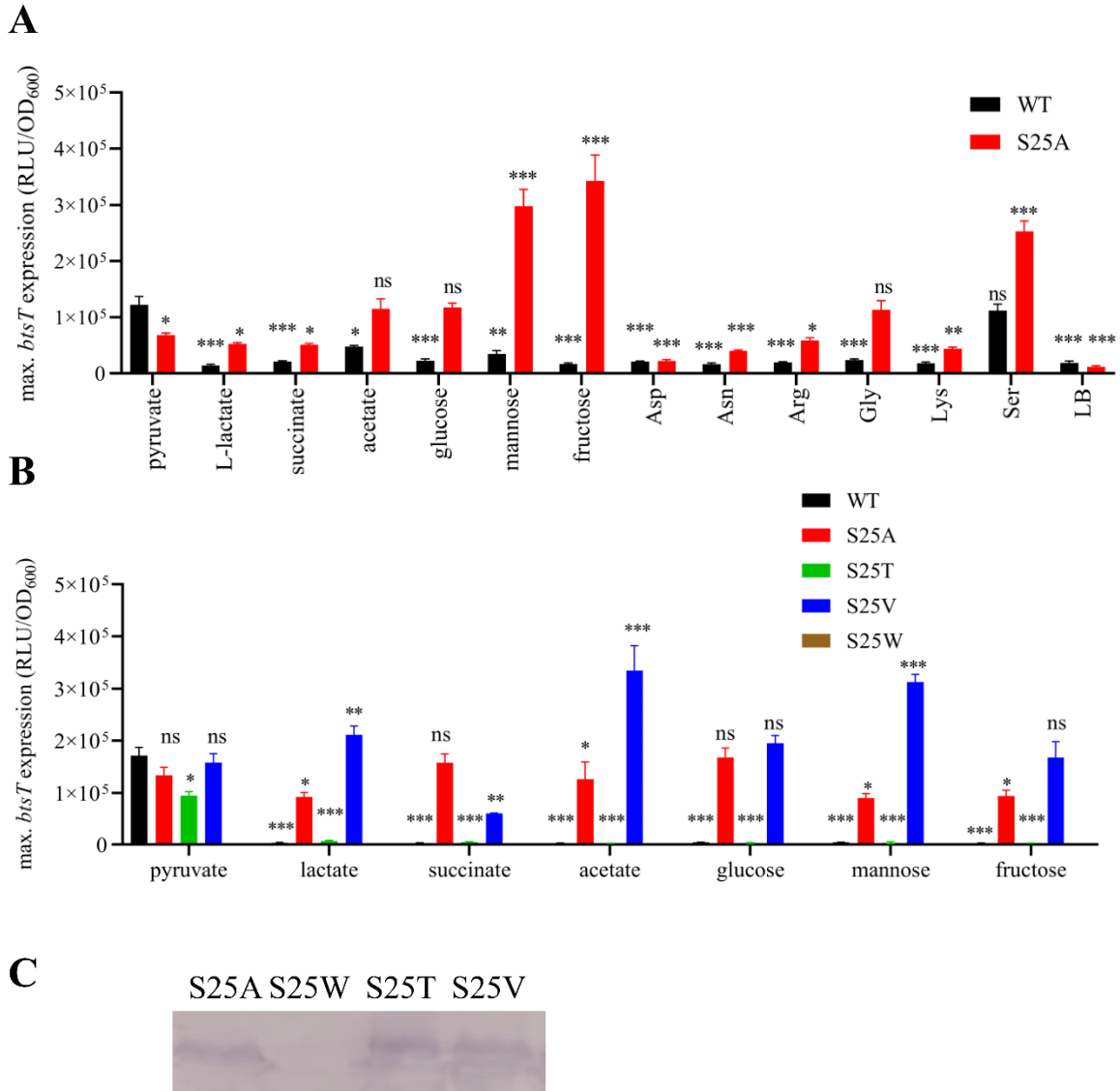
FIG 3.4.1 BtsS-Ser25 affects the BtsS/BtsR system for sensing. pBAD24-*btsSR* or variants were transformed with

E. coli MG1655Δ*btsSR*/pBBR-*btsT-lux*. Growth and the activity of the reporter enzyme luciferase were determined.

(A) Bacteria were cultivated under aerobic conditions in complex medium (LB) or M9 minimal medium with the

indicated carbon sources (20 mM amino acids, 0.5% [wt/vol] all other carbon sources). (B) Cells were grown in M9

minimal medium plus indicated carbon sources (0.5% [wt/vol] carbon sources). Growth and luciferase activity were

monitored continuously. The maximal luciferase activity normalized to an optical density of 1 (RLU/OD$_{600}$) was used

as a measure of the degree of induction of *btsT*. All experiments were performed at least three times, and the error bars

indicate the standard deviations of the means. Statistics: Student's unpaired two-sided t-test (*** p < 0.001; ** p <

0.01; *p < 0.05; ns p > 0.05). (C) Verification of production and integration of BtsS variants in the cytoplasmic membrane of *E. coli*. Cells were disrupted and fractionated, 25 µg protein of the membrane fraction was analyzed by SDS-PAGE and Western blotting. BtsS was detected by a monoclonal mouse antibody against the Flag tag and an alkaline phosphatase-coupled secondary antibody.

3.4.2 Alanine replacement on BtsS-Ser25 can enhance thermostability of BtsS

Besides, thermostability of BtsS and variant BtsS-S25A was detected by nanoDSF. His-tagged BtsS and BtsS-A25A were overproduced in *E. coli* TKR2000 strain and subsequent purification via Ni-NTA-affinity chromatography was performed and determined by SDS-PAGE. Details can be found in [Methods]. Concentration of BtsS in elution fractions E2, E3, E4 and E5 were 0.55 µg/µl, 0.52 µg/µl, 0.50 µg/µl, 0.63 µg/µl and the corresponding amount loaded in per lane was 2.64 ng, 2.46 ng, 2.4 ng and 3.024 ng. Concentration of BtsS-S25A from E2 to E5 fractions were 0.57 µg/µl, 3.45 µg/µl, 1.67 µg/µl and 0.42 µg/µl and the amount was 3.12 ng, 11.76 ng, 8.01 ng and 2.02 ng (FIG 3.4.2).
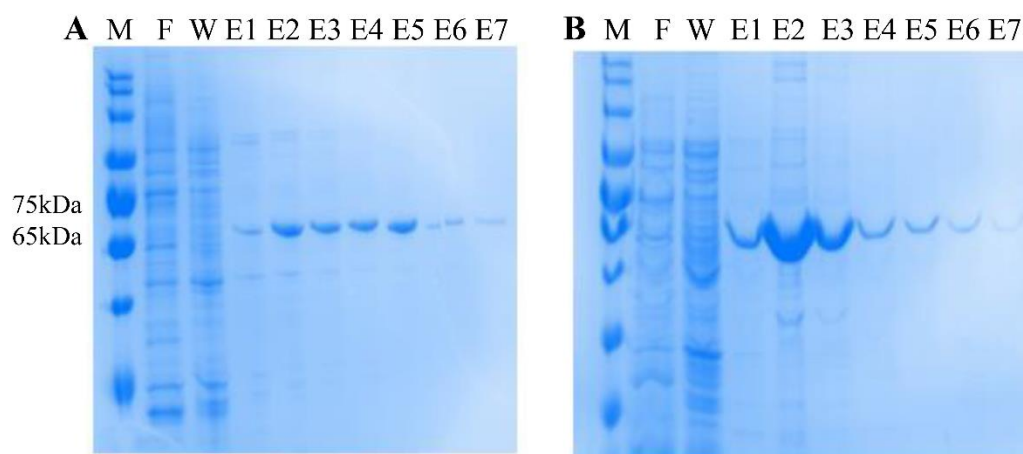
FIG 3.4.2 Purification of (A) BtsS-6His and (B) BtsS-S25A-6His. *E. coli* TKR2000 was transformed with pBAD24-*btsS*-6His or pBAD24-*btsS*-S25A-6His. After inoculation in KML medium (OD_{600}=0.05) cells were grown aerobically at 37°C to an OD_{600} of 0.5 before overproduction of BtsS-6His and BtsS-S25A-6His was induced by the addition of

0.2% (w/v) arabinose. BtsS-6His and BtsS-S25A-6His were purified with Ni-NTA affinity purification. Resin was equilibrated by 30 mM imidazole, 20 mM Tris HCl, pH 8.0, 250 mM NaCl, 1 mM DTT, 10% Glycerol, 0.02% DDM. Elution buffer component is the same as above but with different concentrations of imidazole. E1 was fraction eluted with buffer containing 100 mM imidazole. E2 was fraction eluted with buffer containing 200 mM imidazole. E3 was fraction eluted with buffer containing 300 mM imidazole. E4 was fraction eluted with 400 mM imidazole containing buffer. E5 to E7 were fractions eluted with buffer containing 500 mM imidazole. M: marker, F: flow through fraction, W: wash fraction.

2.5 mg/ml purified BtsS or BtsS-S25A was mixed with several concentrations of pyruvate and lactate. As for wild type, the midpoint temperature of thermal unfolding (T_m) showed a tendency to increase as more pyruvate was added (ΔT_m=5.6±0.6 °C with a range of pyruvate from 0 mM to 250 mM), while T_m value was quite low and barely changed when there was more lactate added (FIG 3.4.3A). It also fits with former results that wild-type BtsS/BtsR is specific for pyruvate response (84). However, T_m value of variant BtsS-S25A was increased when assayed with more pyruvate and lactate. Midpoint temperature tested with 250 mM pyruvate was increased by 20.1±0.3 °C compared with the value tested with 0 mM pyruvate. ΔT_m was 19.2±0.6 °C when tested with lactate in the same concentration as pyruvate, which indicated BtsS-S25A was more stable than BtsS and both pyruvate and lactate could enhance the stability of BtsS-S25A (FIG 3.4.3B).
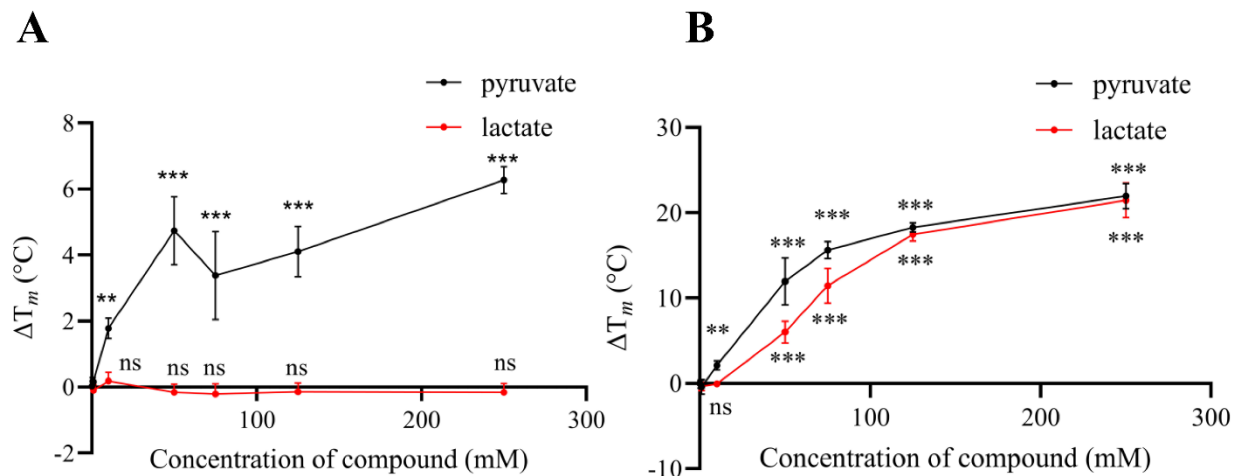
FIG 3.4.3 BtsS-S25A is more thermostable than BtsS. Thermostablility assayed by using nanoDSF for BtsS (A) and BtsS-S25A (B). BtsS-6His and BtsS-S25A-6His were purified from *E. coil* TKR2000. NanoDSF experiment was conducted by adding 0, 0.5 mM, 1 mM, 10 mM, 50 mM, 250 mM pyruvate or lactate with puried proteins. The concentration of purified protein is 2.5 mg/ml. The temperature is set from 40 to 80°C. All experiments were performed in triplicate, and error bars indicate standard deviation of the means. Statistics: Student's unpaired two-sided t-test (*** $p < 0.001$; ** $p < 0.01$; *$p < 0.05$; ns $p > 0.05$).

3.4.3 Replacement BtsS-Ser25 with alanine can increase autokinase activity

Autophosphorylation assay was conducted for both wild type BtsS and variant BtsS-S25A with indicated concentration of pyruvate. Details can be seen in [Method]. Results showed that in each assayed pyruvate concentration, phosphorylation activity of BtsS-S25A was 2 to 4-fold higher than that BtsS. It means the processes before autophosphorylation were functional. Initial rate of BtsS-S25A was also higher than wild type under each concentration of pyruvate tested condition (FIG 3.4.4).

92

A 0 μM pyruvate

B 25 μM pyruvate

C 50 μM pyruvate

D 100 μM pyruvate

E 200 μM pyruvate

F 500 μM pyruvate

G 1000 μM pyruvate

H
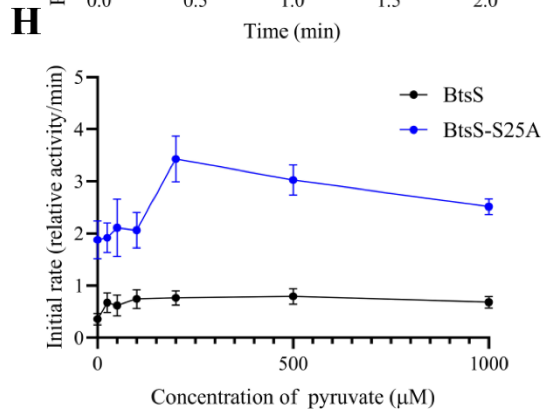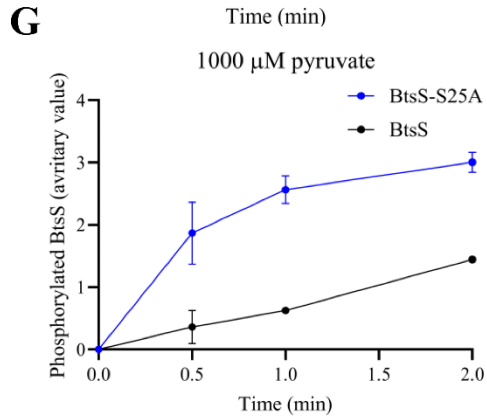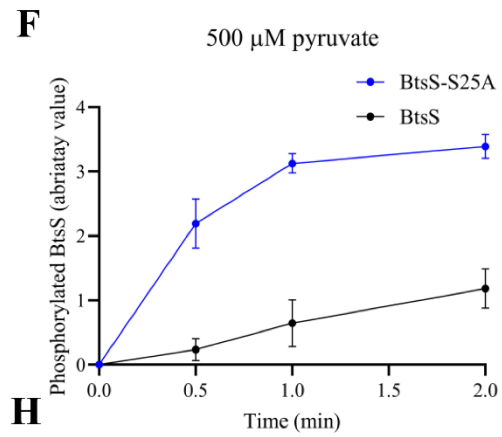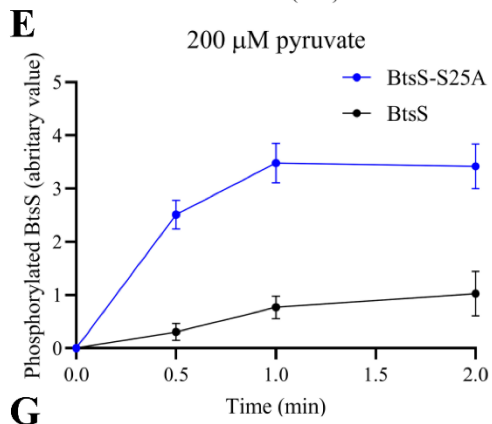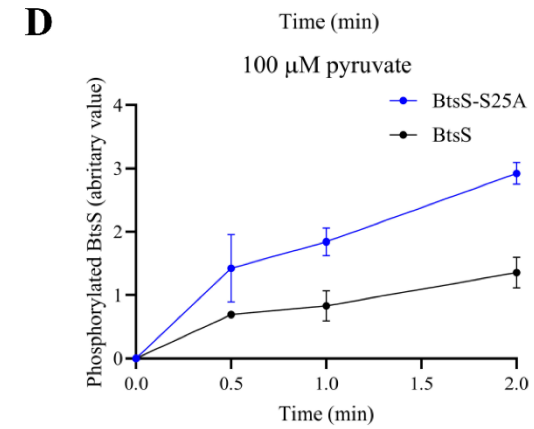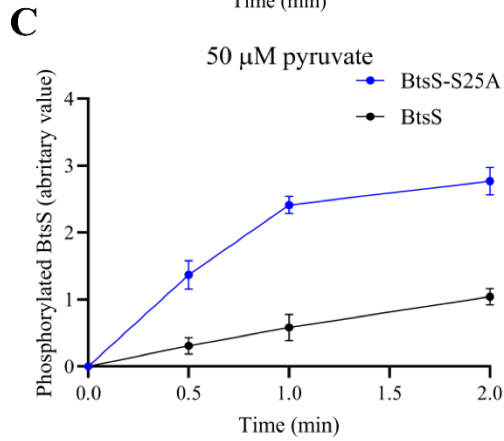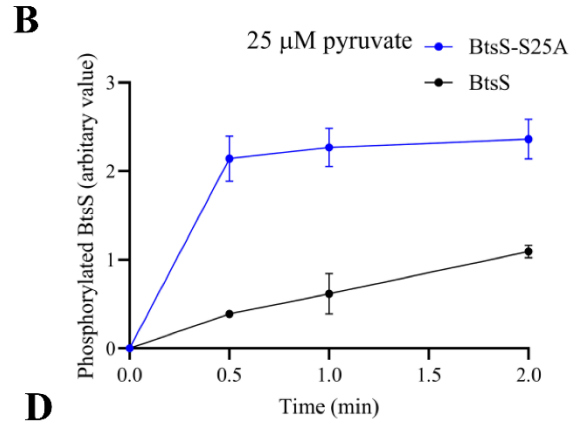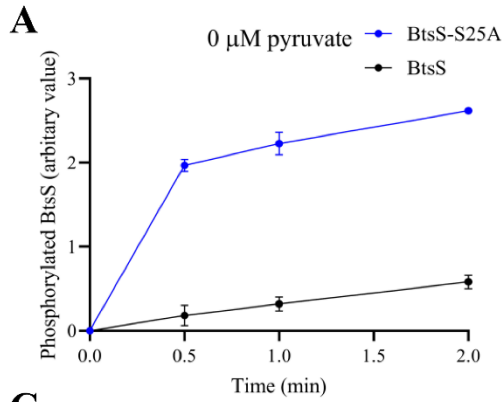
FIG 3.4.4 Autophosphorylation assay of BtsS and BtsS-S25A. (A-G) Influence of increasing pyruvate concentrations on theautophosphorylation activity of BtsS and BtsS-S25A. (H) The effect of increasing pyruvate concentrations on the initial rate of autophosphorylation BtsS and BtsS-S25A. Membrane vesicles prepared from *E. coli* TKR2000 incubated in the presence 50 µM pyruvate. At time zero, 20 µM [γ-^{32}P] ATP (2.38 Ci/mmol) plus either 5 mM MnCl$_2$ was added. Reactions were stopped at the time indicated, and phosphorylated proteins were separated by SDS-PAGE followed by phosphoimage analysis. Activity for WT that incubated with 50 µM pyruvate, 5 mM MnCl$_2$ for 5 min is regarded as 1.

3.4.4 Alanine replacement on BtsS-Ser25 has no effect on BtsS and BtsR interaction

Interaction between BtsS-S25A and BtsR was also detected with bacterial adenylate cyclase based two-hybrid system (23). Wild-type BtsS interacts with BtsR, as indicated by a high β-galactosidase activity that was in the same range as the positive control (yeast leucine zipper protein Zip-Zip) (FIG 3.4.5). Replacement of BtsS-Ser25 with alanine didn't affect the interaction between BtsS and BtsR, as indicated by a higher β-galactosidase activity than that from BtsS/BtsR. Wild type BtsS and variant BtsS-S25A were produced as intact hybrid proteins as confirmed by SDS-PAGE and immunodetection.
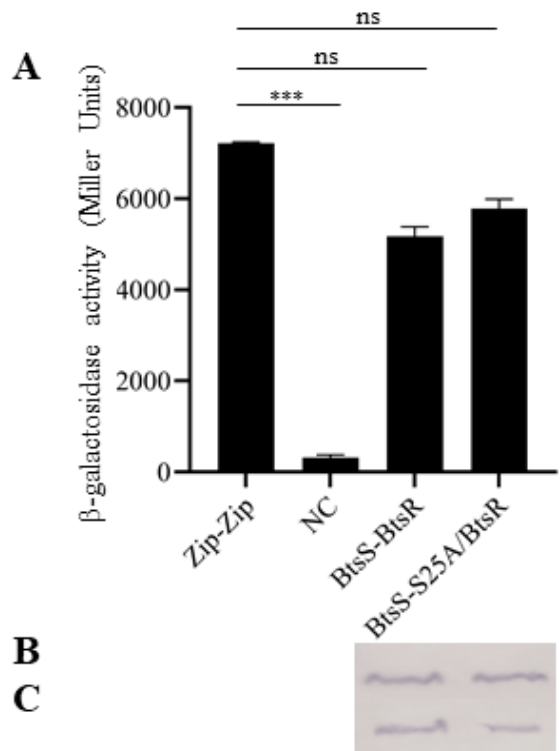
FIG 3.4.5 BACTH-based reporter assay to detect the interaction of BtsS/BtsR and BtsS-S25A/BtsR. (A) *E. coli* BTH101 was co-transformed with plasmid pairs encoding the C-terminal T18 and C-terminal T25 hybrids. Cells were grown in 0.1 x LB medium supplemented with 0.5 mM IPTG and 100 µM pyruvate at 37°C overnight. The activity of the reporter enzyme β-galactosidase was determined and served as a measure of the interaction strength. Dimerization of the yeast leucine zipper protein (Zip-Zip) was used as a positive control. The pUT18 and pKT25N vectors served as negative control (NC). All experiments were performed in triplicate, and error bars indicate standard deviation of the means. Statistical analysis was performed for wild type and mutants using unpaired t-test/Assuming Gaussian distribution. Statistics: Student's unpaired two-sided t-test (*** $p < 0.001$; ** $p < 0.01$; *$p < 0.05$; ns $p > 0.05$). (B) Verification of production and integration of BtsS or BtsS-S25A of *E. coli*. Cells were disrupted and fractionated. 15 µg protein of the membrane fraction was analyzed by SDS-PAGE and Western blotting. BtsS or variant were detected by a monoclonal mouse antibody against the His tag and an alkaline phosphatase-coupled secondary antibody.

3.5 Conversion of BtsS into a lactate sensor

3.5.1 Rational design for BtsS based on pyruvate binding information

Once the pyruvate binding pocket was identified, what to do next is to convert BtsS into a lactate sensor by mutagenesis to convert BtsS as a lactate biosensor to use it in medical field. The structure of pyruvate and lactate was firstly analyzed. Hydroxyl group of lactate requires a strong H-bond acceptor. Arg72 and Arg99 are in contact with the pyruvate carbonyl group. This means that one possibility was to keep Arg99 and replace Arg72 with a Glu residue. Additionally, a nearby Glu117 should be mutated into a neutral Gln, otherwise the two Glu residues would result in a predominantly negative potential so that neither lactate nor pyruvate binds (FIG 3.5.1A). Another possibility was to change the Gln154, which is located near the pyruvate carbonyl group, to a stronger H-bond acceptor Glu and replace the adjacent Glu151 to a Gln, to avoid the negative charged environment (FIG 3.5.1B). Both proposals could possibly stabilize lactate binding by a corresponding new H-bridge.
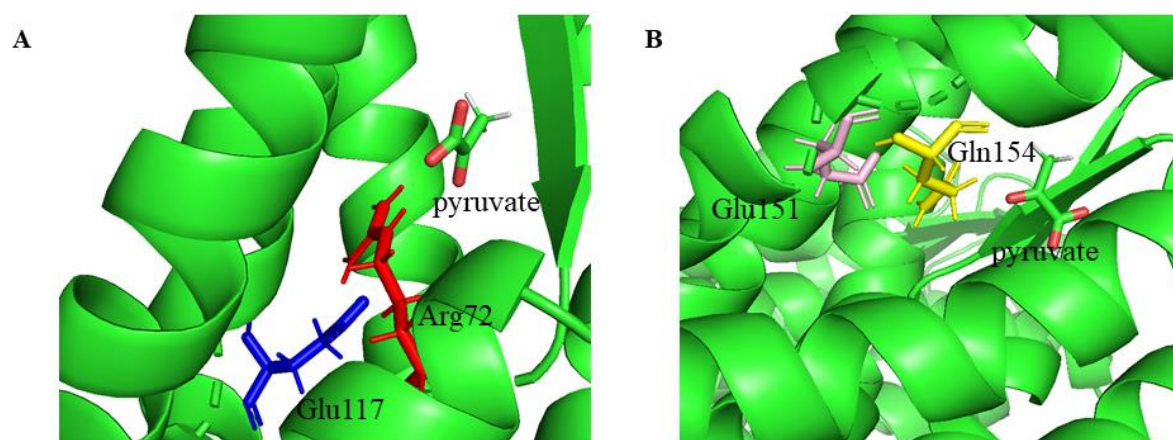
FIG 3.5.1 AlphaFold2.0 based structural model of the BtsS and the arrangement surrounding Arg72 was shown.

(A) Amino acid Glu117 and Arg72 are labeled in blue and red, respectively. (B) Amino acid Glu151 and Gln154 are labeled in pink and yellow, respectively.

Variant BtsS-E117Q/R72E/BtsR and BtsS-E151Q/Q154E/BtsR were constructed. *In vivo btsT* expression was assayed under the same condition as described which can be seen in [Methods].

Results showed that BtsS-E117Q/R72E/BtsR prevented the *btsT* expression under pyruvate or lactate-inducing condition. BtsS-E151Q/Q154E/BtsR could slightly induce *btsT* expression with pyruvate dependency but the level was quite low. But there was almost no *btsT* expression induced when lactate was used as the sole C source (FIG 3.5.2).
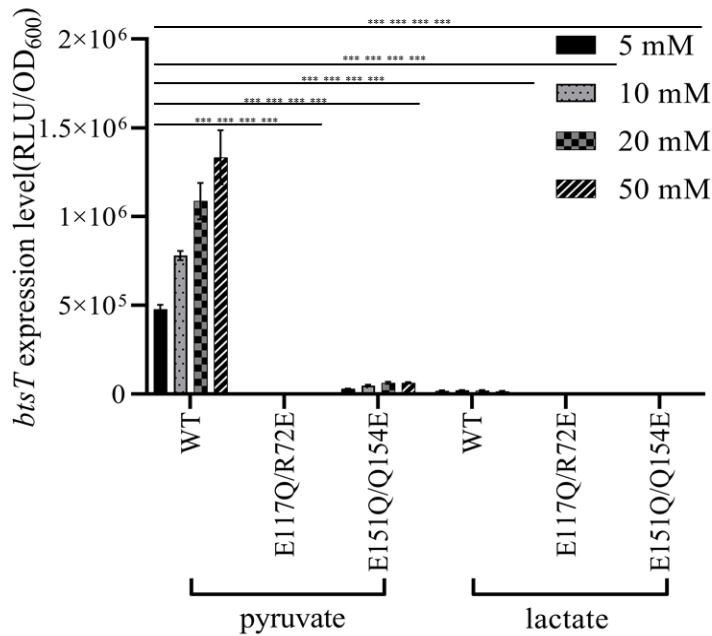
FIG 3.5.2 BtsS-E117Q/R72E/BtsR and BtsS-E151Q/Q154E/BtsR could not sense lactate. pBAD24-*btsS/R* or variants were transformed with *E. coli* MG1655Δ*btsSR*/pBBR-*btsT-lux*. Growth and the activity of the reporter enzyme luciferase were determined. Cells were grown in M9 minimal medium plus indicated concentration of pyruvate supplemented with succinate to make the total carbon sources constant. Growth and luciferase activity were monitored continuously. The maximal luciferase activity normalized to an optical density of 1 (RLU/OD$_{600}$) was used as a measure of the degree of induction of *btsT*. All experiments were performed at least three times, and the error bars indicate the standard deviations of the means. Statistical analysis was performed for wild type and mutants (comparation the value for wild type assayed with pyruvate and mutant or wild type with each concentration of pyruvate or lactate) using unpaired t-test/Assuming Gaussian distribution.

These results showed that replacement of BtsS-E117Q/R72E and BtsS-E151Q/Q154E by site-directed mutagenesis did not convert BtsS into a lactate sensor. But it is not surprising because the pyruvate binding pocket is small compared to the whole BtsS protein size. Besides, the structures of pyruvate and lactate are quite similar, so it is not easy to change the sensing specificity by changing only two amino acids.

3.5.2 Conversion of BtsS into a lactate sensor by random mutagenesis

Random mutagenesis is a well studied strategy for protein directed evolution (FIG 3.5.3). The general idea is to creat mutant library by using physical, chemical or biological strategies. The advantages and drawbacks of different mutagenesis methods were listed (Table 4). Promising mutant can be obtained by using high through-put screening methods. Here, epPCR was performed to mutate *btsS* gene in this study.

Table 4 Advantages and drawbacks for different random mutagenesis strategies.

Method	Advantages	Drawbacks
epPCR	Mutation ratio can be controlled by PCR conditions	Basied towards transitioning due to polymerase
Saturation mutagenesis	Comprehensive substitution study of specific residue with reduced bias	Time consuming to screen the library
DNA shuffling	Recombination of sequences from different genes	Generation of mutation biased libaray
Physical/chemical mutagenesis	Simple to creat broad spectrum mutants compared to biological methods	Toxic, difficult to control the mutation ratio
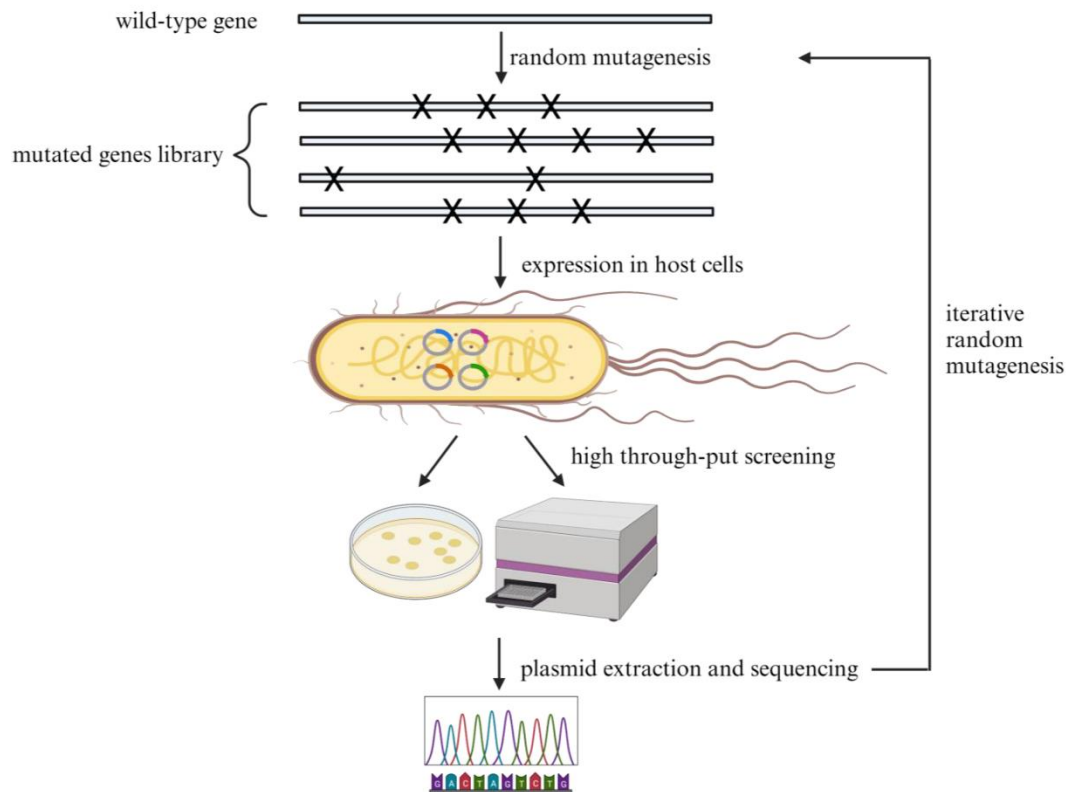
FIG 3.5.3 Principle of directed evolution. Genes are mutated by random mutagenesis and the library can be created. The promising mutant can be obtained after gene expression in host cells and screening by high through-put methods e.g., by white/blue colony screening, by fusing target promoter with gene encoding fluorescent protein. The mutation position on a gene can be known by sequencing. The best functional mutated gene will be used for another round of iterative random mutagenesis. Figure was created with Biorender.com

Nine different epPCR conditions were conducted to amplify the *btsS*-TM fragment (details seen in [Method]) and five of those conditions worked (Table 5). Mutation ratio created under condition #5 and #7 were more suitable and were chosen to generate the library. Besides, a high through-put screening strategy was conducted by using reporter plasmid pBBR-*btsT*-*lacZ*. Expression of *btsT* trigged by BtsS/BtsR was indicated by the activity of β-galactosidase encoded by *lacZ*. Thus, libraries were screened by colored colony grown on M9 minimal medium agar plate supplemented with X-gal plus 50 mM lactate or pyruvate. Mutant turns blue on lactate-containing

plate while turns white on pyruvate-containing plate is promising to be furtherly modified as a lactate sensor. Wild-type colony turned blue when 50 mM pyruvate (FIG 3.5.4B) was used as sole C source and turned white when only 50 mM lactate (FIG 3.5.4B) was used. Thus, 50 mM C source was the concentration in the medium for screening. The screening of library is still going on under this condition. Until now, not a good mutant is obtained due to the limited time. After promising mutant is obtained, it will be sequenced and *in vivo btsT* expression will be assayed by adding lactate and pyruvate as well as other carbon sources in the medium. Details will be discussed in the Outlook part.

Table 5 Mutated ratio calculated for five promising epPCR conditions.

Condition	Template	$MnCl_2$ concentration	Mutated ratio
#1	500 pg	0.4 mM	1 nucleic acids / 300 bp
#2	250 pg	0.4 mM	2 nucleic acids / 80 bp
#4	500 pg	1 mM	2 nucleic acids / 80 bp
#5	250 pg	1 mM	6 nucleic acids / 80 bp
#7	500 pg	2 mM	3 nucleic acids / 80 bp
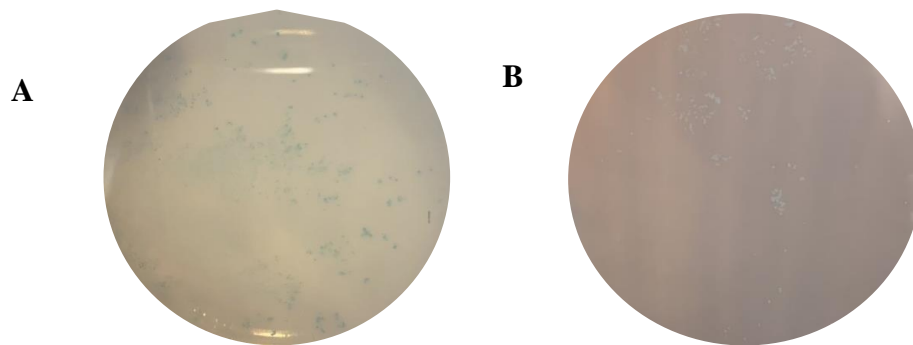
FIG 3.5.4 High through-put screening for lactate-sensing mutant library. MG1655Δ*btsSR*Δ*lacZ* was co-transformed with plasmids mixture of pBAD24-*btsSR*-RM and pBBR-*btsT-lacZ*. Cells were plated on M9 minimal medium supplemented with 50 mM pyruvate or lactate. After inoculation at 37 °C for 48 hours, the plates were checked

to see the colors of colonies. (A) Wild type grows and turns blue on the M9 minimal medium supplemented with 50 mM pyruvate. (B) Wild type grows and turns white on the M9 minimal medium supplemented with 50 mM lactate.

4 Discussion and outlook

4.1 Discussion

Paragraph below was cited from publication: Jin Qiu, Ana Gasperotti, Nathalie Sisattana, Martin Zacharias, and Kirsten Jung. The LytS-type histidine kinase BtsS is a 7-transmembrane receptor that binds pyruvate. mBio. doi: 10.1128/mbio.01089-23. Online ahead of print.

Generally, HKs have an even number of transmembrane helices with N-terminus located towards cytoplasm. However, there are some exceptions for HK AgrC *Staphylococcus aureus* (126) and hybrid HK LuxN *Vibrio harveyi* (127)*,* in which the N-terminus is located outside the cytoplasm and which contains an odd number of transmembrane helices. BtsS/BtsR TCS belongs to the LytS/LytTR-type family which is the second largest family for signal transduction (128). LytS-like HKs have a 5TMR-LYT (<u>5</u> <u>trans</u><u>m</u>embrane <u>r</u>eceptors of the <u>LytS</u>-<u>Y</u>hcK <u>t</u>ype) input domain that is responsible for stimulus perception. This domain is composed with an average of 169 amino acids. It has about 88 different protein architectures and mainly found in histidine kinases, but also occurs in combination with c-di-GMP synthetases (GGDEF domain-containing proteins) (84). Bioinformatic analyses by using TMHMM previously indicated that BtsS has at least five transmembrane helices in TM domain, but models with six or seven transmembrane helices were also obtained, considering that the first 36 amino acids do not belong to the 5TMR-LYT domain (129-131). An input domain containing 7 transmembrane helices was suggested based on the BtsS 3D-model prediction with Alphafold2.0 (FIG 3.1.2A, left panel). The location of the N-terminus of BtsS was detected by using the maltose-binding protein as a reporter. *malE* was fused with the 5'-end of *btsS* and only a hybrid protein in which MalE was localized toward the

periplasm was able to complement a Δ*malE* mutant (indicator: growth with maltose as the sole C source) and sensed pyruvate (FIG 4.1.2). These results indicated that N-terminus of BtsS located to the periplasmic side and this receptor has seven transmembrane helices in TM domain. Seven-transmembrane receptors constitute the largest, most ubiquitous, and most versatile family of membrane receptors in eukaryotes, including rhodopsin, G-protein coupled receptors (132). Comparative genomic analysis also identified several families of seven-transmembrane receptors, e.g., the 7TMR-DISMED1, 7TMR-DISMED2, and 7TMR-HD families in bacteria (84). BtsS was the first known example of a seven-helix receptor belonging to the LytS-like HKs family.

Crystallization structures of several proteins that bind pyruvate can provide clues to the amino acids involved in pyruvate binding. Structure of HK KinD from *Bacillus subtilis* with pyruvate in its binding pocket showed that the hydroxyl group of serine and two arginines could contact with pyruvate carboxyl group. The keto group of pyruvate contacts with serine and tyrosine via a water molecule (PDB: 4JGP) (122). In the pyruvate formate-lyase from *Escherichia coli* (PDB: 1MZO) (25), pyruvate is located in a cleft close to Cys418 and Cys419. Pyruvate carboxyl group is in contact with Arg176 and Arg435 and the methyl group is within van der Waals distance of Phe327. Arg548 and Gln552 are the amino acids to bind pyruvate for the pyruvate carboxylase from *Rhizobium etli* (PDB: 4JX4, 4JX5, 4JX6) (133, 134). For the high-affinity pyruvate receptor BtsS, Arg72, Arg99, Cys110, and Ser113 were identified as amino acids responsible for pyruvate binding. Based on the 3D structure modeling information and MD-based docking with pyruvate, Arg72 and Arg99 formed stable hydrogen bonds with pyruvate. Cys110 was in close contact with pyruvate. Although Ser113 was also in close contact with ligand, no hydrogen bond was formed with

pyruvate, but a close H-bond contact with Arg72 was observed in the model. Therefore, Ser113 may play an important role in positioning the guanidinium group of Arg72 to allow contact with pyruvate (FIG 4.1.6).

BtsS is a high-affinity receptor for extracellular pyruvate and the K_d value is 67.3±10.6 μM as determined (FIG 3.1.4), which is in the same range as previous study (58.6 μM) (84). Replacement of one of these four amino acids could significantly reduce or completely prevent the expression of *btsT in vivo* (FIG 3.1.4). The K_d value measured for BtsS-R72A, BtsS-R99A, BtsS-C110A, and BtsS-S113A for pyruvate were higher than wild-type BtsS (FIG 3.1.5), which means their affinity for pyruvate was lower than that of wild type. Dynamic simulation result showed the predicted interactions between these four amino acids and pyruvate (FIG 3.1.6). However, these substitutions and changes were small and they can not be the only reason that these variants can not induce *btsT* expression even with higher concentration of pyruvate. Besides, these variants also affected signaling transduction by preventing BtsS phosphorylation and dimerization step (FIGs 3.1.7-3.2.1). Sequence alignment analysis using ClustalW (135) showed that arginine at position 72 and 99 in BtsS in *E. coli* are highly conserved. In contrast, amino acid Cys at position 110 and Ser at position 113 in BtsS are 71.4% and 78.6% conserved, respectively (FIG 4.1.1). In some LytS-type kinases, Cys110 is replaced by Tyr and Ser113 is replaced by Ala or Thr (FIG 4.1.1). Replacements in the corresponding positions of Cys110 or Ser113 might affect the ligand specificity, e.g., for lactate, which needs to be verified experimentally further.

FIG 4.1.1 Multiple sequence alignment of BtsS transmembrane domain (aa from1-218) with other LytS kinases.

The species abbreviations are, Bsu-*Bacillus subtilis*; Cte-*Clostridium tetani*; Ec-*Escherichia coli*; Fnu-*Fusobacterium nucleatum*; Gme-*Geobacter metallireducens*; Ooe-*Oenococcus oeni*; Rru-*Rhodospirillum rubrum*; Sag-*Streptococcus agalactiae*; Sau-*Staphylococcus aureus*; Sen-*Salmonella enterica*; Son-*Shewanella oneidensis*; Sep-*Staphylococcus*

epidermidis. Numbers correspond to GenBank (NIH) records. Positions corresponding to Arg72, Arg99, Cys110, Ser113 and Arg192 of BtsS are framed with a black box.

Paragraph below was cited from publication: Jin Qiu, Ana Gasperotti, Nathalie Sisattana, Martin Zacharias, and Kirsten Jung. The LytS-type histidine kinase BtsS is a 7-transmembrane receptor that binds pyruvate. mBio. doi: 10.1128/mbio.01089-23. Online ahead of print.

BtsS autophosphorylation was not able to be detected before (141). In this study, it was detectable *in vitro* for the first time and BtsS autokinase activity was dependent on Mn^{2+}-ATP instead of Mg^{2+}-ATP (FIG 3.1.7A), which is quite rare for HKs. There are some serine/tyrosine kinases and some HKs from plants that prefer Mn^{2+} for kinase activity (70, 71). In bacteria, only the hybrid HK FrzE in *Myxococcus xanthus* is reported that can be auto-phosphorylated in the presence of cofactor Mn^{2+} (72). Mn^{2+} is required as a free ion or a cofactor of superoxide dismutase for resistance to oxidative stress (136). Pyruvate is a known scavenger of reactive oxygen radicals (137, 138). However, a correlation between oxidative stress and BtsS/BtsR activation or pyruvate sensing is still unknown.

Binding of pyruvate could also stimulate the autophosphorylation of BtsS. When assayed with 0 to 100 µM pyruvate, the more pyruvate was added, the higher autokinase activity was detected. Activity reached to saturation at concentrations more than 100 µM (FIG 3.1.7B). The tendency of autokinase activity stimulated by pyruvate concentration fits quite well with the measured affinity of wild-type BtsS for binding pyruvate. What still could not be answered is whether BtsS dimerization is also pyruvate concentration dependent. Since the interacting proteins had to be overproduced for measurement of ß-galactosidase activities with the BACTH assay.

The helix in HK, that spans from the periplasm to the cytoplasm, is involved in signal transduction by helical rotation and helix axis translation following DHp coiled-coil rearrangements (32). Arg at position 192 in BtsS is located in the helix spanning through the membrane and Arg192 in one monomer can form hydrogen bond with Ser25 in another monomer (FIG 4.1.2 and FIG 4.1.3). Replacement BtsS-Arg with alanine may affect DHp conformation because spatial conformation of Arg and Ala side chains are different and hydrogen bond formed by Arg192 and Ser25 was destroyed (FIG 4.1.3). The region where HK interacts with RR is close to DHp domain (32). Thus, the interaction between BtsS-R192A and BtsR could be affected by the rearrangement of DHp domain (32). In addition, studies on HK/RR system ThkA:TrrA in *T. maritima* showed a region close to TM domain of ThkA interacts with regulator TrrA (73). Arg192 in BtsS is located in TM domain of BtsS (FIG 4.1.2). It is also reasonable to propose that BtsS-Arg192 could affect the interaction with BtsR.
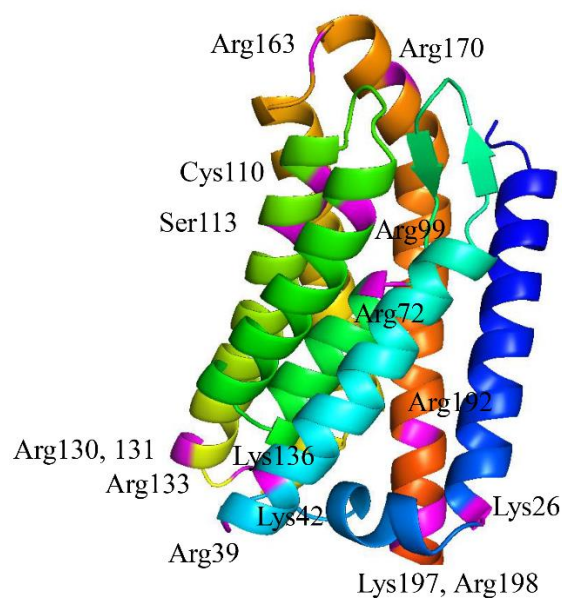
FIG 4.1.2 Alphafold2.0 model of the transmembrane domain of BtsS in rainbow colors. N terminus colored in blue. All positively charged amino acids as well as Cys15 and Ser25 are labeled in purple. Figure was cited from publication: Jin Qiu, Ana Gasperotti, Nathalie Sisattana, Martin Zacharias, and Kirsten Jung. The LytS-type histidine

kinase BtsS is a 7-transmembrane receptor that binds pyruvate. mBio. doi: 10.1128/mbio.01089-23. Online ahead of

print.
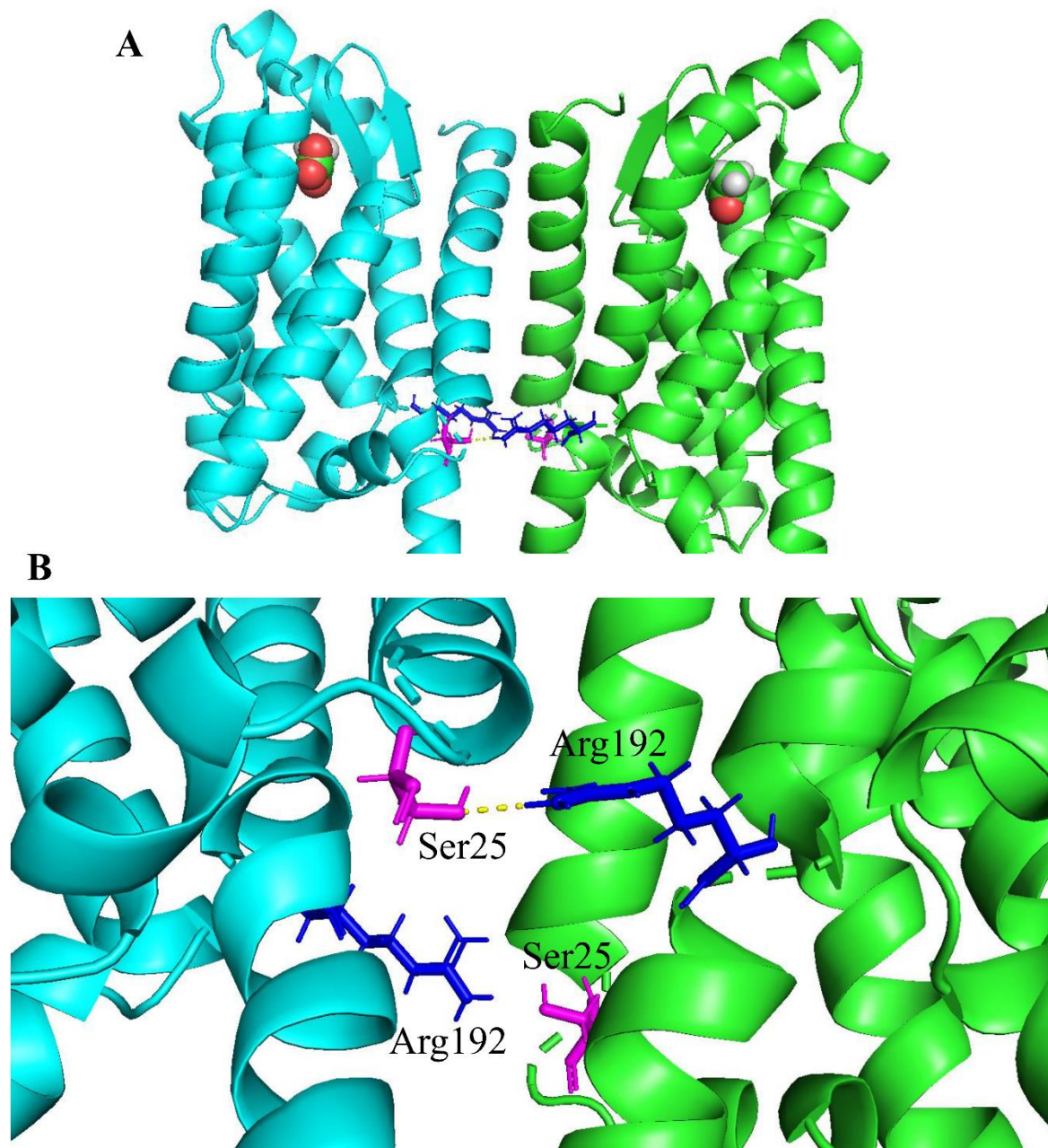
FIG 4.1.3 BtsS-Arg192 in one monomer forms hydrogen bond with BtsS-Ser25 in another monomer. (A)

Overview of BtsS transmembrane domain model. Arg192 is laberled in blue and Ser25 is labeled in purple. (B) Zoom

in the interaction between Ser25 in one monomer and Arg192 in another monomer. Ser25 is labeled in red and Arg192

in labeled in blue. The hydrogen bond form by them is labeled in yellow.

"Positive residue inside rule" also showed that positive charged amino acids like lysine or arginine are always enriched in the transmembrane domains of proteins, that point to cytoplasm to enhance polar interactions (139). Gunnar von Heijne showed that Lys or Arg side chain provide the major part of the stabilization (140). Here, after replacing arginine at position 192 with alanine, downstream of interaction with RR could be reduced since the polor interaction could be destroyed after alanine replacement.

Replacement of Ser25 with alanine, valine, threonine or tryptophan in BtsS showed different signaling transduction patterns (FIG 3.4.1). Especially when BtsS-Ser25 was replaced with alanine or valine, *btsT* was triggered to express when one of these following compounds, pyruvate, lactate, succinate, acetate, glucose, mannose, fructose, serine or glycine, were added to the medium (FIG 3.4.1). The hyphothesis is that replacement of BtsS-Ser25 with alanine or valine could block BtsS in a conformation that could keep the kinase in an ON state, which means BtsS-S25A/BtsR or BtsS-S25V/BtsR system could be always active independent of compound sensing.

Protein thermostability determination by using NanoDSF showed wild type BtsS was more stable after binding ligand pyruvate (FIG 3.4.3A), which can be explained with the principle of equilibrium between binding and protein unfolding (141) (142). BtsS-S25A was more thermostale than wild type (FIGs 3.4.3A and B). Both pyruvate and lactate could enhance the thermostability of BtsS-S25A and there was a concentration-dependent stabilizing effect (FIG 3.4.3B). Ralph P. Diensthuber and colleague clarified there is a correlation between thermostability and protein flexibility, indicating that the less flexible the protein is, the more stable it will be (143). There were hydrophobic amino acids located in the first helix and closed to BtsS-S25A (FIG 4.1.2). Alanine might form hydrophobic interactions with them, e.g., F29. Thus, after replacement of BtsS-Ser25 with alanine, flexibility of BtsS could be decreased and the conformation also changed.

Moreover, autophosphorylation assay results showed that in any tested concentration of pyruvate, autokinase of BtsS-S25A was about three times higher than wild type under the same condition (FIG 3.4.4). BACTH assayed result showed there was an interaction between BtsS-S25A and BtsR and the β-galactosidase activity was in the same range as positive control (FIG 3.4.5). Taken together, it is suggested that BtsS-S25A blocked the kinase BtsS in a specific conformation that could keep ATP binding site and Histidine exposed to an active status leading to BtsS being available to interact with BtsR and the system can always trigger the expression of *btsT*.

BtsS-Ser25 located in the end of first transmembrane helix spanning through the membrane (FIG 4.1.2), which helix could affect the signaling transduction as discussed before (32). The hydroxyl group of serine might form hydrogen bond with water or exposed fatty acid chains in membrane. Replacement of alanine destroyed the hydrogen bond caused by conformation rearrangement. This conformational change could affect the 7th helix (S-helix (32)) movement since Ser25 is surrounded, then ATP binding site in CA domain and the histidine amino acid in DHp domain would be exposed to active. Besides, Ser25 in one monomer is close to Arg192 in another monomer and they can form hydrogen bond between hydroxyl group of Ser and guanidinium group of Arg in the 3D model (FIG 4.1.3). As discussed before, Arg192 is also important for the signaling transduction by affecting BtsS and BtsR interaction. It is reasonable to propose that BtsS-S25A changed the signal transduction since the hydrogen bond was destroyed and turned on the kinase activity. Dynamic simulation studies need to be conducted to furtherly verify these hypothesises.

BACTH results showed that BtsS formed dimer *in vivo*. It is unclear if the dimerization is dependent on pyruvate concentration or not. Once perceived the signal pyruvate, S-helix (32) conformation of BtsS would change, e.g., the distance between cysteine residues and the position of histidine in DHp domain and ATP binding site in CA domain. Here, the distance might did not

get close enough after the amino acids were replaced with alanine since pyruvate could not bind. That is why no BtsS dimer formed after replacement of BtsS-Arg72, BtsS-Arg99, BtsS-Cys110 and BtsS-Ser113 with alanine.

Autokinase activity of BtsS was determined under oxidizing or reducing condition to verify the importance of dimerization. Either Cu (II)(1,10-phenanthroline)$_3$ or I$_2$ was used as an oxidant. Cu (II)(1,10-phenanthroline)$_3$ functioned as a null cross-linker. I$_2$ was used as an oxidant. In contrast, Tris (2-carboxyethyl) phosphine (TCEP) was used to create the reducing environment. It can destroy the disulfide bond while Mn^{2+} will not be changed. Under either of these conditions, there was almost no BtsS autokinase activity detected which means BtsS function as a dimer for kinase function (FIG 3.2.2).

Based on the model predicted by Alphafold2.0, Cys15 was very promising to form disulfide bond for BtsS dimerization. It is located in the interface of each monomer. *In vivo* results showed that there was lower level of *btsT* expressed after the replacement of BtsS-Cys15 with alanine, when pyruvate was used as the sole C source (FIG 3.2.3A). Besides, BtsS-Cys15/BtsR showed pyruvate concentration dependency (FIG 3.2.2B). It means BtsS-Cys15 is likely to form disulfide bond but it is not essential for signal transduction. Studies on histidine kinase KdpD showed it functions as a homodimer but Cys residues between monomers is not responsible for dimer stabilization, but a disulfide bond formed intramolecularly was important for autokinase activity (144, 145). Disulfide bond in CadC, a membrane protein belongs to ToxR-like receptors family, also plays an important role for its function. Without a disulfide bond can result in a semi-active CadC (146).

Except for Cys15, there are other six Cys amino acids in BtsS (Cys46, Cys54, Cys110, Cys299, Cys305 and Cys543). Amino acids Cys46, Cys54, Cys110 are in the transmembrane

domain, Cys298 and Cys305 are in the GAF domain, the last one Cys543 is in DHp domain. According to the model, they are not the promising ones to form disulfide bond between the two monomers since the distance between these Cys with the corresponding ones in another monomer is quite far. But what should be kept in mind is, the model used to analyze is a predicted model, but not a real structure. It is reasonable to propose that maybe the other Cys residues could be involved in dimer formation in the real structure and it should be verified furtherly by performing mutagenesis on these cysteine amino acids and then detecting *in vivo btsT* expression.

Besides, variants BtsS-C15E and BtsS-C15S showed lactate sensing activity although it was low and BtsS-C15E/BtsR was still sensing pyruvate at the same time, but pyruvate sensing ability was quite lower compared with wild type (FIG 3.2.3). These two can be considered as a template for random mutagenesis for lactate sensor generation by increasing the lactate sensing ability meanwhile decrease the pyruvate sensing ability.

After pyruvate binding pocket was identified, the idea was to convert it into a lactate sensor. Variants BtsS-E117Q/R72E and BtsS-E151Q/Q154E were generated to create H-bond accepter for lactate keto group, meanwhile maintained the charged environment for binding (FIG 3.5.1). *In vivo* results showed that none of them could sense lactate (FIG 3.5.1). It is reasonable to explain the result since the pyruvate binding pocket is relatively small compared to the whole size of BtsS (FIG 3.1.6). Moreover, the structure of pyruvate and lactate is also quite similar. Thus, it is not easy or lucky to fully change the ligand specificity by replacement just two amino acids. To continue with the site-directed mutagenesis, what can be done in the future is docking BtsS with lactate. *In vivo btsT* expression should be done by using lactate to check the sensing ability after mutagenesis.

Random mutagenesis was another strategy to try to generate lactate sensor. Two good epPCR conditions were set up which could create suitable mutation ratio (Table 5). A high through-put

screening method using the reporter plasmid pBBR-*btsT-lacZ* was established by screening the mutant by blue or white color on M9 minimal medium agar plate when 50 mM lactate or pyruvate was used as sole carbon source (FIG 3.5.4). Although no good mutant that can sense lactate was obtained until now, these conditions can be used for any gene random mutagenesis in the future.

4.2 Outlook

Hybrid protein is the one created by joining multiple genes which coded for different proteins. Multiple peptides that have different functions derived from each original protein will be created after the hybrid genes translation (147). Here, hybrid kinase can be constructed for lactate sensor by fusing the input domain of a protein that senses lactate with the rest domain of BtsS. Lactate dehydrogenase was usually used as the protein to donate the input domain to sense or transport lactate (148). In this study, sequences alignment was conducted for BtsS in *E. coli* and other HKs belongs to LytS family in different bacteria, e.g., *Bacillus subtilis*, *Clostridium tetani*, *Escherichia coli*, *Fusobacterium nucleatum*, *Geobacter metallireducens*, *Oenococcus oeni*, *Rhodospirillum rubrum*, *Streptococcus agalactiae*, *Staphylococcus aureus*, *Salmonella enterica*, *Shewanella oneidensis*, *Staphylococcus epidermidis*. There is similarity among these sequences, especially in the transmembrane domain. Besides, bacteria *Geobacter metallireducens* is the only one that can live in the environment containing lactate (149). It is reasonable to propose that LytS in *Geobacter metallireducens* might be the HK can sense lactate and use it for growth, which is a nature choice for living in the environment contains lactate. Thus, LytS in *Geobacter metallireducens* was chosen to fuse with BtsS in our research.

Model for LytS and BtsS were predicted with Alphafold 2.0. There is mainly a TM domain (1-200 aa), a GAF domain (211-356 aa) and DHp plus CA domain (357-576 aa) for LytS and a linker with 10 aa between TM domain and GAF domain. Correspondingly, there is a TM domain

(1-205 aa), a GAF domain (218-365 aa) and DHp plus CA domain (366-561 aa) for BtsS a similar linker with 13 aa. There are three possible strategies for hybrid lactate sensor. One is fusion of TM domain of LytS (1-200 aa of LytS) with linker, GAF, DHp and CA domain of BtsS (206-561 aa of BtsS). Second strategy is to fuse TM domain and linker of LytS (1-210 aa of LytS) with GAF, DHp and CA domain of BtsS (218-561 aa of BtsS). Third strategy is the fusion of TM and GAF domain of LytS (1-356 aa of LytS) with the DHp and CA domain of BtsS (366-561 aa of BtsS). Once the corresponding hybrid kinase is expressed, *in vivo btsT* expression assayed will be detected with different carbon sources, e.g., lactate, pyruvate, succinate. If it is specific for lactate sensing, signal output linearization will be detected in mammals for application.

Acknowledgement

I would like to first to say thank you to Prof. Dr. Kirsten Jung, who guided and supervised my project for all these four years. Thank you for giving me this very interesting project. I learnt a lot of knowledge and skills from you, as well as the way to think and the attitude to do research. Every time when we meet the bottleneck for the experiment, you always provide very professional and useful suggestions so that the project can go well and we have very good results. At the beginning when I came here from abroad, you encouraged me to do my best to adapt to the new environment. Thank you for the financially support after my scholarship meet the deadline. I highly appreciate the time and energy that you invested in my publication and this thesis. We can't get such a successful publication without your patience and all the support! I wish you all the best!

I would like to also thank Dr. Ana Gasperottia and Dr. Nathalie Sisattanaa, who helped me with my project and taught me to do some experiments that I never did before. Thank you for always share ideas and guide me when I encountered experimental problems.

Besides, I also want to thank my colleagues in this lab, Bibakhya Saikia, Sebastian Riquelme Barrios, Dania Devassy, Giovanni Gallo, Sophia Beck, Urte Tomasiunaite, Leonardo Vasquez, Elena Fajardo Ruiz, Erica Flora Aveta, Sophie Brameyer, Nicholas Stein, Grazyna Wlodarska-Lauer, Jiawei Cai, Alina Sieber and Kilian Schumacher. You are also my friends abroad and it is very a good experience to working with all of you and it will an unforgettable part of memory in my life.

In addition to that, I want to say thank you to my friend Da Su. You always comfort me when I am down. It is my luck to meet you here and I didn't feel lonely because of you. Thank my friend Zhongying Han, who always encourage me to go through the difficulties during these four years.

Thank Qin Pan for your company and helping me to solve the problems I met in life. I hope all the best for all of you. You are the gifts for me that given by this special four years.

I would also like to thank the China Scholarship Council (CSC) for sponsoring my four years of study in Germany.

Finally, I would like to thank my parents. I feel so lucky that I am your daughter because you always support me with everything that I want to do. Meanwhile, I feel very sorry because I can't be together with you for four years. Thank you for always be on my side.

References

1.   Goudreau PN, Stock AM. 1998. Signal transduction in bacteria: molecular mechanisms of stimulus-response coupling. Curr Opin Microbiol 1:160-169.

2.   Schenk PW, Snaar-Jagalska BE. 1999. Signal perception and transduction: the role of protein kinases. Biochim Biophys Acta 1449:1-24.

3.   Martin-Mora D, Fernandez M, Velando F, Ortega A, Gavira JA, Matilla MA, Krell T. 2018. Functional annotation of bacterial signal transduction systems: progress and challenges. Int J Mol Sci 19:3755-3776.

4.   Ulrich LE, Koonin EV, Zhulin IB. 2005. One-component systems dominate signal transduction in prokaryotes. Trends Microbiol 13:52-56.

5.   Hoch JA. 2000. Two-component and phosphorelay signal transduction. Curr Opin Microbiol 3:165-170.

6.   Campagne S, Allain FHT, Vorholt JA. 2015. Extra cytoplasmic function sigma factors, recent structural insights into promoter recognition and regulation. Curr Opin Struct Biol 30:71-78.

7.   Casino P, Miguel-Romero L, Marina A. 2014. Visualizing autophosphorylation in histidine kinases. Nat Commun 5: 3258-3268.

8.   Pirrung MC. 1999. Histidine kinases and two-component signal transduction systems. Chem Biol 6:167-175.

9.   Robinson VL, Stock AM. 1999. High energy exchange: proteins that make or break phosphoramidate bonds. Structure 7:47-53.

10.   Stock J. 1999. Signal transduction: gyrating protein kinases. Curr Biol 9:364-367.

11.   Kenney LJ. 2010. How important is the phosphatase activity of sensor kinases? Curr Opin Microbiol 13:168-176.

12. Agrawal R, Sahoo BK, Saini DK. 2016. Cross-talk and specificity in two-component signal transduction pathways. Future Microbiol 11:685-697.

13. Mizuno T. 1998. His-Asp phosphotransfer signal transduction. J Biochem 123:555-563.

14. West AH, Stock AM. 2001. Histidine kinases and response regulator proteins in two-component signaling systems. Trends Biochem Sci 26:369-376.

15. Shi XQ, Wegener-Feldbrugge S, Huntley S, Hamann N, Hedderich R, Sogaard-Andersen L. 2008. Bioinformatics and experimental analysis of proteins of two-component systems in *Myxococcus xanthus*. J Bacteriol 190:613-624.

16. Boles BR, Horswill AR. 2008. Agr-mediated dispersal of *Staphylococcus aureus* biofilms. PLoS Pathog 4: e1000052

17. Li M, Lai YP, Villaruz AE, Cha DJ, Sturdevant DE, Otto M. 2007. Gram-positive three-component antimicrobial peptide-sensing system. Proc Natl Acad Sci U S A 104:9469-9474.

18. Beier D, Gross R. 2008. The BvgS/BvgA phosphorelay system of pathogenic *Bordetellae* -structure, function and evolution. Adv Exp Med Biol. 631:149-160.

19. Baker MD, Wolanin PM, Stock JB. 2006. Signal transduction in bacterial chemotaxis. Bioessays 28:9-22.

20. Kaspar S, Bott M. 2002. The sensor kinase CitA (DpiB) of *Escherichia coli* functions as a high-affinity citrate receptor. Arch Microbiol 177:313-321.

21. Itou J, Eguchi Y, Utsumi R. 2009. Molecular Mechanism of transcriptional cascade initiated by the EvgS/EvgA system in *Escherichia coli* K-12. Biosci Biotechnol Biochem73:870-878.

22.   Jung K, Altendorf K. 2002. Towards an understanding of the molecular mechanisms of stimulus perception and signal transduction by the KdpD/KdpE system of *Escherichia coli*. J Mol Microbiol Biotechnol 4:223-228.

23.   Vescovi EG, Soncini FC, Groisman EA. 1994. The Role of the PhoP/PhoQ regulon in *Salmonella* virulence. Res Microbiol 145:473-480.

24.   Behr S, Kristoficova I, Witting M, Breland EJ, Eberly AR, Sachs C, Schmitt-Kopplin P, Hadjifrangiskou M, Jung K. 2017. Identification of a high-affinity pyruvate receptor in *Escherichia coli*. Sci Rep 7:1388-1397.

25.   Aravind L, Ponting CP. 1997. The GAF domain: an evolutionary link between diverse phototransducing proteins. Trends Biochem Sci 22:458-459.

26.   Gao R, Stock AM. 2009. Biological insights from structures of two-component proteins. Annu Rev Microbiol 63:133-154.

27.   Hulko M, Berndt F, Gruber M, Linder JU, Truffault V, Schultz A, Martin J, Schultz JE, Lupas AN, Coles M. 2006. The HAMP domain structure implies helix rotation in transmembrane signaling. Cell 126:929-940.

28.   Taylor BL, Zhulin IB. 1999. PAS domains: Internal sensors of oxygen, redox potential, and light. Microbiol Mol Biol Rev 63:479-506.

29.   Finn RD, Tate J, Mistry J, Coggill PC, Sammut SJ, Hotz HR, Ceric G, Forslund K, Eddy SR, Sonnhammer ELL, Bateman A. 2008. The Pfam protein families database. Nucleic Acids Res 36:281-288.

30.   Singh M, Berger B, Kim PS, Berger JM, Cochran AG. 1998. Computational learning reveals coiled coil-like motifs in histidine kinase linker domains. Proc Natl Acad Sci U S A 95:2738-2743.

31.   Marina A, Waldburger CD, Hendrickson WA. 2005. Structure of the entire cytoplasmic portion of a sensor histidine-kinase protein. Embo J 24:4247-4259.

32.   Buschiazzo A, Trajtenberg F. 2019. Two-component sensing and regulation: How do histidine kinases talk with response regulators at the molecular level? Annu Rev Microbiol 73:507-528.

33.   Gao R, Bouillet S, Stock AM. 2019. Structural basis of response regulator function. Annu Rev Microbiol 73:175-197.

34.   Galperin MY. 2010. Diversity of structure and function of response regulator output domains. Curr Opin Microbiol 13:150-159.

35.   Fabret C, Feher VA, Hoch JA. 1999. Two-component signal transduction in *Bacillus subtilis*: How one organism sees its world. J Bacteriol 181:1975-1983.

36.   Lukat GS, Mccleary WR, Stock AM, Stock JB. 1992. Phosphorylation of bacterial response regulator proteins by low-molecular-weight phospho-donors. Proc Natl Acad Sci U S A 89:718-722.

37.   Baikalov I, Schroder I, KaczorGrzeskowiak M, Grzeskowiak K, Gunsalus RP, Dickerson RE. 1996. Structure of the *Escherichia coli* response regulator NarL. Biochemistry 35:11053-11061.

38.   Lee SY, De la Torre A, Yan DL, Kustu S, Nixon BT, Wemmer DE. 2003. Regulation of the transcriptional activator NtrC1: structural studies of the regulatory and AAA$^{(+)}$ ATPase domains. Genes Dev 17:2552-2563.

39.   MartinezHackert E, Stock AM. 1997. Structural relationships in the OmpR family of winged-helix transcription factors. J Mol Biol 269:301-312.

40. Nikolskaya AN, Galperin MY. 2002. A novel type of conserved DNA-binding domain in the transcriptional regulators of the AlgR/AgrA/LytR family. Nucleic Acids Res 30:2453-2459.

41. Romeo T. 1998. Global regulation by the small RNA-binding protein CsrA and the non-coding RNA molecule CsrB. Mol Microbiol 29:1321-1330.

42. Liu MY, Gui G, Wei B, Preston JF, 3rd, Oakford L, Yuksel U, Giedroc DP, Romeo T. 1997. The RNA molecule CsrB binds to the global regulatory protein CsrA and antagonizes its activity in *Escherichia coli*. J Biol Chem 272:17502-17510.

43. West AH, Martinez-Hackert E, Stock AM. 1995. Crystal structure of the catalytic domain of the chemotaxis receptor methylesterase, CheB. J Mol Biol 250:276-290.

44. Tamayo R, Tischler AD, Camilli A. 2005. The EAL domain protein VieA is a cyclic diguanylate phosphodiesterase. J Biol Chem 280:33324-33330.

45. Paul R, Weiser S, Amiot NC, Chan C, Schirmer T, Giese B, Jenal U. 2004. Cell cycle-dependent dynamic localization of a bacterial response regulator with a novel di-guanylate cyclase output domain. Genes Dev 18:715-727.

46. Karatan E, Saulmon MM, Bunn MW, Ordal GW. 2001. Phosphorylation of the response regulator CheV is required for adaptation to attractants during *Bacillus subtilis* chemotaxis. J Biol Chem 276:43618-43626.

47. Mitchell SL, Ismail AM, Kenrick SA, Camilli A. 2015. The VieB auxiliary protein negatively regulates the VieSA signal transduction system in *Vibrio cholerae*. BMC Microbiol 15:59-74.

48. Stock AM, Martinezhackert E, Rasmussen BF, West AH, Stock JB, Ringe D, Petsko GA. 1993. Structure of the Mg^{2+}-bound form of CheY and mechanism of phosphoryl transfer in bacterial chemotaxis. Biochemistry 32:13375-13380.

49.   Wemmer DE, Kern D. 2005. Beryllofluoride binding mimics phosphorylation of aspartate in response regulators. J Bacteriol 187:8229-8230.

50.   Hastings CA, Lee SY, Cho HS, Yan D, Kustu S, Wemmer DE. 2003. High-resolution solution structure of the beryllofluoride-activated NtrC receiver domain. Biochemistry 42:9081-9090.

51.   Fernandez I, Otero LH, Klinke S, Carrica MD, Goldbaum FA. 2015. Snapshots of conformational changes shed light into the NtrX receiver domain signal transduction mechanism. J Mol Biol 427:3258-3272.

52.   Ocasio VJ, Correa F, Gardner KH. 2015. Ligand-induced folding of a two-component signaling receiver domain. Biochemistry 54:1353-1363.

53.   Pappalardo L, Janausch IG, Vijayan V, Zientz E, Junker J, Peti W, Zweckstetter M, Unden G, Griesinger C. 2003. The NMR structure of the sensory domain of the membranous two-component fumarate sensor (histidine protein kinase) DcuS of *Escherichia coli*. J Biol Chem 278:39185-39188.

54.   Matsushika A, Mizuno T. 1998. The structure and function of the histidine-containing phosphotransfer (HPt) signaling domain of the *Escherichia coli* ArcB sensor. J Biochem 124:440-445.

55.   Schell MA, Denny TP, Huang J. 1994. VsrA, a second two-component sensor regulating virulence genes of *Pseudomonas solanacearum*. Mol Microbiol 11:489-500.

56.   Eraso JM, Kaplan S. 1995. Oxygen-insensitive synthesis of the photosynthetic membranes of *Rhodobacter sphaeroides*: a mutant histidine kinase. J Bacteriol 177:2695-706.

57.   Mosley CS, Suzuki JY, Bauer CE. 1994. Identification and molecular genetic characterization of a sensor kinase responsible for coordinately regulating light harvesting and reaction center gene expression in response to anaerobiosis. J Bacteriol 176:7566-7573.

58. Bilwes AM, Alex LA, Crane BR, Simon MI. 1999. Structure of CheA, a signal-transducing histidine kinase. Cell 96:131-141.

59. Kramer G, Weiss V. 1999. Functional dissection of the transmitter module of the histidine kinase NtrB in *Escherichia coli*. Proc Natl Acad Sci U S A 96:604-609.

60. Wang L, Grau R, Perego M, Hoch JA. 1997. A novel histidine kinase inhibitor regulating development in *Bacillus subtilis*. Genes Dev 11:2569-2579.

61. Stock JB, Ninfa AJ, Stock AM. 1989. Protein-phosphorylation and regulation of adaptive responses in bacteria. Microbiol Rev 53:450-490.

62. Parkinson JS, Kofoid EC. 1992. Communication modules in bacterial signaling proteins. Annu Rev Genet 26:71-112.

63. Humphrey W, Dalke A, Schulten K. 1996. VMD: Visual molecular dynamics. J Mol Graph. 14:33-38.

64. Puttick J, Baker EN, Delbaere LTJ. 2008. Histidine phosphorylation in biological systems. Biochim Biophys Acta 1784:100-105.

65. Attwood PV, Piggott MJ, Zu XL, Besant PG. 2007. Focus on phosphohistidine. Amino Acids 32:145-56.

66. Casino P, Rubio V, Marina A. 2009. Structural insight into partner specificity and phosphoryl transfer in two-component signal transduction. Cell 139:325-336.

67. Pena-Sandoval GR, Georgellis D. 2010. The ArcB sensor kinase of *Escherichia coli* autophosphorylates by an intramolecular reaction. J Bacteriol 192:1735-1739.

68. Swanson RV, Bourret RB, Simon MI. 1993. Intermolecular complementation of the kinase activity of CheA. Mol Microbiol 8:435-441.

69. Maguire ME, Cowan JA. 2002. Magnesium chemistry and biochemistry. Biometals 15:203-210.

70. Singh TJ. 1993. Insulin receptor serine kinase activation by casein kinase 2 and a membrane tyrosine kinase. Mol Cell Biochem 121:167-174.

71. Gamble RL, Coonfield ML, Schaller GE. 1998. Histidine kinase activity of the ETR1 ethylene receptor from *Arabidopsis*. Proc Natl Acad Sci U S A 95:7825-7829.

72. Mccleary WR, Zusman DR. 1990. Purification and characterization of the *Myxococcus-Xanthus* Frze protein shows that it has autophosphorylation activity. J Bacteriol 172:6661-6668.

73. Yamada S, Sugimoto H, Kobayashi M, Ohno A, Nakamura H, Shiro Y. 2009. Structure of PAS-linked histidine kinase and the response regulator complex. Structure 17:1333-1344.

74. Zapf J, Sen U, Madhusudan, Hoch JA, Varughese KI. 2000. A transient interaction between two phosphorelay proteins trapped in a crystal lattice reveals the mechanism of molecular recognition and phosphotransfer in signal transduction. Structure 8:851-862.

75. Dubey BN, Lori C, Ozaki S, Fucile G, Plaza-Menacho I, Jenal U, Schirmer T. 2016. Cyclic di-GMP mediates a histidine kinase/phosphatase switch by noncovalent domain cross-linking. Sci Adv 2: e1600832.

76. Batchelor E, Goulian M. 2003. Robustness and the cycle of phosphorylation and dephosphorylation in a two-component regulatory system. Proc Natl Acad Sci U S A 100:691-696.

77. Cleland WW, Hengge AC. 2006. Enzymatic mechanisms of phosphate and sulfate transfer. Chem Rev 106:3252-3278.

78. Kirby JR, Kristich CJ, Saulmon MM, Zimmer MA, Garrity LF, Zhulin IB, Ordal GW. 2001. CheC is related to the family of flagellar switch proteins and acts independently from CheD to control chemotaxis in *Bacillus subtilis*. Mol Microbiol 42:573-585.

79.	Zhao R, Collins EJ, Bourret RB, Silversmith RE. 2002. Structure and catalytic mechanism of the *E. coli* chemotaxis phosphatase CheZ. Nat Struct Biol 9:711-711.

80.	Perego M, Hanstein C, Welsh KM, Djavakhishvili T, Glaser P, Hoch JA. 1994. Multiple protein-aspartate phosphatases provide a mechanism for the integration of diverse signals in the control of development in *B. subtilis*. Cell 79:1047-1055.

81.	Ohlsen KL, Grimsley JK, Hoch JA. 1994. Deactivation of the sporulation transcription factor Spo0A by the Spo0E protein phosphatase. Proc Natl Acad Sci U S A 91:1756-1760.

82.	Silversmith RE, Levin MD, Schilling E, Bourret RB. 2008. Kinetic characterization of catalysis by the chemotaxis phosphatase CheZ. Modulation of activity by the phosphorylated CheY substrate. J Biol Chem 283:756-765.

83.	Grenha R, Rzechorzek NJ, Brannigan JA, de Jong RN, Ab E, Diercks T, Truffault V, Ladds JC, Fogg MJ, Bongiorni C, Perego M, Kaptein R, Wilson KS, Folkers GE, Wilkinson AJ. 2006. Structural characterization of Spo0E-like protein-aspartic acid phosphatases that regulate sporulation in *bacilli*. J Biol Chem 281:37993-38003.

84.	Anantharaman V, Aravind L. 2003. Application of comparative genomics in the identification and analysis of novel families of membrane-associated receptors in bacteria. Bmc Genomics 4:34-53.

85.	Behr S, Kristoficova I, Witting M, Breland EJ, Eberly AR, Sachs C, Schmitt-Kopplin P, Hadjifrangiskou M, Jung K. 2017. Identification of a high-affinity pyruvate receptor in *Escherichia coli*. Sci Rep 7:1388-1397.

86.	Kraxenberger T, Fried L, Behr S, Jung K. 2012. First insights into the unexplored two-component system YehU/YehT in *Escherichia coli*. J Bacteriol 194:4272-4284.

87.   Fried L, Behr S, Jung K. 2013. Identification of a target gene and activating stimulus for the YpdA/YpdB histidine kinase/response regulator system in *Escherichia coli*. J Bacteriol 195:807-815.

88.   Miyake Y, Inaba T, Watanabe H, Teramoto J, Yamamoto K, Ishihama A. 2019. Regulatory roles of pyruvate-sensing two-component system PyrSR (YpdAB) in *Escherichia coli* K-12. FEMS Microbiol Lett.366: fnz009.

89.   Galperin MY. 2008. Telling bacteria: Do not LytTR. Structure 16:657-659.

90.   Behr S, Brameyer S, Witting M, Schmitt-Kopplin P, Jung K. 2017. Comparative analysis of LytS/LytTR-type histidine kinase/response regulator systems in gamma-proteobacteria. PLoS One 12:e0182993.

91.   Behr S, Heermann R, Jung K. 2016. Insights into the DNA-binding mechanism of a LytTR-type transcription regulator. Biosci Rep 36:e00326.

92.   Sidote DJ, Barbieri CM, Wu T, Stock AM. 2008. Structure of the *Staphylococcus aureus* AgrA LytTR domain bound to DNA reveals a beta fold with an unusual mode of binding. Structure 16:727-735.

93.   Kristoficova I, Vilhena C, Behr S, Jung K. 2018. BtsT, a novel and specific pyruvate/H$^{(+)}$ symporter in *Escherichia coli*. J Bacteriol 200:e00599-17.

94.   Romeo T, Vakulskas CA, Babitzke P. 2013. Post-transcriptional regulation on a global scale: form and function of Csr/Rsm systems. Environ Microbiol 15:313-324.

95.   Behr S, Fried L, Jung K. 2014. Identification of a novel nutrient-sensing histidine kinase/response regulator network in *Escherichia coli*. J Bacteriol 196:2023-2029.

96.   Gasperotti A, Going S, Fajardo-Ruiz E, Forne I, Jung KR. 2020. Function and regulation of the pyruvate transporter CstA in *Escherichia coli*. Int J Mol Sci 21: 9068-9084.

97.   Paulini S, Fabiani FD, Weiss AS, Moldoveanu AL, Helaine S, Stecher B, Jung K. 2022. The biological significance of pyruvate sensing and uptake in *Salmonella enterica* serovar Typhimurium. Microorganisms 10: 1751-1771.

98.   Going S, Gasperotti AF, Yang Q, Defoirdt T, Jung K. 2021. Insights into a pyruvate sensing and uptake system in *Vibrio campbellii* and its importance for virulence. J Bacteriol 203: e00296-21.

99.   Vilhena C, Kaganovitch E, Shin JY, Grunberger A, Behr S, Kristoficova I, Brameyer S, Kohlheyer D, Jung K. 2018. A single cell view of the BtsSR/YpdAB pyruvate sensing network in *Escherichia coli* and its biological relevance. J Bacteriol 200: e00536-17.

100.   Rathee K, Dhull V, Dhull R, Singh S. 2016. Biosensors based on electrochemical lactate detection: A comprehensive review. Biochem Biophys Rep 5:35-54.

101.   Alam F, RoyChoudhury S, Jalal AH, Umasankar Y, Forouzanfar S, Akter N, Bhansali S, Pala N. 2018. Lactate biosensing: The emerging point-of-care and personal health monitoring. Biosens Bioelectron 117:818-829.

102.   Saeidi N, Wong CK, Lo TM, Nguyen HX, Ling H, Leong SSJ, Poh CL, Chang MW. 2011. Engineering microbes to sense and eradicate *Pseudomonas aeruginosa*, a human pathogen. Mol Syst Biol 7:521-531.

103.   Xu X, Xu R, Hou S, Kang Z, Lu C, Wang Q, Zhang W, Wang X, Xu P, Gao C, Ma C. 2022. A selective fluorescent L-lactate biosensor based on an L-lactate-specific transcription regulator and forster resonance energy transfer. Biosensors (Basel) 12:1111-1124.

104.   Meselson M, Yuan R. 1968. DNA restriction enzyme from *E. coli*. Nature 217:1110-1114.

105.   Kraxenberger T, Fried L, Behr S, Jung K. 2012. First insights into the unexplored two-component system YehU/YehT in *Escherichia coli*. J Bacteriol 194:4272-4284.

106. Karimova G, Pidoux J, Ullmann A, Ladant D. 1998. A bacterial two-hybrid system based on a reconstituted signal transduction pathway. Proc Natl Acad Sci U S A 95:5752-5756.

107. Kollmann R, Altendorf K. 1993. ATP-driven potassium transport in right-side-out membrane vesicles via the Kdp system of *Escherichia coli*. Biochim Biophys Acta 1143:62-66.

108. Jung K, Odenbach T, Timmen M. 2007. The quorum-sensing hybrid histidine kinase LuxN of *Vibrio harveyi* contains a periplasmically located N terminus. J Bacteriol 189:2945-2948.

109. Guzman LM, Belin D, Carson MJ, Beckwith J. 1995. Tight regulation, modulation, and high-level expression by vectors containing the arabinose P_{BAD} promoter. J Bacteriol 177:4121-4130.

110. Zhong C, You C, Wei P, Zhang YH. 2017. Simple cloning by prolonged overlap extension-PCR with application to the preparation of large-size random gene mutagenesis library in *Escherichia coli*. Methods Mol Biol 1472:49-61.

111. Behr S, Brameyer S, Witting M, Schmitt-Kopplin P, Jung K. 2017. Comparative analysis of LytS/LytTR-type histidine kinase/response regulator systems in gamma-proteobacteria. PLoS One 12:e0182993.

112. Schramke H, Tostevin F, Heermann R, Gerland U, Jung K. 2016. A dual-sensing receptor confers robust cellular homeostasis. Cell Rep 16:213-221.

113. Jung K, Tjaden B, Altendorf K. 1997. Purification, reconstitution, and characterization of KdpD, the turgor sensor of *Escherichia coli*. J Biol Chem 272:10847-10852.

114. Behr S, Fried L, Jung K. 2014. Identification of a novel nutrient-sensing histidine kinase/response regulator network in *Escherichia coli*. J Bacteriol 196:2023-2039.

115. Roelofs KG, Wang J, Sintim HO, Lee VT. 2011. Differential radial capillary action of ligand assay for high-throughput detection of protein-metabolite interactions. Proc Natl Acad Sci U S A 108:15528-15533.

116. Sonnhammer EL, von Heijne G, Krogh A. 1998. A hidden Markov model for predicting transmembrane helices in protein sequences. Proc Int Conf Intell Syst Mol Biol 6:175-182.

117. Krogh A, Larsson B, von Heijne G, Sonnhammer EL. 2001. Predicting transmembrane protein topology with a hidden Markov model: application to complete genomes. J Mol Biol 305:567-580.

118. Wilkins MR, Gasteiger E, Bairoch A, Sanchez JC, Williams KL, Appel RD, Hochstrasser DF. 1999. Protein identification and analysis tools in the ExPASy server. Methods Mol Biol 112:531-552.

119. Buchan DW, Minneci F, Nugent TC, Bryson K, Jones DT. 2013. Scalable web services for the PSIPRED protein analysis workbench. Nucleic Acids Res 41:349-357.

120. Jumper J, Evans R, Pritzel A, Green T, Figurnov M, Ronneberger O, Tunyasuvunakool K, Bates R, Zidek A, Potapenko A, Bridgland A, Meyer C, Kohl SAA, Ballard AJ, Cowie A, Romera-Paredes B, Nikolov S, Jain R, Adler J, Back T, Petersen S, Reiman D, Clancy E, Zielinski M, Steinegger M, Pacholska M, Berghammer T, Bodenstein S, Silver D, Vinyals O, Senior AW, Kavukcuoglu K, Kohli P, Hassabis D. 2021. Highly accurate protein structure prediction with AlphaFold. Nature 596:583-589.

121. Ueguchi C, Ito K. 1990. *Escherichia coli* sec mutants accumulate a processed immature form of maltose-binding protein (MBP), a late-phase intermediate in MBP export. J Bacteriol 172:5643-5649.

122. Wu R, Gu M, Wilton R, Babnigg G, Kim Y, Pokkuluri PR, Szurmant H, Joachimiak A, Schiffer M. 2013. Insight into the sporulation phosphorelay: Crystal structure of the sensor domain of *Bacillus subtilis* histidine kinase, KinD. Protein Sci 22:564-576.

123. Lehtio L, Leppanen VM, Kozarich JW, Goldman A. 2002. Structure of *Escherichia coli* pyruvate formate-lyase with pyruvate. Acta Crystallogr D Biol Crystallogr 58:2209-2212.

124. Grebe TW, Stock JB. 1999. The histidine protein kinase superfamily. Adv Microb Physiol 41:139-227.

125. Casino P, Miguel-Romero L, Marina A. 2014. Visualizing autophosphorylation in histidine kinases. Nat Commun 5:3258-3268.

126. Lina G, Jarraud S, Ji G, Greenland T, Pedraza A, Etienne J, Novick RP, Vandenesch F. 1998. Transmembrane topology and histidine protein kinase activity of AgrC, the agr signal receptor in *Staphylococcus aureus*. Mol Microbiol 28:655-662.

127. Freeman JA, Lilley BN, Bassler BL. 2000. A genetic analysis of the functions of LuxN: a two-component hybrid sensor kinase that regulates quorum sensing in *Vibrio harveyi*. Molecular Microbiology 35:139-149.

128. Geer LY, Domrachev M, Lipman DJ, Bryant SH. 2002. CDART: Protein homology by domain architecture. Genome Res. 12:1619-1623.

129. Jones DT. 2007. Improving the accuracy of transmembrane protein topology prediction using evolutionary information. Bioinformatics 23:538-544.

130. Krogh A, Larsson B, von Heijne G, Sonnhammer ELL. 2001. Predicting transmembrane protein topology with a hidden Markov model: Application to complete genomes. J Mol Biol. 305:567-580.

131. Viklund H, Elofsson A. 2008. OCTOPUS: improving topology prediction by two-track ANN-based preference scores and an extended topological grammar. Bioinformatics 24:1662-1668.

132. Pierce KL, Premont RT, Lefkowitz RJ. 2002. Seven-transmembrane receptors. Nat Rev Mol Cell Biol 3:639-650.

133. Duangpan S, Jitrapakdee S, Adina-Zada A, Byrne L, Zeczycki TN, St Maurice M, Cleland WW, Wallace JC, Attwood PV. 2010. Probing the catalytic roles of Arg548 and Gln552 in the carboxyl transferase domain of the *Rhizobium etli* pyruvate carboxylase by site-directed mutagenesis. Biochemistry 49:3296-3304.

134. Lietzan AD, St Maurice M. 2013. A substrate-induced biotin binding pocket in the carboxyltransferase domain of pyruvate carboxylase. J Biol Chem 288:19915-19925.

135. Oliver T, Schmidt B, Nathan D, Clemens R, Maskell D. 2005. Using reconfigurable hardware to accelerate multiple sequence alignment with ClustalW. Bioinformatics 21:3431-3432.

136. Takeda Y, Avila H. 1986. Structure and gene expression of the *E. coli* Mn-superoxide dismutase gene. Nucleic Acids Res 14:4577-4589.

137. Guarino VA, Oldham WM, Loscalzo J, Zhang YY. 2019. Reaction rate of pyruvate and hydrogen peroxide: assessing antioxidant capacity of pyruvate under biological conditions. Sci Rep 9:19568.

138. Asmus C, Mozziconacci O, Schoneich C. 2015. Low-temperature NMR characterization of reaction of sodium pyruvate with hydrogen peroxide. J Phys Chem A 119:966-977.

139. Hristova K, Wimley WC. 2011. A look at arginine in membranes. J Membr Biol.239:49-56.

140.   von Heijne G. 1992. Membrane protein structure prediction. Hydrophobicity analysis and the positive-inside rule. J Mol Biol 225:487-494.

141.   Lerch-Bader M, Lundin C, Kim H, Nilsson I, von Heijne G. 2008. Contribution of positively charged flanking residues to the insertion of transmembrane helices into the endoplasmic reticulum. Proc Natl Acad Sci U S A 105:4127-4132.

142.   Nakamura H, Kumita H, Imai K, Iizuka T, Shiro Y. 2004. ADP reduces the oxygen-binding affinity of a sensory histidine kinase, FixL: The possibility of an enhanced reciprocating kinase reaction. Proc Natl Acad Sci U S A 101:2742-2746.

143.   Diensthuber RP, Bommer M, Gleichmann T, Moglich A. 2013. Full-length structure of a sensor histidine kinase pinpoints coaxial coiled coils as signal transducers and modulators. Structure 21:1127-1136.

144.   Heermann R, Altendorf K, Jung K. 1998. The turgor sensor KdpD of *Escherichia coli* is a homodimer. Biochim Biophys Acta 1415: 114–124.

145.   Jung K, Heermann R, Meyer M, Altendorf K. 1998. Effect of cysteine replacements on the properties of the turgor sensor KdpD of *Escherichia coli*. Biochim Biophys Acta 1372: 311-332.

146.   Tetsch L , Koller C, Dönhöfer A, Jung K. 2011. Detection and function of an intramolecular disulfide bond in the pH-responsive CadC of *Escherichia coli*. BMC Microbiol 11:74-85.

147.   Yang H, Liu L, Xu F. 2016. The promises and challenges of fusion constructs in protein biochemistry and enzymology. Appl Microbiol Biotechnol 19: 8273-8281.

148.   Hiraka K, Tsugawa W, Asano Ryutaro, Yokus MA, Ikebukuro K, Daniele MA, Sode K. 2021. Rational design of direct electron transfer type L-lactate dehydrogenase for the development of multiplexed biosensor. Biosens Bioelectron 176:1-10.

149.   Lovley DR, Giovannoni SJ , White DC , Champine JE, Phillips EJP, Gorby YA , Goodwin
S.1993. *Geobacter metallireducens* gen. nov. sp. nov., a microorganism capable of
coupling the complete oxidation of organic compounds to the reduction of iron and other
metals. Arch Microbiol 159:336-344.